Predicting erosion of vegetated dunes during hurricanes

Assessing the representation of vegetation effects in XBeach

Sebastian Cuevas Salgado

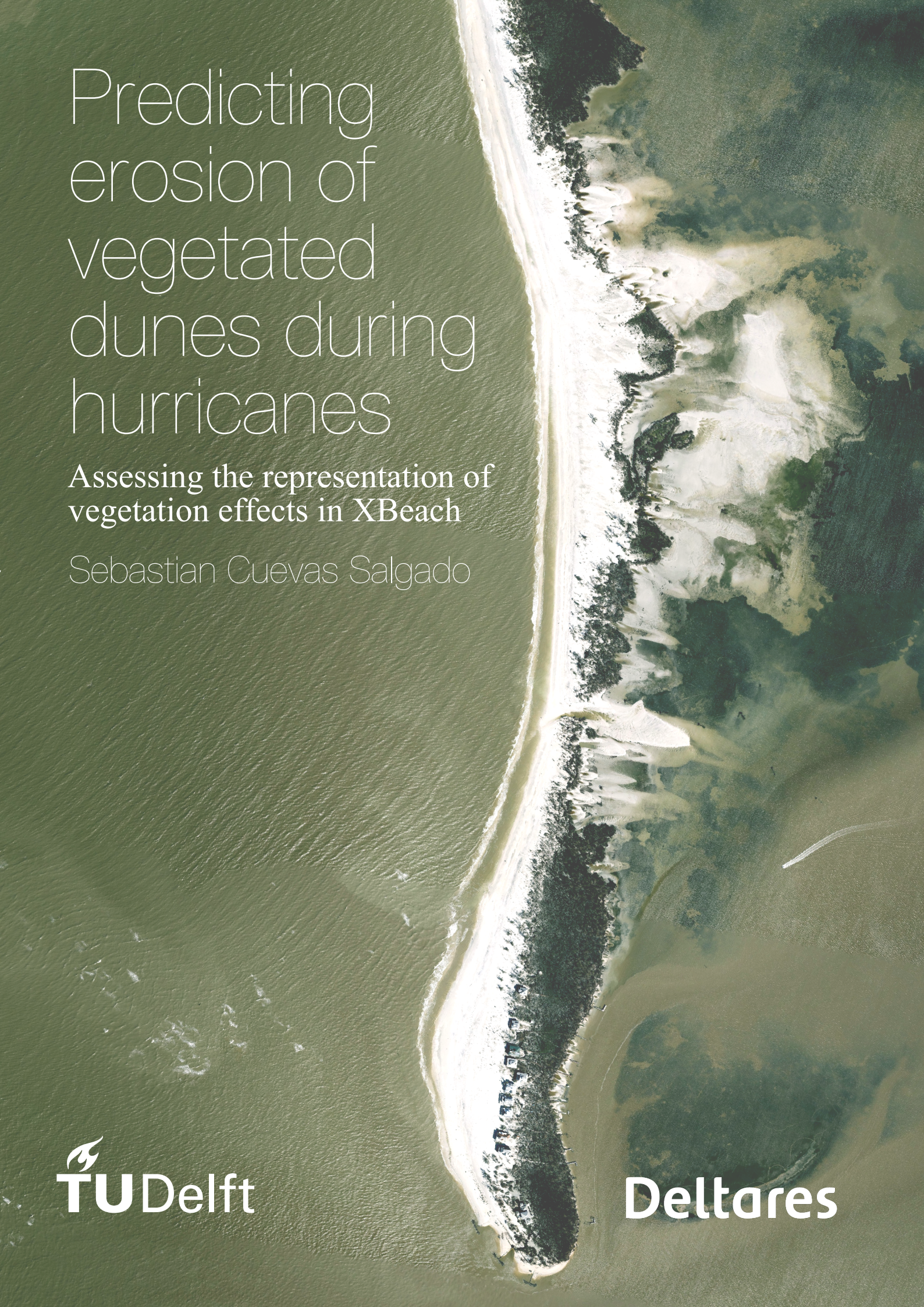

TU Delft

Deltares

Predicting erosion of vegetated dunes during hurricanes

Assessing the representation of vegetation effects in XBeach

Thesis report

by

Sebastian Cuevas Salgado

to obtain the degree of Master of Science
at the Delft University of Technology
to be defended publicly on Friday October 13^{th}, 2023 at 13:00.

Thesis committee:	Dr. ir. S. de Vries,	TU Delft, chair
	Dr. M.F.S. Tissier,	TU Delft
	ir. E. Quataert,	Deltares
	Dr. ir. A. van Dongeren,	Deltares

Place:	Faculty of of Civil Engineering and Geosciences, Delft
Project Duration:	February 1^{st}, 2023 - October 13^{th}, 2023
Student number:	5325110

TU Delft Delft University of Technology

enabling delta life

Abstract

Coastal dunes serve as the primary defence mechanism against coastal storms for many coastal communities around the world. Vegetation plays a role in increasing dune resiliency as it enables dune growth, however not enough is known about its effects during storms. Research has shown that the current climate crisis will increase the intensity of coastal storms as the sea level rises and global temperatures increase. It is therefore of utmost importance to understand the effects of vegetation on coastal dunes. Particularly with current trends of nature-based solutions to plant vegetation in dune restoration projects.

In this master thesis, the impact of Hurricane Ian on two barrier islands is analyzed and modelled. The primary focus of the study was to investigate how dune vegetation influenced the erosional effects of the storm, with a particular emphasis on enhancing the existing methodologies for incorporating vegetation into morphological models such as XBeach. The research findings derived from the data analysis revealed that the most resilient dunes are high, broad and have a dense vegetation coverage. Moreover, the model outcomes highlight the substantial improvement in predictive accuracy achieved by integrating vegetation as a bed roughness coefficient within the XBeach model. Adding vegetation to the model directly influences current velocities, but does not affect water levels, wave heights, or infragravity waves. The primary influence of vegetation becomes pronounced when an island is inundated or breached, significantly reducing the currents and sediment transport caused by water level gradients. An additional effect of vegetation was observed in a comparative analysis between vegetated and unvegetated models. This analysis highlighted a delay in dune crest lowering when vegetation was present, showcasing the importance of vegetation in shaping the response of barrier islands during storm events.

Numerical modelling can help understand the complex processes that shape barrier islands during storms. This research emphasized the necessity of including vegetation in XBeach models to enhance their predictive capabilities. The best predictions occur when high-resolution bathymetric data is combined with land use land cover (LULC) data to include vegetation as a constant bed roughness parameter. Furthermore, reducing the land classes to four different ones based on dune vegetation zones improves the results of the model and facilitates the calibration of bed friction coefficients.

The most effective models applied in this study demonstrated impressive skill, ranging from good to excellent, accurately predicting breaches in the precise areas they occurred for both islands under investigation. This research contributes to the continued improvements of modelling with XBeach and provides a detailed method of analyzing the effects of dune vegetation on dune erosion to determine the impact of Hurricanes in coastal dunes.

Acknowledgements

This master's thesis work marks the culmination of my two-year journey as a Civil Engineering Master's Student at the Deft University of Technology. This period has been enriched with memorable experiences during which I gained invaluable knowledge from the expert faculty at TUD, as well as from my engaging internships at Rijkswaterstaat and Witteveen+Bos. A major highlight was the conclusion of my masters at a world-renowned research institute such as Deltares.

Completing this master's thesis would not have been possible without the help of many people. I extend my sincere gratitude to my university supervisors, Sierd de Vries and Marion Tissier, for their insightful feedback and guidance throughout my thesis and time at TUD. Additionally, I express my thanks to my supervisors at Deltares, Ap van Dongeren and Ellen Quartaert, for their unwavering support, detailed explanations, and mentorship.

Of course, this accomplishment would not have been possible without the constant support of my parents. No words can express my gratitude for their help, inspiration and love. A special thank you go to Dick Heijboer, Casper Thorsturp, Paulina Rodriguez and Michael Smolinski, who were kind enough to provide a home for me during the final two months of my thesis. Lastly, I would like to thank my friends who not only helped with the thinking process during my thesis but also provided nice distractions and activities outside of work - you know who you are.

Happy reading!

Sebastian Cuevas Salgado
Utrecht, October 5^{th}, 2023

Contents

List of Figures

List of Tables

Nomenclature

List of Abbreviations

BSS Brier Skill Score

C-CAP Coastal Change Analysis Program

CHM Canopy Height Model

DEM Digital Elevation Model

DSM Digital Surface Model

FDEP Florida Depatment of Environmental Protection

HWM High Water Mark

LiDAR Light Detection and Ranging

LK Lovers Key

LULC Land use and land cover

MHW Mean High Water

NAVD88 North American Vertical Datum of 1988

NCI North Captiva Island

NGS National Geodetic Survey

NOAA National Oceanic and Atmospheric Administration

NOPP National Oceanographic Partnership Program

NRL U.S. Naval Research Laboratory

ONR Office of Naval Research

RMW Radius of maximum winds

ROTO Remove Off-terrain Objects

SfM Structure for Motion

SSHS Saffir–Simpson hurricane wind scale

USGS United States Geological Survey

List of Symbols

RR Relative relief

Δz_b Bed level change

ϕ Dune slope

d^* Root depth

D_{crest} Dune crest location

D_{hill} Dune hill location

D_{toe} Dune toe location

H Dune height

h^* Vegetation height

H_{ig} Infragravity wave height

H_s Significant wave height

n Manning roughness coefficient

R_{high} Highest runup

R_{low} Lowest runup

RR_c Relative relief center of window

$V_{deposited}$ Deposited volumes

V_{eroded} Eroded volumes

W Dune width

z_b Bed level

z_{c0} Initial dune crest elevation

z_{cf} post-storm elevation at pre-storm dune crest

z_{crest} Dune crest elevation

z_c Elevation at center of window

z_{max} Maximum elevation

z_{min} Minimum elevation

1

Introduction

Human settlements in coastal areas have proliferated because of the availability of resources, socio-economic benefits, appealing landscapes, and ecosystem services, resulting in significant population growth and infrastructure development (Luijendijk et al., 2018; Small & Nicholls, 2003). This is exemplified by the 15 megacities located along the coast (Blackburn et al., 2019). This rapid growth and continued development of the coastal zone combined with long-term coastal erosion has led to significant coastal squeeze, increasing both the risk and exposure of coastal communities to coastal hazards (Luijendijk et al., 2018). Furthermore, climate change has led to an increase in temperatures around the globe, and a recent study by Bhatia et al., 2019 has linked warming temperatures to an increase in storm intensity in the Atlantic Ocean. This increase in storm intensity combined with sea-level rise (SLR) poses one of the major coastal hazards for coastal areas worldwide as they can drastically change the coastal landscape within a short time frame (Sherwood et al., 2021).

Coastal dunes provide the primary line of defence against coastal storms for most low-lying sandy beaches, as they can withstand to a certain extent hydrodynamic forces (Shiflett & Backstrom, 2023). This has resulted in several projects and studies to restore or strengthen dunes, as there is a new shift towards nature-based solutions. Vegetation is believed to play a key role in increasing dune resiliency as it facilitates sediment cohesion, wave energy dampening and dune growth through the capture of aeolian-transported sediment (Bryant et al., 2019; Shiflett & Backstrom, 2023; Sigren et al., 2023). Given the importance of dunes for flood safety and current dune restoration practices almost always include planting vegetation (Sigren et al., 2023), there is a need to further research the effects of dune vegetation during storms.

One of the current research projects is being conducted in a consortium of Deltares, the U.S. Geological Survey (USGS), the U.S. Naval Research Laboratory (NRL), and IHE Delft to develop forecasting models for surges, waves, floods, and dune erosion during hurricanes for the Atlantic and Gulf of Mexico coastlines in the United States. This research will focus on the morphological modelling of dune erosion using XBeach and improve the current methods for including vegetation in XBeach models based on data gathered during Hurricane Ian.

1.1. Research objective

The impact of coastal hazards can be reduced by improving our current forecasting practices for extreme storms and the accurate prediction of dune erosion in such events. XBeach is a morphodynamic model that was developed to model morphological changes during storm events. This model has shown satisfactory results across different case studies, however, this can be further improved by including a better representation of the physical processes taking place and by reducing the uncertainty of the models. One process that needs further investigation in the model is the interaction of dune vegetation and the role it plays in erosional processes. To contribute to the current body of knowledge, this study will investigate the role vegetation played in a set of barrier islands located near Cape Coral, Florida during Hurricane Ian 2022. The data gathered pre and post-storm for these islands will be used to conduct data analysis and to improve and adapt current methods used to include vegetation in XBeach models. The ultimate research goal is to improve current methods to include vegetation in XBeach for forecasting dune erosion during hurricanes. With this in mind, we come to the following research objective and subsequent research questions:

Improve the inclusion of vegetation in XBeach models to reduce uncertainty in predicting dune and beach erosion during storms.

1. What was the erosional impact of Hurricane Ian and what was the influence of vegetation?

2. How can we improve the inclusion of dune vegetation in XBeach?

3. What are the most significant uncertainties in the inclusion of vegetation in XBeach models?

1.2. Approach and methodology

To determine the effects of vegetation during storms, data analysis and morphodynamic modelling are conducted for two barrier islands that experienced significant morphological change during Hurricane Ian. First, pre and post-storm data are analyzed, focusing on extracting dune characteristics, vegetation data, and erosion volumes to evaluate the storm impact and the role of vegetation. Secondly, two XBeach models are set up to simulate the morphological change throughout the storm for Lovers Key and North Captiva Island. In this phase, different representation methods of vegetation are tested in XBeach. Including different vegetation data sets derived from land use land cover (LULC) data and temporal vegetation models that can be applied statically or dynamically. The effects and uncertainties of including vegetation are assessed by looking at model performance metrics, effects of hydrodynamic conditions and storm regimes. Knowing the uncertainties of including vegetation will help determine the effects of including vegetation relative to other known uncertainties in XBeach models. Finally, the results of the data analysis and XBeach models are discussed and conclusions are drawn. These steps are taken as shown in Fig. 1.1 with the thesis outline.

1.3. Thesis outline

To answer the overall research objective and each sub-research question the thesis is divided into the following chapters:

Chapter 1: Introduction to the master thesis topic and research objective. **Chapter 2:** An extensive literature review of the state-of-the-art regarding dunes, dune vegetation, morphological modelling with XBeach and current methods to include vegetation in XBeach. **Chapter 3:** The selection of the storm and the reasons for selecting the two study areas are discussed, along with an overview of the pre and post-storm data available. **Chapter 4:** In this chapter, the methodology to identify relationships between dune properties, dune vegetation and dune erosion from pre and post-storm data is presented followed by the results for the two case studies. **Chapter 5:** This chapter begins by detailing the methodology used to model the two cases in XBeach during Hurricane Ian and the varying methods to incorporate vegetation into the models. It then delves into the presentation of results, showcasing diverse simulation outcomes under varying vegetation conditions. **Chapter 6:** The results of the data analysis and morphodynamic modelling will be discussed in this section, with an overall focus on the effects of vegetation both in the data and the model, along with the research limitations. **Chapter 7:** Conclusions are drawn based on the results and discussion sections. Finalized with recommendations based on the research outcomes.

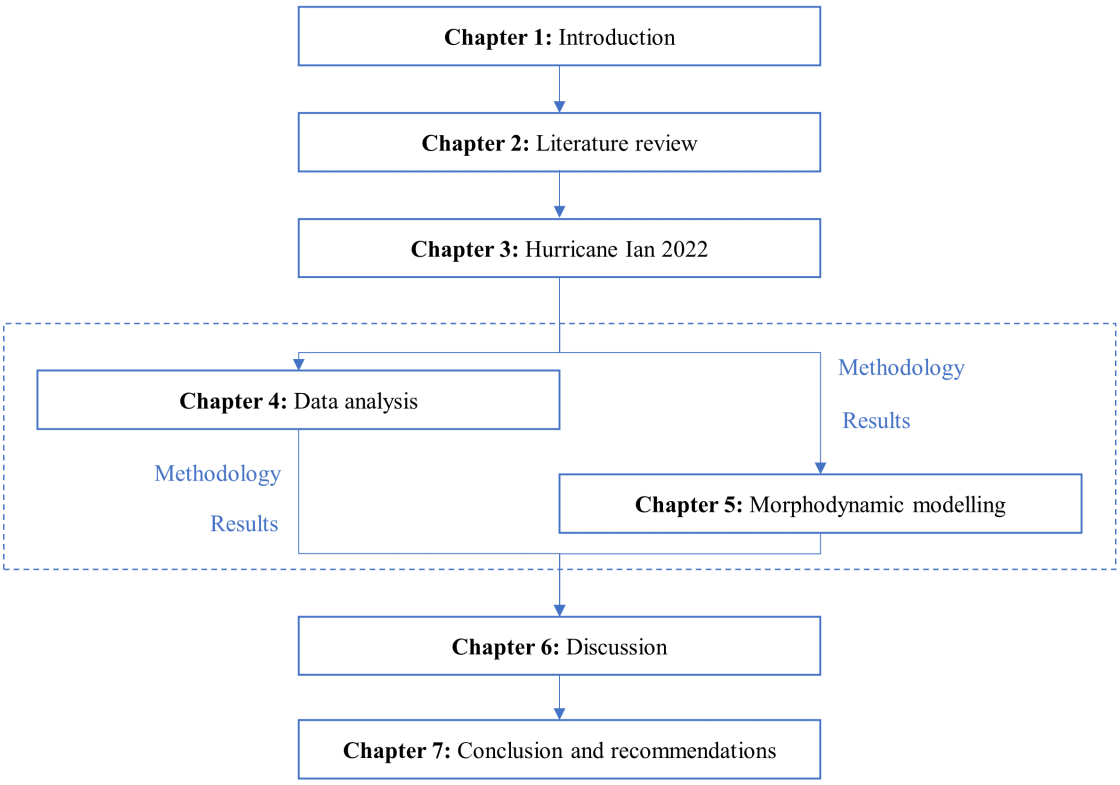

Figure 1.1: *Thesis outline*

2

Literature Review

This section reviews the current state-of-the-art literature regarding coastal dunes, dune erosion, dune vegetation, morphological modelling of dune erosion with XBeach, and methods for including vegetation in XBeach models. From this literature review, knowledge gaps are identified and addressed in the following sections of this thesis.

2.1. Coastal Dunes

Coastal dunes are well distributed across the world and can be found at any latitude (Martínez & Psuty, 2004). They provide a natural primary line of defence against storms for coastal communities (Wernette et al., 2016). These coastal ecosystems develop from the intricate interactions between sediment supply, vegetation, wind, waves and water levels (De Battisti & Griffin, 2020). While the system provides a front-line defence mechanism, their interaction with hydrodynamics during storms can result in sudden large-scale morphological changes caused by erosional and accretion processes. The capacity of coastal dunes to withstand a storm is a function of their geomorphic characteristics (Houser et al., 2008).

Dunes have three distinctive morphological features that can help determine their extent and height. Namely, the toe, crest and hill. Definitions and methods to locate these morphological features are varied across the literature. The following list summarizes some of the definitions found in the literature.

- **Dune toe (D_{toe})** can be considered the transition point between beach and dune (Mitasova et al., 2011) or from the maximum slope change
- **Dune crest (D_{crest})** are topographic peaks, however, some literature defines it as the maximum crest of the most landward dune (Lentz & Hapke, 2011) while other authors differ and suggest that the dune crest is the elevation peak within a user-defined beach (Stockdon et al., 2009). The user-defined beach can be selected based on local knowledge of the area, and surroundings such as human infrastructure.
- **Dune hill (D_{hill})** is defined as a geographical depression located landward of the dune crest (Wernette et al., 2016).

Dune characteristics can be used to compute geomorphic parameters of the dune system, such as slope Φ, width W, height H and aspect ratio (Cohn et al., 2019; Doyle & Woodroffe, 2018). Figure 2.1 shows a dune schematic with morphological features and geomorphic parameters. The dune slope Φ is calculated as the angle between the dune crest and toe, the dune height is the vertical distance between the toe and the crest, and the dune width is the horizontal distance between the dune toe and the dune hill.

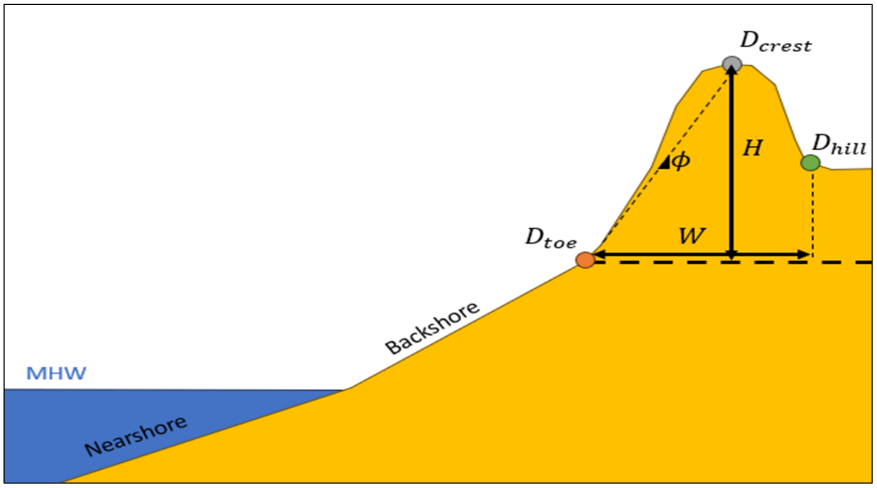

Figure 2.1: *Coastal dune with its distinctive morphological features and geomorphic parameters. Where D_{crest} is the dune crest, D_{toe} is the dune toe, D_{hill} is the dune hill, H is the dune height, W is the dune width and Φ is the dune slope.*

2.2. Dune erosion

Dune erosion during storms is driven by four main nearshore processes: infragravity waves, avalanching, turbulence and force generated on wave impact (Van Rijn, 2009; Van Thiel De Vries et al., 2008). In a large dune experiment conducted at the Delta flume, Van Thiel De Vries et al., 2008 found that for the dune erosion process, both incident and long waves are important but the latter becomes more important as the sediment eroded from the dune develops a new foreshore. Infragravity waves also play an important role as these low-frequency motions can contribute to large offshore sediment transport during storms but also reach the dunes without losing much energy and induce overwash, dune erosion and breaching (Bertin et al., 2018; Masselink, 1995). Van Thiel De Vries et al., 2008 also discuss that the turbulence generated by wave breaking enhances suspended sediment concentrations and therefore the capacity of the water to transport eroded sediment in the offshore or alongshore directions. Finally, gravity causes the avalanching of slumps of sand as the base of the dune starts to erode and the wet sand loses cohesion (Davidson et al., 2020; Sallenger, 2000).

The erosional impact of a storm on a beach is influenced by both the hydrodynamic forcing and the pre-storm coastal morphology (Sallenger, 2000). By taking this into account, Sallenger, 2000 categorized the erosional and accretion processes of a storm into four regimes: swash, collision, overwash and inundation. These regimes are determined based on the dune characteristics such as the toe or crest and the run-up and round-down of the combined hydrodynamics effects, including tides, storm surge, and waves and are shown in Fig. 2.2.

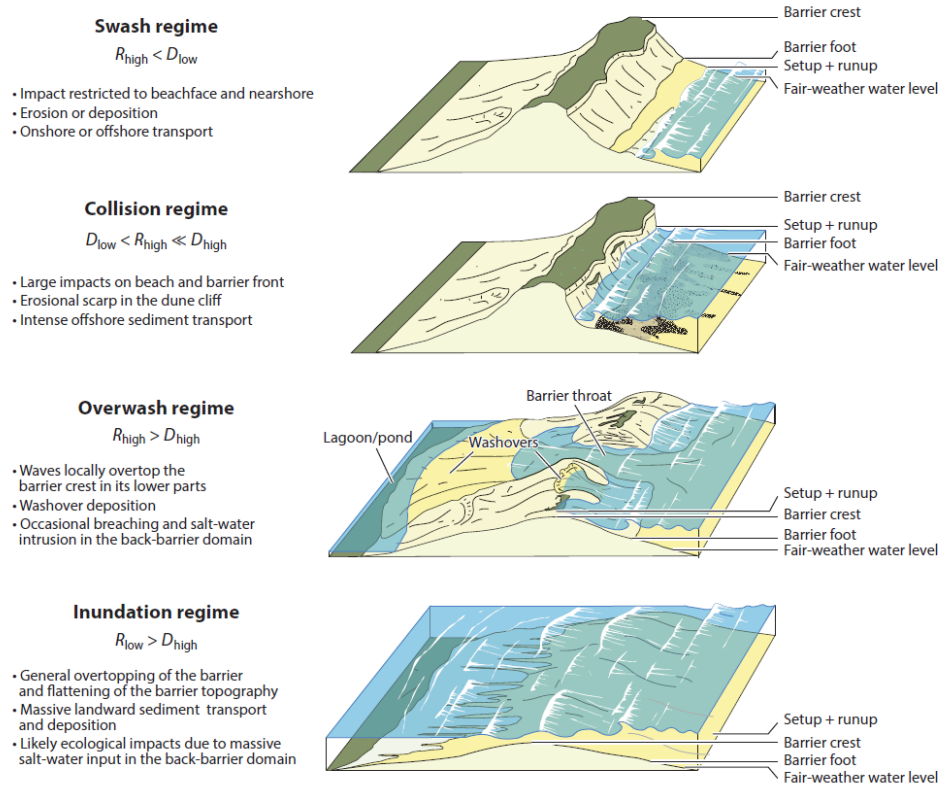

Figure 2.2: *Sallenger, 2000 storm impact regimes. The figure is taken from (Sherwood et al., 2021).*

Swash $R_{high} < D_{toe}$
The swash regime occurs when the wave run-up does not reach the dune base. During storms, cross-shore sediment transport is in the offshore direction and later returned onshore under calm wave conditions.

Collision $D_{toe} < R_{high} < D_{crest}$
The collision regime takes place when the incident or infragravity waves reach the dune face but the wave swash does not overtop the dune crest. In this regime, dune scarping occurs and the eroded sediment is then subsequently transported offshore or alongshore (Sallenger, 2000; Sherwood et al., 2021). The sediment is transported back to the beach under calm wave conditions and over time it returns to the dunes using aeolian transport (De Vries et al., 2012). An important distinction noted by Sallenger, 2000 is that for beaches without dunes, there is no collision regime, it goes from the swash regime to the overwash regime.

Overwash $R_{high} > D_{crest}$
In the overwash regime, some waves overtop the dune crest and transport sediment landward. The recovery of sediment lost during overwash is not as reversible compared to the collision regime and this generally leads to net landward migration of barrier islands.

Inundation $R_{low} > D_{crest}$
When the storm-induced wave setup exceeds the dune crest, the dunes are completely submerged and the inundation regime begins. This can occur locally in areas where the dune crest is lower, in which a breach can form and the main driver of sediment transport becomes the channel current velocities.

Storm surge ebb

An additional regime referred to as the ”storm surge ebb” is not included by Sallenger, 2000. This storm surge ebb takes place when the storm subsides, the water level in the back basin of a barrier can be higher than the seaside water level and this gradient causes return flows that result in the formation of new channels or deepening of existing channels (Goff et al., 2010; Goff et al., 2019; Harter & Figlus, 2017; Lennon, 1991; Over et al., 2021; Sherwood et al., 2021; Van Der Lugt et al., 2019).

Additional studies have shown that dune erosion is strongly dependent on pre-storm morphology and hydrodynamic forcing. Houser et al., 2008 found that erosional processes are stronger in steep narrow beaches compared to mild sloping wide beaches. Higher dunes are typically found along these narrow steep beaches and show the highest erosion rates during storms with high water levels (Cohn et al., 2019; Houser et al., 2008). However, recent studies have shown that dune vegetation also plays an important role in the erosional process. Wave flume experiments using both artificial vegetation and cores taken from dunes show a significant reduction in dune erosion (Bryant et al., 2019; De Battisti & Griffin, 2020; Figlus et al., 2022; Figlus et al., 2017; Sigren et al., 2018) and pre and post-storm surveys have shown that vegetation can mitigate erosion (Davidson et al., 2020; Maximiliano-Cordova et al., 2021).

2.3. Dune vegetation

Coastal dune vegetation is characterized by a gradual decline in environmental stresses caused by marine environments as one moves inland, including exposure to winds, storms, salinity and sand (McLachlan, 1991). This results in increasing vegetation coverage and complexity landwards. Figure 2.3, divided the dune vegetation into three zones, primary, secondary and tertiary vegetation zones. The primary vegetation zone is located in the incipient dunes and is characterized by its low vegetation height. The secondary zone is along the foredune area and has a greater diversity in vegetation types and denser coverage. Finally, the tertiary zone is located in the hind dunes and has the greatest canopy heights and fauna diversity.

Nature-based coastal defences have emerged as more sustainable options compared to hard engineering solutions. This has led to several dune restoration projects and studies to understand the role of dune vegetation (Maximiliano-Cordova et al., 2021; Sigren et al., 2014; Sigren et al., 2018). Wave flume experiments comparing vegetated dunes against bare dunes have shown a total eroded dune volume reduction of 30% (Bryant et al., 2019; De Battisti & Griffin, 2020; Feagin et al., 2019; Figlus et al., 2022; Figlus et al., 2017). Figlus et al., 2022 conclude that aboveground vegetation plays an important role in dissipating wave energy and uprush/backwash velocities. While the belowground vegetation anchors the surrounding sediment, thus increasing the strength and reducing avalanching. In their flume experiment, Bryant et al., 2019 tested belowground biomass, and one with above and belowground biomass, including both the collision and overwash regime. Their results show that belowground biomass is the most effective in decreasing erosion by reducing scarping in the collision regime and overtopping in the overwash regime. One important effect he noted is that vegetation delayed the regime shift between collision and overwash. These studies reach a general agreement that root biomass significantly reduces erosion and increases the shear strength of dune sediment. However, these experiments were conducted in small flumes and the authors highlight the complexity of scaling down vegetation. Another limitation is that only one of these studies experimented with collision and overwash regimes. It is stipulated that in reality, the erosion mitigation by vegetation is lower than what these experiments show, as

replicating the architecture of vegetation and strength in scale is extremely difficult Bryant et al., 2019. Further research needs to be conducted at a real scale on the differences between dune vegetation species, density, maturity, cover extent and uprooting processes.

Recent remote sensing techniques combined with high-resolution imagery have led to significant improvements in land use and land cover (LULC) data. This data has been recently used in some studies to determine if the inclusion of vegetation and urban areas in morphodynamic models like XBeach results in improved model skill, for examples, see (Passeri et al., 2018; Schambach et al., 2018; Van Der Lugt et al., 2019). With the increasing availability of high-resolution LULC data, there are new promising ways to assess the influence of dune vegetation during storms using models like XBeach.

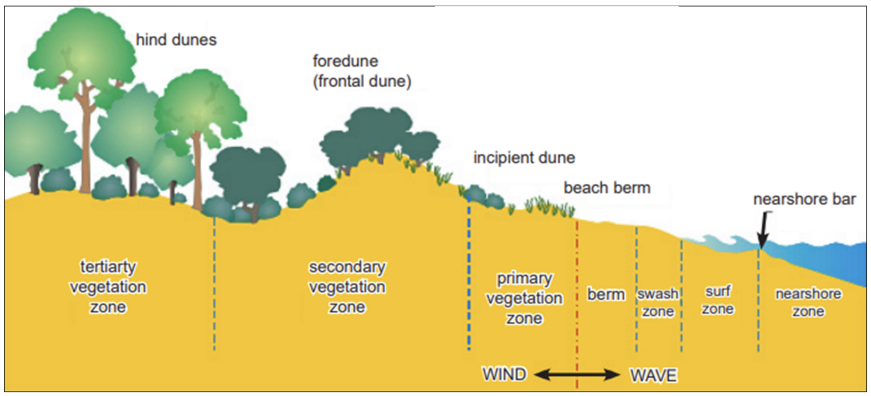

Figure 2.3: *Typical dune cross-section and vegetation distribution (Livingston, n.d.).*

2.4. XBeach

XBeach was developed by Roelvink et al., 2009 to model the physical processes that take place across the different Sallenger regimes under extreme storm events. It is a process-based model capable of resolving coupled wave energy, flow, infragravity wave motions, sediment transport and bed level change to determine dune and beach erosion (McCall et al., 2010; Roelvink et al., 2009).

XBeach solves short-wave action using the shallow water momentum and balance equations. To solve these, the wave energy density, propagation, frequency, and energy dissipation that includes wave rollers are needed. This is then used to compute radiation stress tensors to be used in the shallow water equations. For low-frequency waves, the shallow water equations are adapted to a Generalized Lagrangian Mean (GLM) formula that includes the effects of Coriolis, eddy viscosity, water depth, Eularian bed shear stresses, water level, and the radiation stresses tensors. These equations are responsible for computing wave-induced mass fluxes.

Bed shear stress in XBeach is modelled by the Ruessink et al., 2001 formulation and plays a direct role in the Eulerian flow velocities. In this formulation, the bed friction coefficient is derived from the Chezy coefficient which is directly related to the Manning coefficient.

The advection-diffusion equation is used in XBeach to compute sediment transport. To resolve this equation, depth average sediment concentrations, Eulerian velocities, sediment diffusion

coefficient, sediment fall velocities and water depth are needed. This equation combined with the wave calculations will lead to sediment transport vectors that will be used to compute bed-level changes.

Swash dynamics are resolved by a 2DH (depth-averaged) description of wave groups, it is an approach that resolves long waves but averages short waves and resolves them with a time and space-varying wave group energy. This method enables the simulation of infragravity wave motions and longshore and cross-shore currents. In the collision regime, dune erosion takes place by a wetting and drying process caused by swash runup, which eventually leads to the avalanching of the dune face. This is done by an avalanching algorithm that lowers dune elevation and transports the sediment onshore. This algorithm considers the drying and wetting process that affects the dune sand cohesion, as saturated sediments erode faster than dry ones. To simulate the overwash regime, XBeach uses the wave group forcing combined with a drying/wetting and sediment transport formulation. Finally, the inundation regime is implemented by using a semi-empirical model to predict how a breach will develop based on a schematic uniform cross-section.

To summarize, the hydrodynamic processes modelled by XBeach include short wave propagation, shallow water equations and undertow and for the morphodynamic processes, XBeach simulates sediment transport, bed updates, avalanching, dune erosion, overwash and breaching. It first computes waves, then hydrodynamics, and finally sediment transport as described above to update bottom changes. It then loops through this process for the duration of the storm. For a more detailed description of the inner working and hydrodynamic and sediment transport formulations used in XBeach see Harter and Figlus, 2017; McCall et al., 2010; Roelvink et al., 2009.

2.5. Modelling vegetation

There are different methods to include vegetation in morphological models. XBeach has a vegetation module that is used to model wave dissipation by mangroves, kelp or salt marshes. Nevertheless, for dune vegetation, the most common method is to increase the surface roughness or bed friction in vegetated areas of the dune Lodewijk et al., 2015. However, new alternatives have been developed that adopt the critical velocity in vegetated areas. These different methods and their applications are further described below.

Manning roughness coefficient

The Manning roughness coefficient n can be used to take into account frictional losses and is extremely difficult to determine as it is governed by many different hydraulic parameters and it varies both in time and space (De Doncker et al., 2009; Mckay & Fischenich, 2011). There are many different methods to estimate the Manning coefficient including direct measurements and field assessments (Mckay & Fischenich, 2011). Field measurements are generally difficult, time-consuming and costly, resulting in the common use of field assessments across different engineering applications. Mckay and Fischenich, 2011 note that field assessments generally consist of photographic comparison, table estimates, Cowan's analytical method and professional judgement. The Manning roughness coefficients derived from a photographic comparison of densely vegetated floodplains by Arcement and Schneider, 1989 were adapted for a coastal numerical model by Mattocks and Forbes, 2008 using LULC data. Lodewijk et al., 2015 applied a higher friction coefficient for vegetated areas to simulate the effects of vegetation. Vegetation obstructs the flow of water and lowers the current velocities. To simulate this in XBeach, the

bed friction coefficient is increased as it reduces the flow velocities. This in turn reduces erosion as with reduced flows the erosional capacity of the water is reduced. Since then, this adaptation has been used in several XBeach research projects that use varying Manning bed roughness coefficients based on LULC data to effectively reduce the flow in the area where vegetation is present (Schambach et al., 2018; Van Der Lugt et al., 2019). One exception is the study conducted by Passeri et al., 2018 for which a different Manning roughness classification was used that is obtained from the Coastal Change Analysis Program (C-CAP). These coefficients vary slightly compared to the ones used by Mattocks and Forbes, 2008. This difference in roughness coefficients is likely attributed to the fact that bed friction is commonly used as a calibration parameter in many hydro and morphodynamic models.

Van Der Lugt et al., 2019 use space-varying Manning friction coefficients in two XBeach models based on LULC data. In their study, they introduce a novel dynamic roughness method that takes into account the time-varying processes of vegetation getting covered by sand or eroded. Fig 2.4 shows a schematic that describes the dune vegetation module. The dynamic model takes a root depth d^* and vegetation height h^* and as soon as there is a positive or negative bed level change the manning roughness coefficient increases/decreases linearly back to the manning value for sand n_{sand}. This method showed promising results in forecasting dune erosion, deposition, and breach formation for two barrier islands under Hurricane forcing.

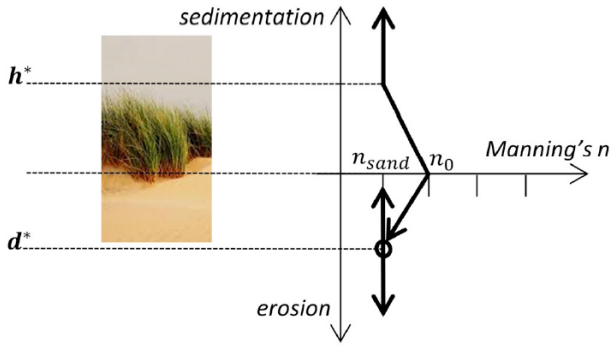

Figure 2.4: *Dynamic vegetation model for XBeach by Van Der Lugt et al., 2019.*

Critical velocity

An alternative to using only the adjusted Manning roughness coefficients based solely on LULC data is to include an increase in critical velocity in vegetated areas (Schweiger & Schuettrumpf, 2021a, 2021b). Increasing the critical velocity reduces the ability of the flow to pick up and erode sediment in vegetated areas. Schweiger and Schuettrumpf, 2021a introduce this in a new XBeach module and combine it with the dynamic roughness from Van Der Lugt et al., 2019. The results show that this works and reduces erosion in vegetated areas. However, this XBeach model was set up for a wave flume and it is yet to be tested in field-scale XBeach models.

XBeach vegetation module

The vegetation module of XBeach developed by Van Rooijen et al., 2014 is intended to simulate the dissipation effects of vegetation for waves and currents in front of beaches. The applications can be used for coastal areas that have mangroves, kelp forests, salt marshes and other types of vegetation. However, this XBeach module has only been used for wave dissipation in the nearshore and its applicability for vegetation located in the dunes is yet to be tested.

2.6. Knowledge gap

From the previous literature study, some knowledge gaps can be highlighted that can improve our understanding of dune vegetation and its inclusion in XBeach models. With the ultimate goal of increasing our capabilities to accurately predict the erosion of dunes during storms. Currently, vegetation in XBeach models for the prediction of erosional dune process during storms has been included by adjusting the bed roughness based on LULC. This has shown promising results, but large uncertainties remain in the selection of Manning roughness coefficients for each LULC. The effects of vegetation removal during storms can also be included in XBeach models. Van Der Lugt et al., 2019 implemented a new novel dynamic roughness scheme that accounts for the erosion of vegetation and coverage of vegetation. However, they kept constant uprooting depths and vegetation heights, and the sensitivity of these constant values is not known. Schweiger and Schuettrumpf, 2021a went a step further by including a dynamic critical velocity factor in vegetated areas, this was tested in an XBeach model for a flume dune experiment but has yet to be implemented in real scale. Another process that is yet to be included in the XBeach model is the increased shear strength by belowground biomass that reduces avalanching, this effect could be implemented in the XBeach avalanching module. Roots systems in dunes have been shown to increase the shear strength of the soil and erosion resistance (Figlus et al., 2022; Schweiger & Schuettrumpf, 2021a, 2021b). However, implementing this effect on the XBeach model to reduce slumping has not been studied. Adjusting the XBeach module for avalanching in vegetated areas to account for below-ground biomass can potentially improve model results.

This study will focus first on assessing the influence of vegetation during storms. As mentioned above, several studies have concluded that vegetation plays an important role in dune resiliency. However, it is not clear yet how important the vegetation is relative to dune morphology or the hydrodynamic conditions. To further understand the role of vegetation, data collected before and after a storm will be analyzed. To improve the current methods of including vegetation in XBeach, this study will focus on studying the effects of selecting different Manning roughness classifications as well as testing different vegetation maps derived from LULC data. Finally, this study will aim to further understand the effects of varying root depths in the Van Der Lugt et al., 2019 model and how this model compares to a static one that does not remove vegetation.

3

Hurricane Ian 2022

Hurricane Ian originated as a tropical storm near the southeast of Jamaica on September 24, 2022. While travelling northward from the Caribbean into the Gulf of Mexico, Ian steadily gained strength and evolved into a hurricane. Upon entering the Gulf of Mexico, Ian's intensity continued to escalate until reaching Category 5 (Cat-5) on the Saffir–Simpson hurricane wind scale (SSHS) about 70 km off the southwest coast of Florida, USA. Finally, on September 28, 2022, Hurricane Ian made landfall as a Cat-4 hurricane along a series of barrier islands near Cape Coral, Florida, resulting in catastrophic storm surges, winds, and freshwater flooding. Leaving a toll of $112 billion in damages and more than 150 lives lost in its wake, making it one of the most devastating hurricanes in United States History (Bucci et al., 2023). Ian re-entered the Atlantic Ocean and made landfall again as a Cat-1 in South Carolina before converting back into a tropical storm.

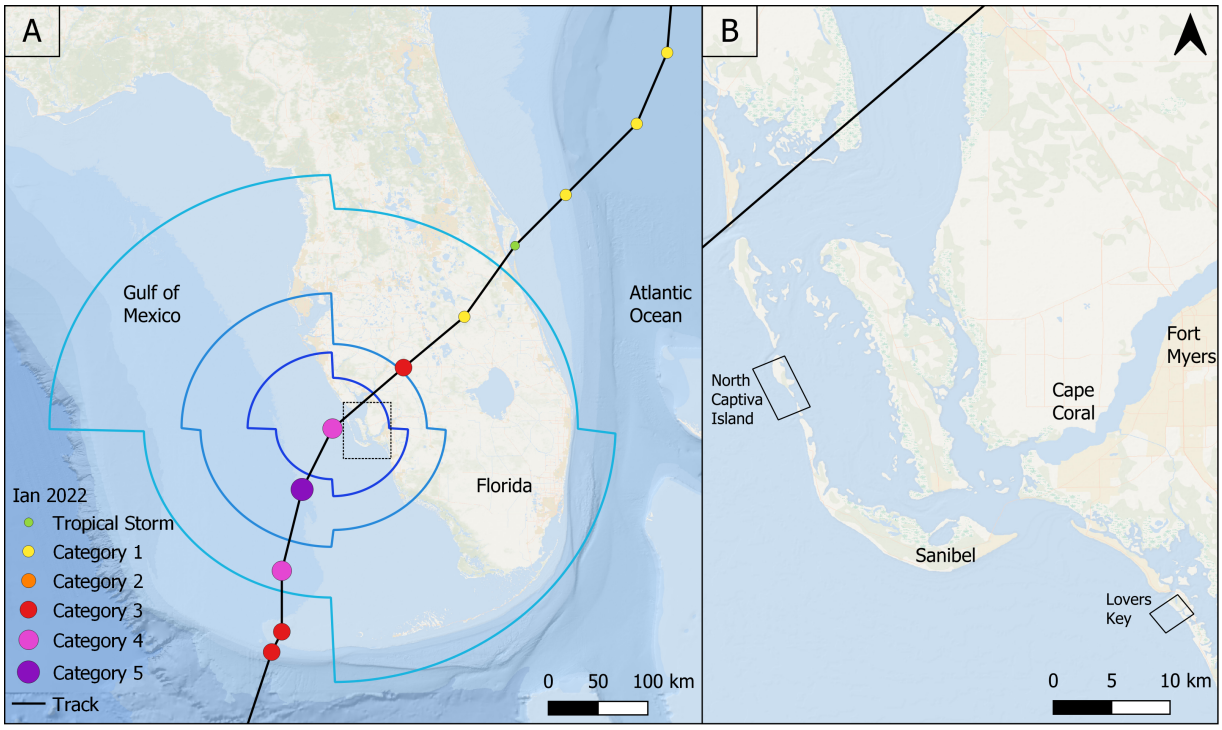

Figure 3.1: *A) Hurricane Ian track near the west coast of Florida, USA. With markers showing storm intensity on the SSHS scale and radii showing the extent of the storm. B) Area of largest impact, highlighting the XBeach model domains for the two islands selected for this study, North Captiva Island (NCI) and Lovers Key (LK).*

Hurricane Ian caused morphological changes along the series of barrier islands where it made landfall. Two of these islands remain largely uninhabited and have minimal human infrastructure. Namely, North Captiva Island (NCI) and Lovers Key (LK), with the study domains for these two islands shown in Fig. 3.1 B. Both islands have extensive vegetation coverage and experienced extreme morphological changes during the storm, thus making them suitable study areas for this research.

3.1. Lovers Key

Lovers Key (LK) is currently a State Park and is also a low-lying barrier island that is susceptible to morphological shifts. The island is well vegetated in the northern and southern ends however it lacks some vegetation in the middle of the island (Fig. 3.2 C). Efforts have been carried out by the government since Hurricane Charley to restore dunes and dune vegetation by means of nourishments and planting vegetation completed in 2014 (FDEP, 2005). During the storm, the closest recording hydrograph with wave data is the same as mentioned previously with wave height of up to 1.5 m. However, LK experienced much higher water levels compared to NCI as it was located closer to Ian's radius of maximum winds (RMW) (approximately 37 km at landfall) (Bucci et al., 2023). The recorded high water marks reached up to 3.47 m (USGS, 2023); well above the average crest height of 1.6m in LK. This resulted in extreme morphological changes, including breaches, and storm surge ebb channels (Fig 3.2 D). The area with the largest impact was the middle section by the beach with a breach with a width of 13 m at its narrowest section. In addition, the north of the island had numerous storm surge ebb channels and vegetation removal.

3.2. North Captiva Island

North Captiva Island (NCI) is a low-lying barrier island that is subject to morphological change caused by hurricanes and winter storms (Kelly & Jose, 2021). The island is characterized by a wide section in the north of the island with extensive vegetation coverage, and a thinner section in the south with reduced vegetation (Fig. 3.2 A.). The storm destroyed a lot of measuring devices but a hydrograph located approximately 22 km southeast recorded wave heights at the dune toe ranging between 1 and 1.5 m. The highest watermarks were measured at approximately 1.34 m above the NAVD88 datum (USGS, 2023). Given that the average ridge height relative to NAVD88 is 1.9 m for NCI, the combination of storm surge and wave heights resulted in a breach and several overwash fans all over the southern end of the island. The new breach was approximately 10 m wide and the overwash fans extended up to 175m horizontally (Fig. 3.2 B).

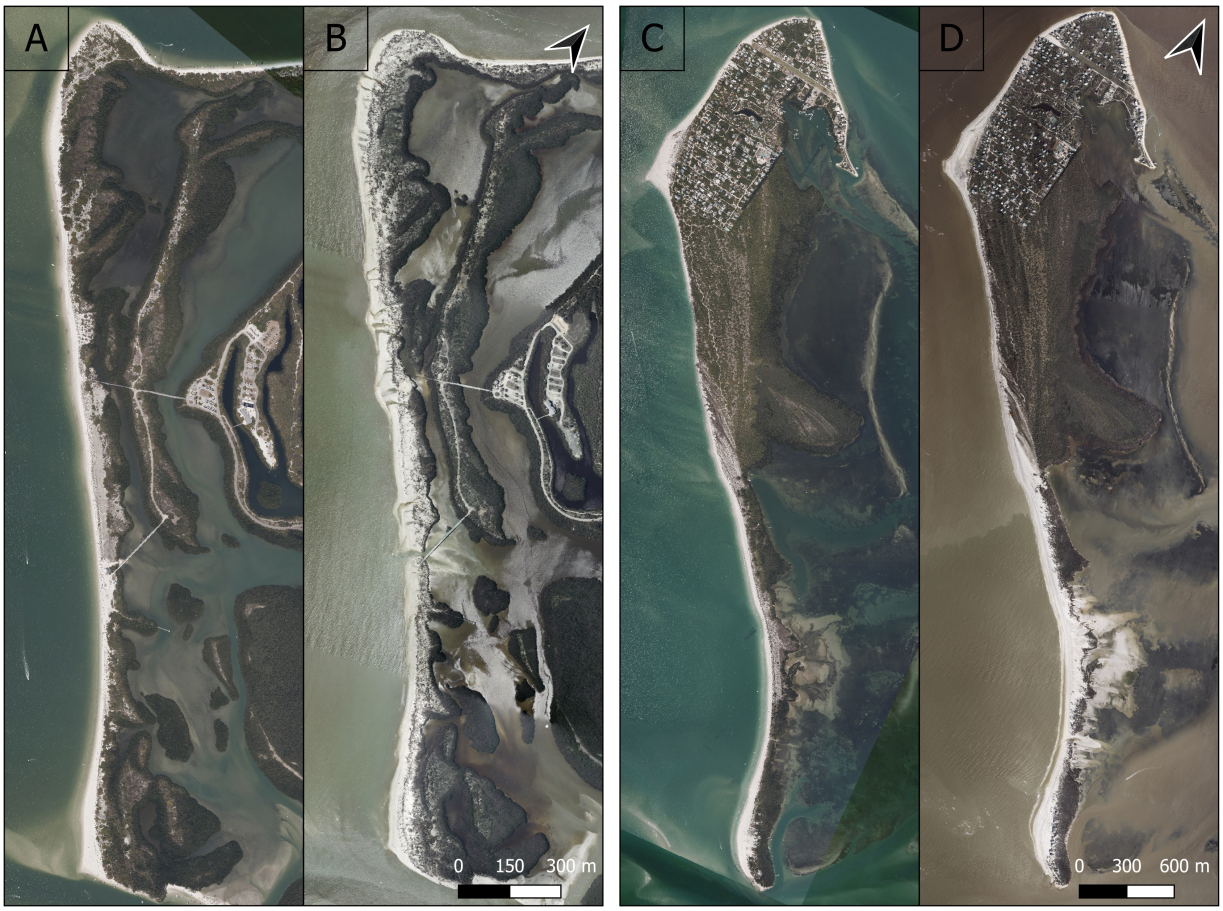

Figure 3.2: *2022 NOAA NGS pre and post-event high-resolution oblique RGB (0.3 m) for both LK and NCI. A) LK pre-storm, B) LK post-storm, C) NCI pre-storm and D) NCI post-storm.*

3.3. Data overview

Several measurement campaigns took place pre and post-Hurricane Ian, as well as during the storm. The data used for this research is listed below and Figures 3.3 and 3.4 display some of the data. Note that both islands have the same data sets except that LK is missing the pre-storm DSM.

Hydrodynamic data
The nearest water level and wave height measurements that recorded data during the storm and survived are from a pressure sensor located at the toe of a dune on-site FLLEE26290 in Sanibel island (USGS, 2023). In addition, a series of high water marks were recorded in the area at different locations, shown in Fig 4.5.

Topographic data
The topographic data sets include DEM and DSM collected pre and post-storm. The pre-storm data sets were collected by Light Detection and Ranging (LiDAR) in 2018 with a resolution of 0.5 m, the DSM (OCM-Partners, 2023c) is shown in Fig. 3.4B and the DEM (OCM-Partners, 2023b) are shown in Fig. 3.3A and 3.4A. Unfortunately, that is the latest high-resolution topographic survey conducted before Ian. Post-storm elevation data was collected Structure from Motion (SfM) technology to derive DSM data sets for both islands in 2022 (Fig.3.3C and 3.4D. Both the LiDAR and SfM data sets only include points above MHW.

Bathymetric data

The bathymetric data for the area is obtained from the Continuously Updated Digital Elevation Model (CUDEM) and it dates back to 2018 (NOAA, 2018). The data is shown in Fig. 3.5.

LULC data

Two main sources for LULC data are available for the two study areas. The first one is obtained from the National Land Cover Database (NLCD) 2019 product (Dewitz, 2021). This NLCD 2019 data set is derived from satellite imagery and has a resolution of 30 m. The second one is from the National Oceanographic Partnership Program (NOPP) 2019 and is a data set that fusions high-resolution LULC data with satellite imagery to achieve resolutions ranging from 1 to 30 m. This data set is displayed in Fig. 3.3B and 3.4C.

Aerial imagery

High-resolution RGB imagery collected by NOAA has been collected since 2006 and contains pre and post-storm data for multiple storms (NOAA, 2023). Including Hurricane Charley taken in 2006 (OCM-Partners, 2023a), Irma taken in 2017 pre-storm (NGS, 2023c) and post-storm (NGS, 2023b), and Ian taken in 2022 pre-storm (NGS, 2023a) and post-storm (NGS, 2023d). The aerial images for Ian are displayed in Fig. 3.2.

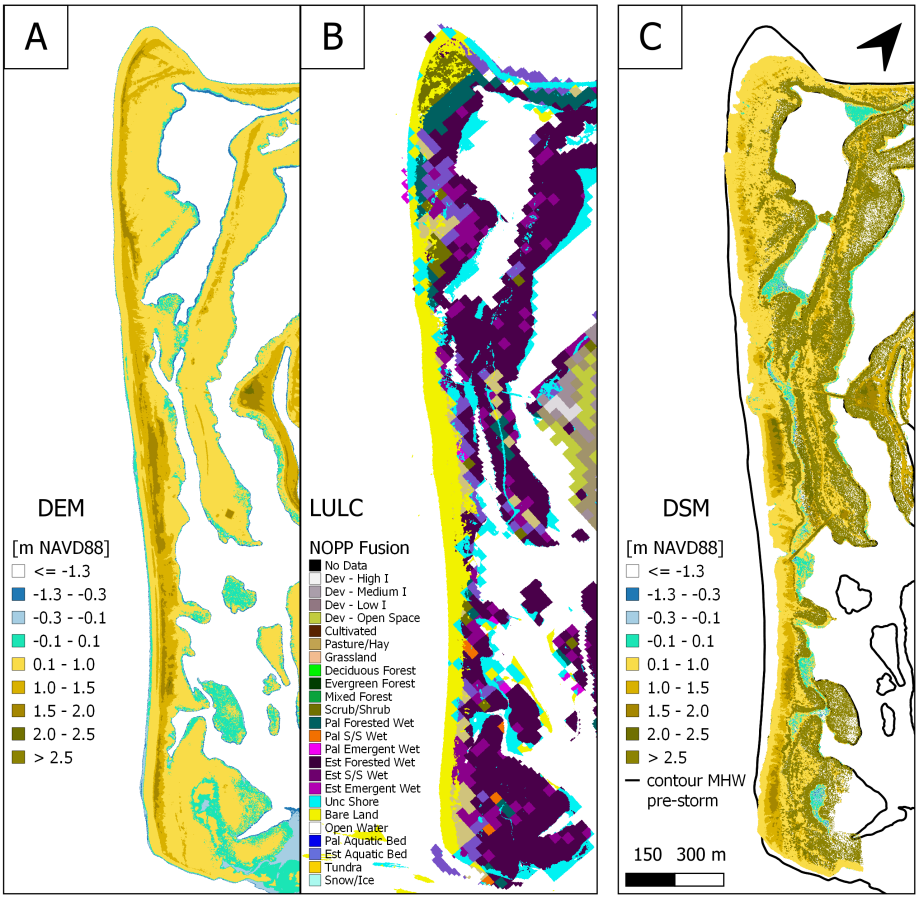

Figure 3.3: *Hurricane Ian data LK. A) LIDAR-derived DEM taken before the storm in 2018 (NOAA, 2023). B) LiDAR-derived DSM taken in 2018 (NOAA, 2023). C) LULC data from the USGS-NOPP fusion product with the latest data from 2019. D) Post-Hurricane Ian SfM DSM data taken in 2022, MHW contour is at 0.1 m NAVD88*

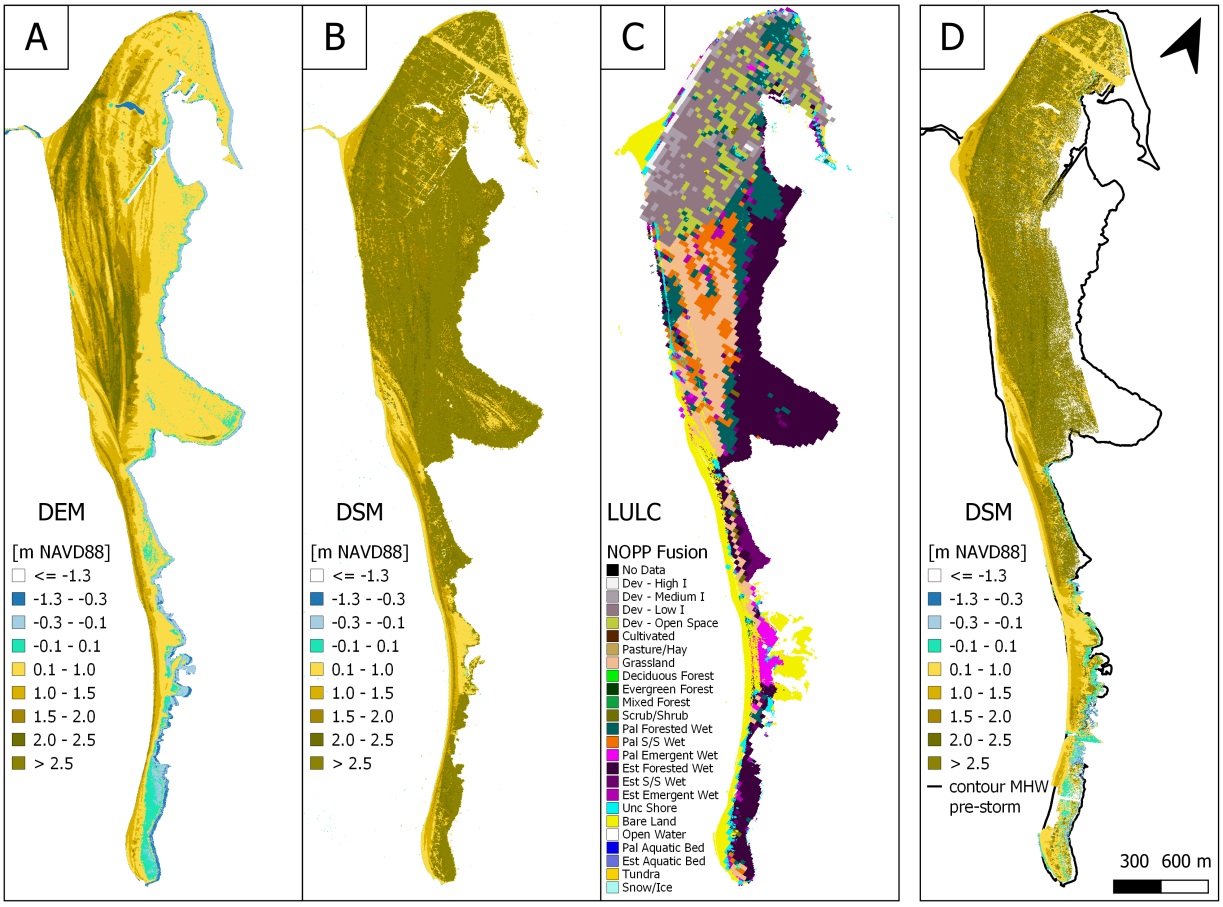

Figure 3.4: *Hurricane Ian data NCI. A) LIDAR-derived DEM taken before the storm in 2018 (NOAA, 2023). B) LiDAR-derived DSM taken in 2018 (NOAA, 2023). C) LULC data from the USGS-NOPP fusion project with the latest data from 2019. D) Post-Hurricane Ian SfM DSM data taken in 2022, MHW contour is at 0.1 m NAVD88*

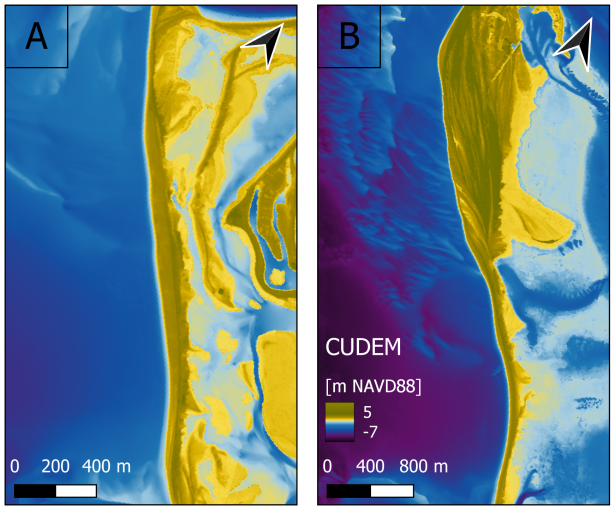

Figure 3.5: *CUDEM 2018 bathymetric data (NOAA, 2018) for both LK and NCI*

4

Data analysis

This chapter delves into the analysis of pre and post-Hurricane Ian data, aiming to assess the storm impact and understand the role of vegetation. The chapter is divided into two main sections. The first section outlines the methodologies employed to analyze the available data for Hurricane Ian, including aerial imagery, digital elevation models (DEM), digital surface models (DSM), and land use/land cover data (LULC). The subsequent section discusses the results of the data analysis and gauges the impact of the storm. The focus is on the morphological changes that took place and the influence of vegetation in the erosional processes for both Lovers Key (LK) and North Captiva Island (NCI).

4.1. Methodology

To analyze Hurricane Ian's data, first, the data is post-processed to obtain dune characteristics, geomorphic features, and erosion/sedimentation volumes. Secondly, vegetation data is derived from DSM, DEM and LULC data to obtain vegetation maps that exclude anthropogenic features and classify vegetation based on height and type. Finally, a method is developed to determine if the island remains in a collision regime or went into a flooding regime based solely on pre and post-storm topography.

4.1.1. DSM to DEM

The first data post-processing step is to convert the post-storm DSM into a DEM. These data sets are common geospatial products that can be derived from measurements taken by aerial vehicles with Laser imaging Detection And Ranging (LiDAR) or Structure from Motion (SfM) technologies. These technologies result in point cloud data that can be subsequently interpolated into a DSM or DEM. If all point cloud data is interpolated, the result is a DSM, which is a height map that includes bare earth points and vegetation and structure heights. While DEMs are elevation maps that only include ground points. These maps are particularly useful to estimate erosion or assess morphological changes after a storm.

The post-storm data from Hurricane Ian was collected with SfM cameras and posteriorly converted into a DSM. To be able to use the post-storm data for analysis and model calibration/validation, the DSM was converted to a DEM. For this, the tool Remove Off-terrain Objects (ROTO) developed by Lindsay, 2018 was used. This tool removes off-terrain objects from high-resolution DSM based on slope threshold and kernel size. This algorithm works particularly well for areas with small slope variability which was the case for both islands.

Figure 4.1 shows the results of applying the ROTO tool on the DSM derived from SfM. The tool successfully removed vegetation and urban features. However, the tool struggles to convert the DSM data into ground points in some areas around the urbanised zone and no-data pixels. Higher elevation points relative to the surroundings can still be observed in those areas of the DSM (black arrows in Fig 4.1. These areas also coincide with densely vegetated or urbanized zones where almost no bare ground sections are visible. Overall, this method successfully removes vegetation and urban features for low to medium-density areas and careful assessment of dense areas needs to be conducted. Unfortunately, there is insufficient data to validate the accuracy of vegetation removal. This is particularly an issue for the northern end of NCI.

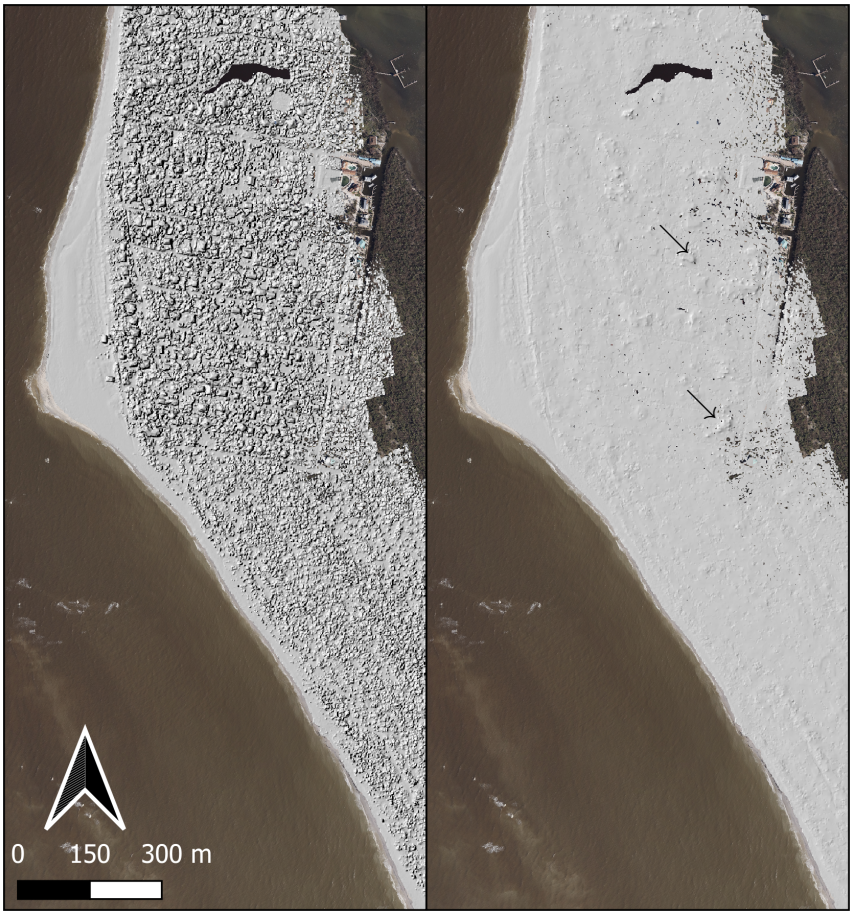

Figure 4.1: *Northern NCI: The left panel displays the DSM hillshade derived from the SfM data. The right panel shows the DEM hillshade after applying the ROTO tool (Lindsay, 2018) to remove off-terrain objects. The black arrows point out some areas in which the tool did not work as well.*

4.1.2. Dune characteristics

To determine the dune characteristics, the elevation data from pre-storm DEM is analyzed. The first step is to determine the dune crest location. For this, Stockdon et al., 2009 definition is used, which means the dune crest will be the maximum elevation point within a user-defined beach. The user-defined beach for the two barrier islands was defined as any natural area between the coastline and any anthropogenic infrastructure (Doyle & Woodroffe, 2018) or the bay side on the opposite side of the island. For the wider area in NCI, the dune was determined to be within the first 200 m of the beach.

With the beach area defined, perpendicular transects to the coast are placed at 5 m intervals to extract dune characteristics, geomorphic characteristics and vegetation data along each transect. To establish the dune toe and hill locations along the beach transects, the relative relief method by (Wernette et al., 2016) is used. The relative relief represents the variation in height between a morphological feature to its surroundings and is calculated using Equation 4.1. Where RR_c is the relative relief at the centre of the window, z_c is the elevation at the centre of the window, z_{max} is the maximum elevation within the window, z_{min} is the minimum elevation within the window, a is the vertical distance between the centre of the window and z_{min}, and R is the elevation range within a window. The window size is important to determine the amount of topographic features that want to be captured to determine the relative relief (see Fig. 4.2).

$$RR_c = \frac{z_c - z_{min}}{z_{max} - z_{min}} = \frac{a}{R} \tag{4.1}$$

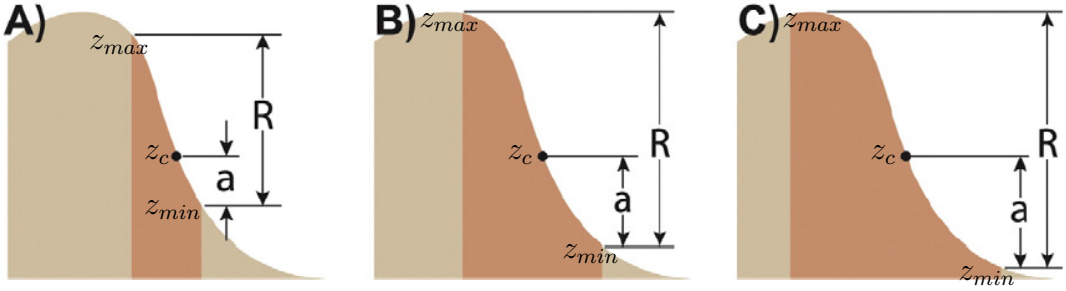

Figure 4.2: *Relative relief based on different window sizes selected, taken from (Wernette et al., 2016). Where RR_c is the relative relief at the centre of the window, z_c is the elevation at the centre of the window, z_{max} is the maximum elevation within the window, z_{min} is the minimum elevation within the window, a is the vertical distance between the centre of the window and z_{min}, and R is the elevation range within a window.*

Dune crest D_{crest}

The dune crest is selected as the maximum elevation point along each transect. The dune crests are uniformly distributed alongshore, except for areas that have local depressions such as the area that breached in LK and NCI (See Fig. 4.8). The locations of the dune crests are important as they will help determine the locations of the dune toe, dune hill, geomorphic features, and the sections of the beach that remained in a collision or flooded regime.

Dune toe D_{toe}

The dune toe was determined using the relative relief method described by Wernette et al., 2016. In their paper, the dune toe location was determined with a window size ranging between 21 and 25 m and as the first landward point located above 0.2 m above mean sea level that has a RR_c lower than 0.2. They selected this value as the dune toe is likely to be located within the lower 20^{th} percentile of the topography (see Fig. 4.3). However, they note that these values must be selected based on local knowledge of the morphology and water levels.

For LK and NCI the dune toe would be located between any elevation above MHW which is approximately 0.1 m above NAVD88 and below the dune crest elevation. To calculate the relative relief several window sizes were tested and a final one of 20 m was selected by assessing the location of the toe with respect to the pre-storm DEM as shown in Fig. 4.8. Similarly to Wernette et al., 2016, the dune toe was chosen as the first point that crossed the threshold of $RR_c = 0.2$.

Dune hill D_{hill}
Similarly to the dune toe, the dune hill was determined using the methods described by Wernette et al., 2016. The only difference is the window size selected, the RR_c threshold and that the hill is located landward of the crest. A wider window size was selected to account for the greater topographic variability landward of the crest. Multiple window sizes were tested again, however, this ranged between 20 and 40 m. With a final 30 m window size selected as the best-performing window for the local topography. The RR_c threshold was increased to the 40^{th} percentile as dune the dune hill is also a topographic low (Wernette et al., 2016). However, it can be located in a wider range of the lower topography compared to the toe, Fig. 4.3.

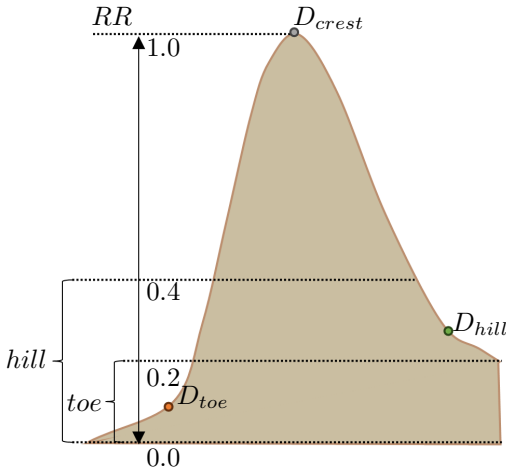

Figure 4.3: *Relative relief for dune crest, hill and toe. This conceptual figure shows the relative relief ranges in which the dune hill and toe are likely located based on the relative relief (Wernette et al., 2016).*

4.1.3. Dune geomorphic features

With the dune crest, toe and hill locations determined for the dune, it is now possible to derive geomorphic features. These features can be analyzed to determine their alongshore effect on erosion processes when compared to other dune characteristics such as vegetation (Doyle & Woodroffe, 2018). The dune slope Φ is calculated by taking the slope between the dune crest and dune toe locations as shown in Chapter Fig. 2.1. The dune height H for this study is defined as the vertical distance between the dune crest and the dune toe (Fig. 2.1). Dune width W is established as the horizontal distance between the dune toe and the dune hill locations (Fig. 2.1). The dune aspect ratio is defined as the dune height over the dune width. The dune aspect ratio is a useful dimensionless parameter that can be used for analyzing the effects of morphometric variables as it is correlated to the dune height, dune width and dune slope (Itzkin et al., 2021).

4.1.4. Dune erosion

Dune erosion volumes are calculated from the pre and post-storm DEM data. This is done for each cross-shore profile for which dune characteristics and geomorphic features are derived. Each profile averages the elevation data over 5 m alongshore intervals. The erosion or sedimentation volumes were obtained by subtracting the pre-storm profile from the post-storm profile. For which positive values correspond to sedimentation volumes and negative values to eroded volumes. Note that all erosion/sedimentation calculations were done for areas located above MHW, as the

LiDAR and SfM do not include elevation points below the water line. Therefore, net erosion is expected as a closed sediment transport balance is not possible.

4.1.5. Dune vegetation

To assess the influence of vegetation during the storm, dune vegetation data can be extracted from the pre-storm DEM, DSM and LULC data. Different vegetation parameters can be derived from these data sets, including the spatial distribution of vegetation, vegetation height, vegetation types, and coverage per area. For this study, vegetation variables were extracted along the same cross-shore transects used for geomorphic features by averaging vegetation data over a width of 5 m. This ensured enough vegetation data was represented in each transect as done by Doyle and Woodroffe, 2018.

Canopy Height Models (CHM)
Vegetation data can be extracted from DSM's and DEM's by calculating Canopy Height Models (CHM). These can be simply calculated by using equation 4.2. This results in a map that contains the height of any non-ground points measured in a DSM, including both vegetation and urban structures. The spatial distribution of vegetation and its height can be determined from a CHM. Given the available data, it was only possible to compute a CHM for NCI, shown in Fig. 4.4A.

$$CHM = DSM - DEM \tag{4.2}$$

Vegetation spatial distribution
The spatial distribution of vegetation is first derived from LULC data by removing all the no vegetation classes (Table 4.1) from the data set. Once all urban structures are removed, this data set can be combined with a CHM to achieve a higher-resolution vegetation map. This is shown in Fig. 4.4B, where all the urban features are removed and only vegetation data remains in NCI. It was not possible to derive a combined LULC-CHM vegetation map for LK as no pre-storm DSM was available, therefore, only the LULC data was used for that location in this analysis.

NOPP class name	New classification
Unconsolidated Shore, Bare land, Open water, Palustrine and Estuarine Aquatic Bed, Developed all intensities	No vegetation
Cultivated Crops, Pasture/Hay, Grassland/Herbaceous, Palustrine and Estuarine Emergent Wetland	Low vegetation
Scrub/Shrub, Palustrine and Estuarine Scrub/Shrub Wetland	Medium vegetation
Palustrine and Estuarine Forested Wetland	High vegetation

Table 4.1: *Classification of vegetation types*

Vegetation type

The vegetation types are derived directly from the different LULC classes. There is a total of 10 different vegetation types present in the two barrier islands. To simplify the analysis, the vegetation classes were divided into no vegetation, low vegetation, medium vegetation and high vegetation. Table 4.1 summarizes the new classification compared to the NOPP class names and the resulting vegetation map is displayed in Fig. 4.4B. Note that this classification is different to the one used in Chapter 5, Table 5.3. The difference is medium and high vegetation are combined in Chapter 5. Once the vegetation data was reclassified, the vegetation type per transect was determined by taking the dominant vegetation type per transect or no vegetation in cases where the transect was unvegetated.

Vegetation coverage

The vegetation coverage was determined by calculating the percentage of cells that have vegetation data located between the dune toe and the dune hill. Given that these islands went into an overwash regime it is important to consider the vegetation in front of the dune crest as well as in the back of the dune crest. When islands go into overwash or inundation, sediment transport in the back side of the dune increases and therefore vegetation in the back of the dune should be taken into account for this analysis.

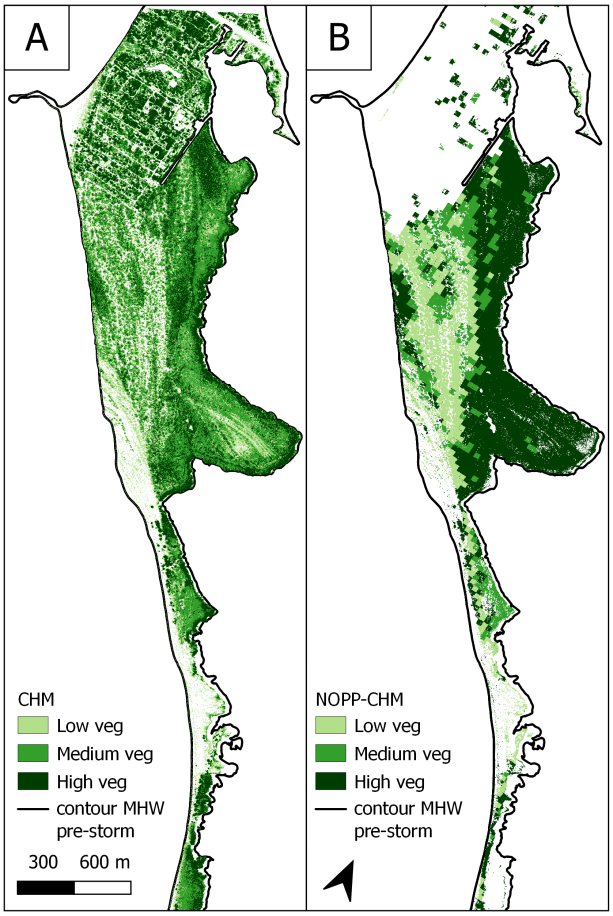

Figure 4.4: *NCI vegetation maps. A) Canopy Height Map (CHM) derived from DEM and DSM. Note that urban features are still included in this map. Particularly in the northern end of the island. B) Vegetation map obtained by combining CHM with LULC data to remove urban features and classified based on vegetation types (Table 4.1).*

4.1.6. Storm regimes

The Sallenger, 2000 storm regimes are useful for classifying the level of destruction caused by a storm in coastal dune environments. However, to determine these regimes, hydrodynamic conditions are necessary as described in Chapter 2. This type of data was not recorded during the storm. To determine the level of impact of the storm a new method was developed to derive storm regimes from pre and post-storm elevation data and high water marks (HWM) data collected after the Hurricane. Given the lack of hydrodynamic data, it is only possible to determine the storm impact in terms of the Sallenger storm regimes by combining overwash and inundation into a flood regime and the no-flood regime consisting of the collision regime.

High water marks (HWM)

As mentioned in Chapter 3, HWM measurements were taken along the coastline that suffered the most extensive impact during Ian. Figure 4.5, shows the locations and measurements of the HWM closest to the two barrier islands chosen for this study. To obtain the maximum water levels along the two barrier islands, linear interpolation was conducted between the two closest measurements taken near the barrier islands. These values are subsequently used to determine the storm regime experienced at each island as discussed in the following subsections.

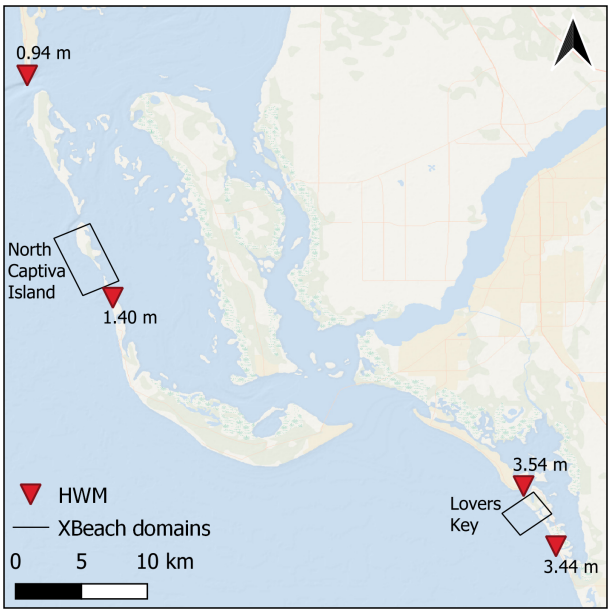

Figure 4.5: *High water marks (HWM) locations and measured values relative to NAVD88. The HWM shown are the closest measurements to both islands. For reference, the two XBeach domains in this study are shown.*

Flood regime

The flood regime consists of both the overwash and inundation regimes. To determine this regime, first, the alongshore dune crest locations need to be identified. Then the pre and post-storm elevation at those locations is determined. If the pre-storm bed level at that location is below the HWM, then that section of the island went into flood regime. If that is not the case, but the post-storm elevation along the crest is lower than the pre-storm bed level, it also means that the location is flooded.

Collision regime

The collision regime is whenever the pre-storm dune crest is higher than the HWM and the post-storm dune crest elevation remains the same as the pre-storm dune elevation.

Figure 4.6 outlines the algorithm used to determine the flood and collision storm regimes. Where HWM is the high water mark, z_{c0} is the initial dune crest elevation, and z_{cf} is the post-storm elevation at the same location as the pre-storm dune crest.

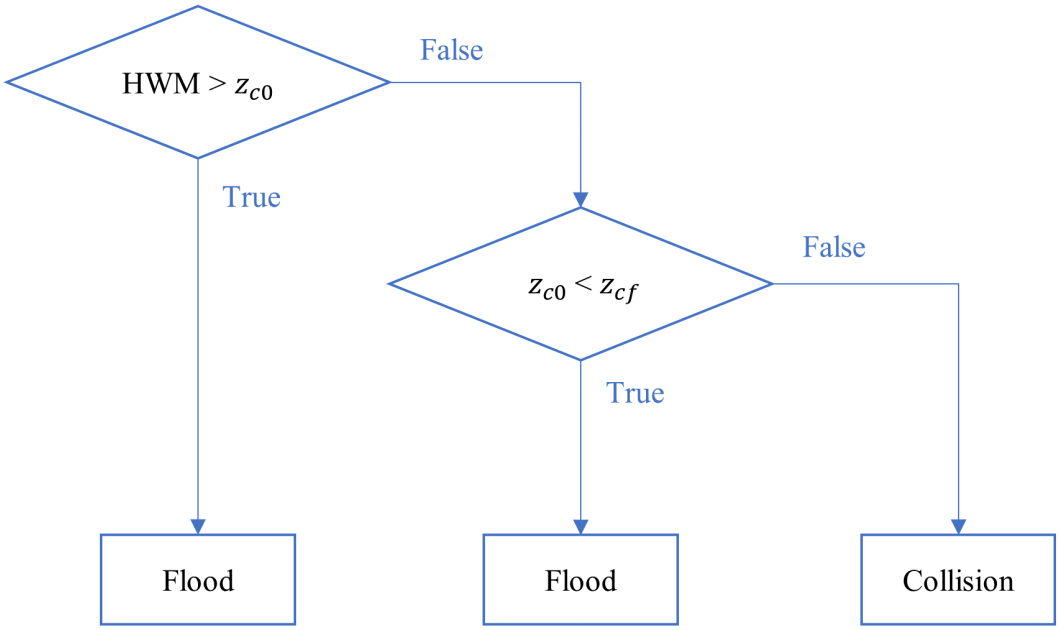

Figure 4.6: *Storm regimes algorithm with simple if statements to determine flood and collision storm regimes.*

4.2. Results: Data analysis

Current literature on the effects of dune vegetation in erosional processes during storms is based on several flume experiments and limited field observations. This section further investigates the role of vegetation in dune erosion by analyzing the processed data from Hurricane Ian. First, historical aerial images are analyzed to determine if vegetation played a role in areas with major morphodynamic change. Then storm regimes are determined along the shores of LK and NCI to assess the storm impact on both islands. Finally, dune characteristics and geomorphic features are compared against vegetation characteristics and dune erosion/sedimentation volumes.

4.2.1. Historical hurricanes

The region of Cape Coral has been impacted by three major Hurricanes since the start of the century. Namely, Hurricane Charley 2004 (Cat-4), Irma 2017 (Cat-3) and Ian 2022 (Cat-4). These storms were selected based on a 50 km radius from Cape Coral; which is consistent with the average radius of maximum winds for Hurricanes (Hsu & Yan, 1998). High-resolution aerial imagery taken by the NOAA National Geodetic Survey (NGS) provides sufficient resolution to observe vegetation and storm erosional impact at different scales. This imagery is analyzed to identify potential trends that led to breaches in the region. Focusing on the areas that were breached during Ian for both LK and NCI.

Lovers Key breach 2022
Row A in Fig. 4.7 shows the area that was breached during Hurricane Ian in LK. The first image A1, shows the impact Charley had, which removed vegetation almost entirely. To aid the recovery of the island after Charley, a management plan was put in place in 2005 that included dune and vegetation restoration (FDEP, 2005). The nourishments and vegetation planting were completed by 2014 and planted sections of vegetation can be observed in image A2. An unvegetated path remained (red arrows) in the area that resulted in an overwash fan during Irma and subsequently breached during Ian. This unvegetated path coincides with a local topographic depression along the dune crest. The LK breach was 15 m wide at its narrowest point and a series of storm surge ebb channels formed at the northern end of the island. Large extents of vegetation were removed, but vegetation close to the bay side showed greater resiliency.

North Captiva Island breach 2022
Row B in Fig 4.7 shows the area that was breached during Ian in NCI. At that location, Charley caused a large overwash fan extending 145 m and all vegetation was removed along the fan. While the rest of the island showed impressive vegetation recovery, the location of the breach remained with an unvegetated path (red arrow image B2). This unvegetated path remained there until Hurricane Ian and aligned with a local dune depression. The breach during Ian occurred at this exact location and it was 7 m wide at its narrowest point with an overwash fan extending approximately 180 m.

North Captiva Island breach 2004
Row C in Fig 4.7 shows the area that was breached during Charley in NCI. This breach was significantly larger than the ones caused during Ian. However, the area showed impressive recovery over the next decade, vegetation recovered and the island width increased locally thanks to the post-Charley morphological changes. This area had minimal effects during Irma and experienced large overwash fans during Ian. However, it did not breach again.

The observed impacts of the storm suggest that erosional channels tend to form along existing unvegetated paths, while this may be coincidental for these two islands and Hurricane Ian, it has also been observed along beach access points in other areas during this storm and other hurricanes. Hindrance of vegetation growth along ”paths” caused naturally or by humans combined with local land depressions may result in local weak points that lead to breaching. In addition, the vegetation at the sides of the path has the potential to further drive local erosion along the unvegetated path.

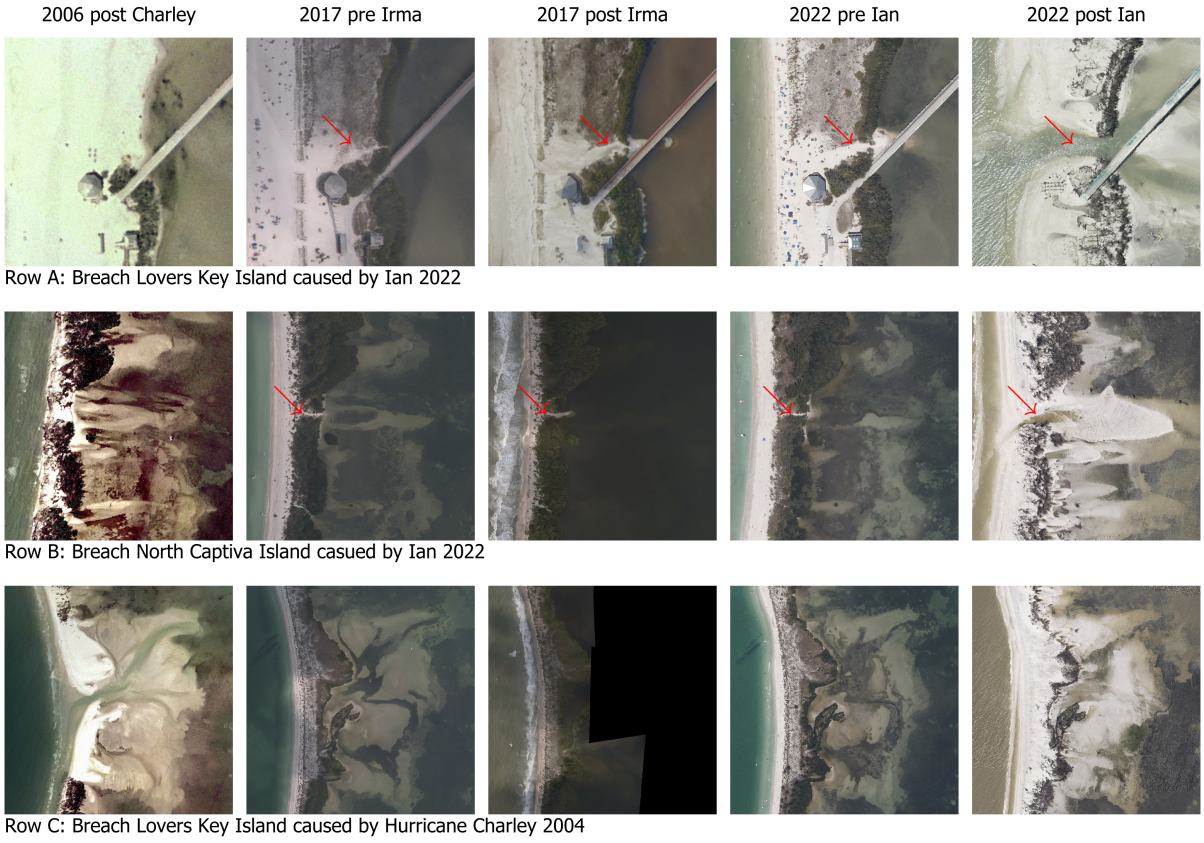

Figure 4.7: *Row A: location of LK Ian breach, Row B: location of NCI Ian breach, Row C: location of NCI Charley breach. From left to right, high-resolution aerial images(NOAA, 2023) showing pre and post-storm erosion for the three hurricanes that hit the Cape Coral area since the 2000s.*

4.2.2. Storm regimes

To calculate the regimes, the method described in Section 4.1.6 was used. Once the dune crest locations were identified along each cross-shore profile the regimes were determined. In Fig. 4.8 the flooded regimes are shown at the locations of the crest with the cyan colour and the collision regimes are shown at the crest location in black. The HWM for LK were higher in elevation for all transects than the maximum dune crest elevation, as a result, the whole island went into the flood regime. That was not the case for NCI, where most dune crest elevations were above the HWM. Nevertheless, significant erosion took place in the southern end of the island. This resulted in most of the southern island going into flood regimes, which accounts for 55% of the island. The northern end, particularly after the 2.5 alongshore km remains in the collision regime. This area, on average had higher dune crests and more vegetation cover.

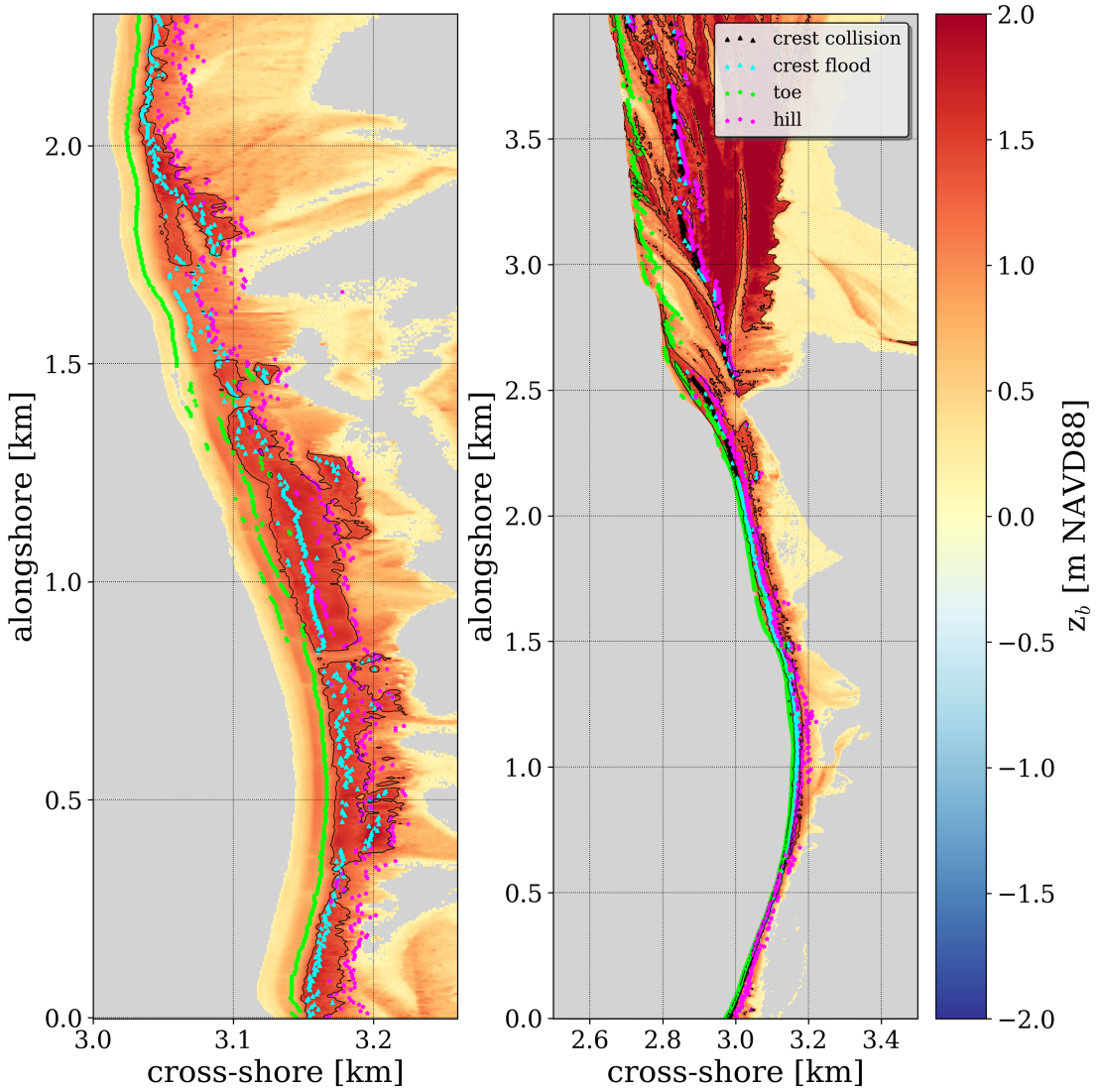

Figure 4.8: *Pre-storm topography for LK (left panel) and NCI (right panel), with dune crest, toe and hill locations are shown. The crest collision (black) represents transects that remained in the collision regime, and the crest flood (cyan) shows transects that experienced floods.*

4.2.3. Dune geomorphic features, erosion/sedimentation and vegetation

The dune toe, crest and hill locations were determined as described in Section 4.1 and the results are shown in Fig. 4.8. The respective locations of the toe, crest and hill align nicely throughout both islands with the areas of maximum change in slope for the toe and hill, and with the highest elevated points for the crest. Particularly for LK, the distribution of the toe, crest and hill follow very similar patterns in the alongshore direction, except for the areas with more complex topography, which occur around low-lying areas. There is a significant difference between the southern end of NCI and the northern end. The south end has a much narrower beach, resulting in dunes with low width and the northern end has a much larger width and higher dunes with their crests located further in land.

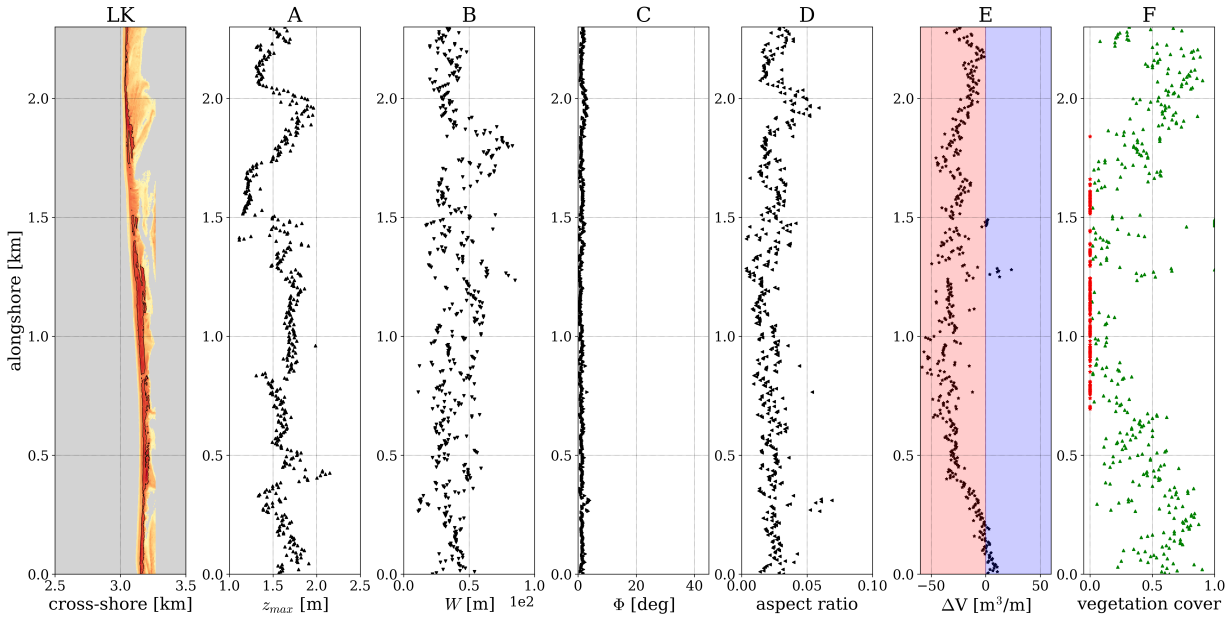

Figure 4.9: *LK alongshore geomorphic features, erosion and vegetation cover per 5 m transect. From left to right: pre-storm topography LK, A) alongshore dune crest z_{crest}, B) alongshore dune width W, C) alongshore dune slope Φ, D) alongshore dune aspect ratio, E) along shore eroded/deposited volumes ΔV (red eroded and blue deposited), and F) alongshore dune vegetation cover (red no vegetation in the transect, green vegetated transect).*

Dune height H

The dune heights for LK are on average 40 cm lower than the dune heights in NCI. However, the maximum crest for NCI is 1 m higher than the crest at LK. With the max for LK being 2.1 m and for NCI 3.1 m. When looking at the alongshore crest variability for LK in Fig. 4.9A, it is mostly uniform except for a low-lying area around the 1.5 km mark. In comparison, there is a more drastic difference in the alongshore dune height variability for NCI. The northern end of NCI has much larger dune heights compared to the southern end as shown in Fig. 4.10A. This change occurs near the 2.5 km alongshore, and the dune heights in the northern end are on average 60 cm higher. To summarize, the dune heights in LK are on average 1.6 m and are comparable to the NCI southern end dune heights which are on average 1.7 m. However, the northern end of NCI has higher dune heights, with an average of 2.3 m.

Dune width W

The dune widths for LK vary alongshore between 25 and 60 m and are on average 40 m wide (Fig. 4.9B. In comparison, the average dune width for NCI is 66 m. However, similarly to the dune height, the northern end and southern end of the island are different. The dune widths in the south are on average 26 m and in the north 133 m. The northern end can be easily differentiated from the south along the 2.5 km mark (see Fig. 4.10B).

Dune slope Φ

Both LK and NCI are low-lying barrier islands, which result in alongshore uniform mild slopes with means around 2 degrees. A slight difference can be observed between the north and south of NCI, with steeper slopes at the southern end (see Fig. 4.9C and 4.10C).

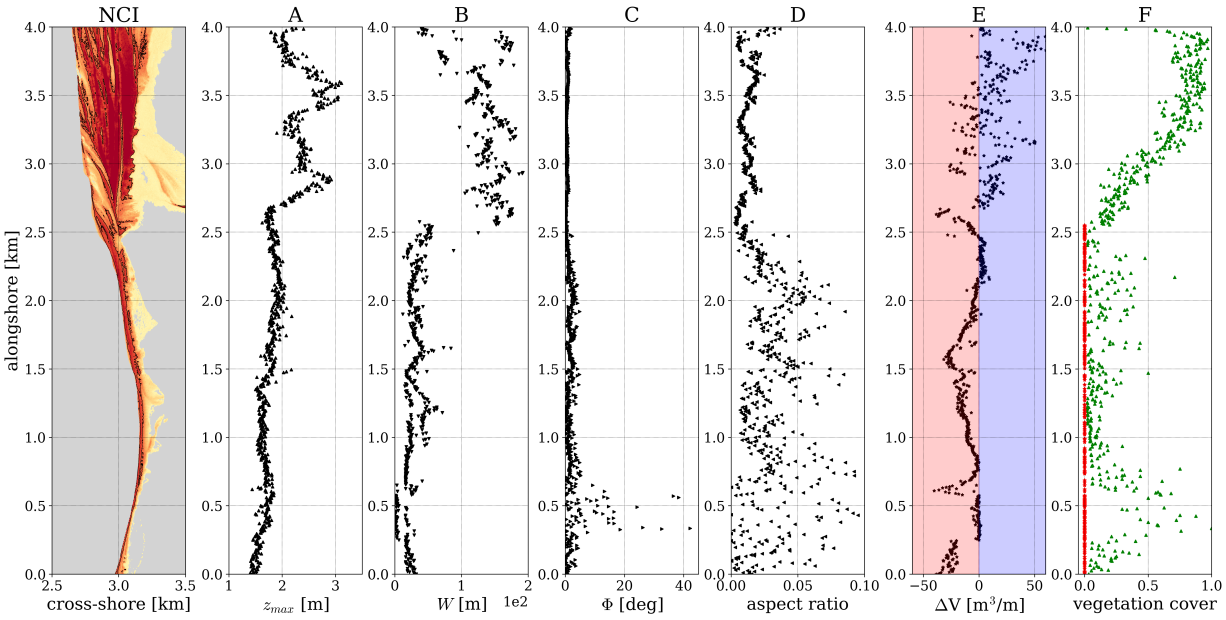

Figure 4.10: *NCI alongshore geomorphic features, erosion and vegetation cover per 5 m transect. From left to right: pre-storm topography LK, A) alongshore dune crest z_{crest}, B) alongshore dune width W, C) alongshore dune slope Φ, D) alongshore dune aspect ratio, E) along shore eroded/deposited volumes ΔV (red eroded and blue deposited), and F) alongshore dune vegetation cover (red no vegetation in the transect, green vegetated transect).*

Dune aspect ratio

Both islands have low dune aspect ratios as the dunes are much wider than they are higher. LK is alongshore uniform and in the case of NCI, the south has much larger dune aspect ratios compared to the northern end (see Fig. 4.9D and 4.10D).

Dune erosion/sedimentation volumes ΔV

LK experienced much larger erosion volumes per transect compared to NCI and had almost no sedimentation above MHW. The island averaged 23 m^3/m of erosion, with the largest sediment losses occurring in the middle section of the island (see Fig. 4.9E). The maximum erosion volume was 71 m^3/m and aligns nicely with the area that breached. Similarly to the geomorphic features, NCI island has a clear distinction between the north and south (Fig. 4.10E). Most of the southern end experiences erosion, while the north has higher deposited volumes. On average the south averaged 10 m^3/m of erosion and the north averaged 8 m^3/m of deposition. The maximum eroded volume was 40 m^3/m, and just like in LK, this value aligns with the area of the NCI breach.

Vegetation cover

The alongshore variability in vegetation coverage for LK can be observed in Fig. 4.9F. The northern and southern ends have significantly more vegetation coverage compared to the middle section of the island. The middle section has many transects without vegetation and the ones that do have much less vegetation. In NCI, the vegetation coverage also differs for the northern end and southern end just like the geomorphic features (Fig. 4.10F). The northern end is entirely vegetated and has much more coverage than the southern end. The southern end consists of many unvegetated transects and much lower vegetation density.

4.2.4. Vegetation effects in dune erosion

To determine if vegetation played a significant role in erosion volumes and storm regimes during Hurricane Ian, the vegetation coverage and vegetation types are compared against the erosion volumes and storm regimes that occurred during the storm. The erosion volumes are also compared with important geomorphic features such as the dune aspect ratio, dune height and dun width. This is done to determine if the erosion volumes are correlated to vegetation or the dune geomorphic features. The results for both islands are discussed in the following subsections.

Lovers Key

The vegetation cover in LK is much higher in the northern and southern end, with little to no vegetation along the middle section of the island. During the storm, LK experiences predominantly dune erosion as the entire island goes into the flood regime. When comparing the dune erosion volumes along each transect to the vegetation cover a clear trend is visible (see Fig. 4.11 left panel). Higher erosion volumes are found in areas with little to no vegetation. In contrast, the densely vegetated areas have less erosion and experience sedimentation in some transects. This can also be observed in Fig. 4.9E and 4.9F, where the areas with no vegetation align with the higher erosion volumes. The geomorphic features at LK are mostly alongshore uniform. Fig. 4.12, shows that higher eroded volumes are present in areas with low vegetation cover, and that dune geomorphic features have little influence over the eroded volumes. This reinforces the link that low vegetation cover results in higher erosion volumes during Hurricane Ian in LK.

When studying the different vegetation types on the island in Fig. 4.11 right panel it is clear that the different types of vegetation are well distributed along the island. In the case of LK, as the whole island goes into a flood regime, it is not possible to recognize if vegetation played a role in the storm regimes experienced along the island. It is also not possible to discern if vegetation types had a significant role in erosion levels as all the different types of vegetation also show high

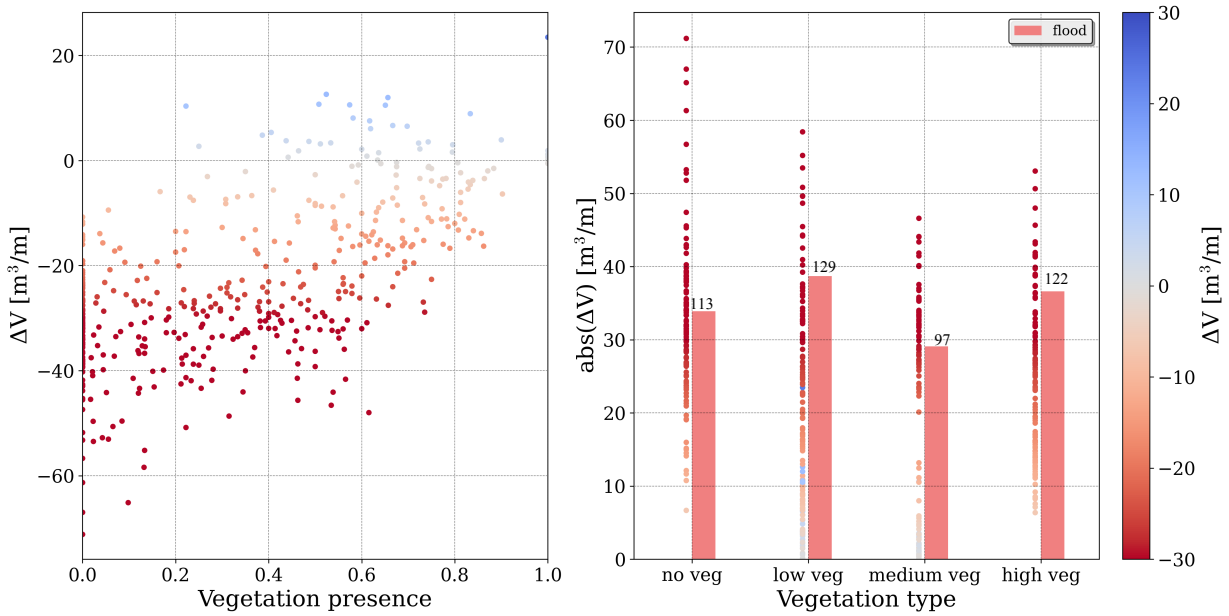

Figure 4.11: *LK eroded/deposited volumes and storm regimes vs vegetation. The left panel scatter plot compares the eroded/deposited volumes ΔV per transect to the vegetation cover per transect (eroded in red, deposited in blue). The right panel compares the dominant vegetation type distribution per transect to the absolute eroded/deposited volumes and storm regime experienced in LK. Note that LK experienced floods everywhere.*

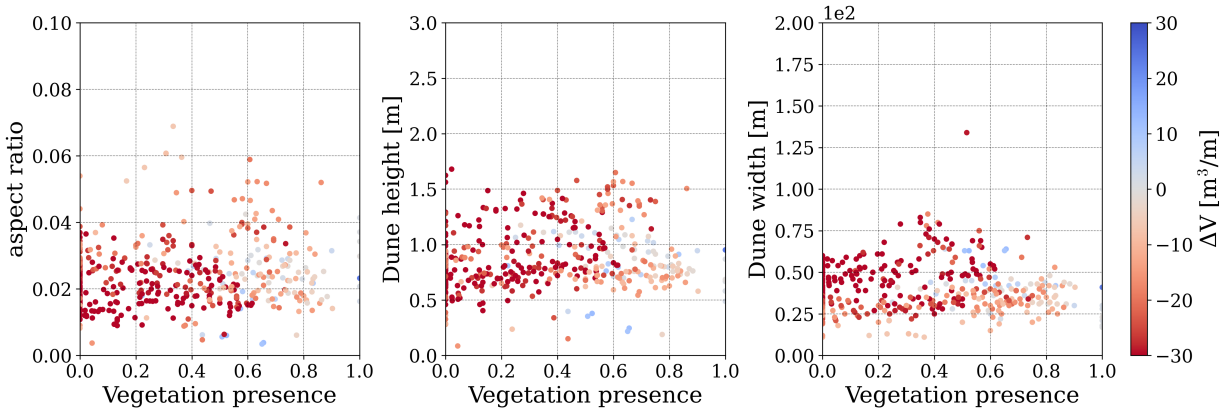

Figure 4.12: *LK dune geomorphic characteristics vs eroded/deposited volumes vs vegetation. From left to right: the dune aspect ratio, dune height H, and dune width W are compared to volume changes and vegetation cover.*

erosion volumes in the right panel of Fig. 4.11. To summarize, the data collected at LK indicates that higher vegetation coverage is correlated to lower erosion volumes and higher sedimentation. Other variables such as vegetation type and geomorphic features do not appear to play a significant role in dune erosion volumes.

North Captiva Island

The erosional impact of Hurricane Ian in NCI was different than what occurred in LK. This is likely due to a combination of their different types of vegetation cover, geomorphic features and the much lower water levels experienced during the storm. The left panel of Fig. 4.13 compares the dune erosion and sedimentation volumes to the vegetation cover along each transect. The results are similar to the ones observed for LK, in which higher vegetation presence is correlated to lower erosion volumes and higher deposited volumes. However, unlike in LK, the geomorphic features are also correlated to changes in dune erosion volumes in NCI. This can be observed in Fig. 4.14, where the higher dunes and wider dunes have much higher sedimentation and lower erosion volumes. A similar result is also visible in Fig. 4.10, where the higher and wider dunes located at the northern end of the island have much more vegetation coverage and lower erosion volumes. In contrast, the southern end of the island has much lower and narrower dunes, with less vegetation coverage and higher erosion volumes. During the processing of the data, the conversion of DSM to DEM could have some errors in the estimation of ground points. These errors are likely in densely vegetated areas which coincide with these sedimentation points.

NCI island experienced both the collision and flood regimes. With the northern end of the island experiencing mostly collision and the southern end flood regime. These regimes are compared against different vegetation types in the right panel of Fig. 4.13. The results mainly show that transects with no vegetation experienced flood regimes almost three times as much as they did the collision regime in the case of NCI. In the case of vegetated transects, regardless of the vegetation height, this difference is not as extreme between the different storm regimes. It is also visible from the scatter plot within the same figure, that the unvegetated transects experienced higher erosion volumes than the vegetated transects. Nevertheless, different vegetation heights do not seem to play a significant role in terms of the eroded or deposited volumes.

The data at LK and NCI island indicate a strong relationship between vegetation coverage per transect and eroded volumes. However, for NCI, this also coincides with higher and wider dunes in the areas that have the most vegetation cover. Therefore, both geomorphic features and vegetation cover played an important role in the dune resilience of NCI.

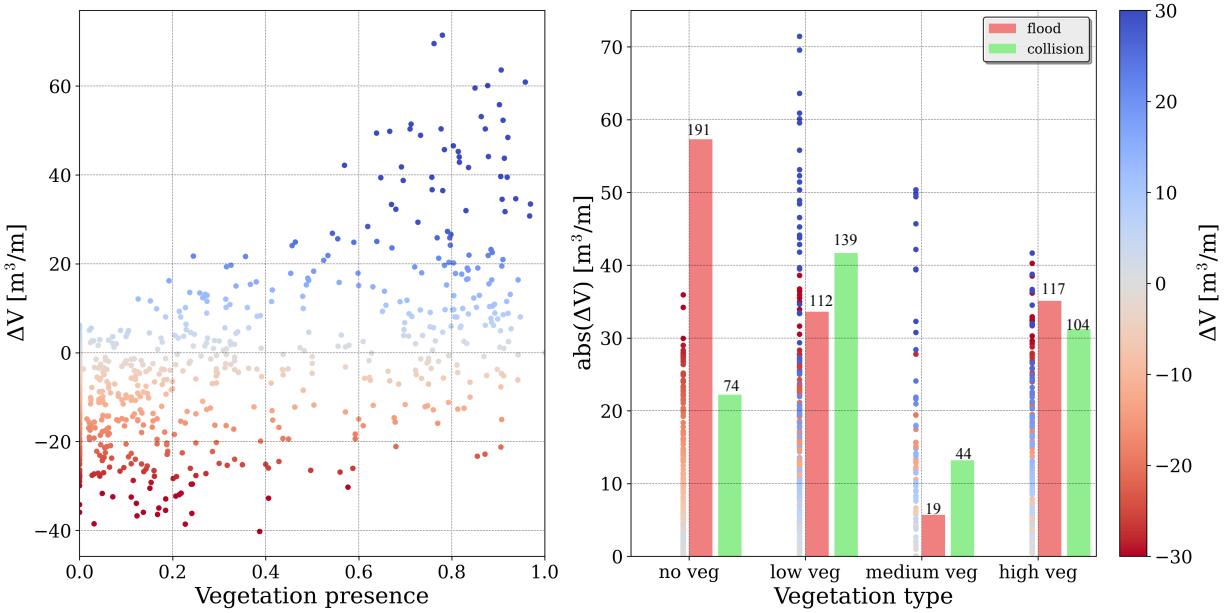

Figure 4.13: *NCI eroded/deposited volumes and storm regimes vs vegetation. The left panel scatter plot compares the eroded/deposited volumes ΔV per transect to the vegetation cover per transect (eroded in red, deposited in blue). The right panel compares the dominant vegetation type distribution per transect to the absolute eroded/deposited volumes and storm regime experienced in NCI.*

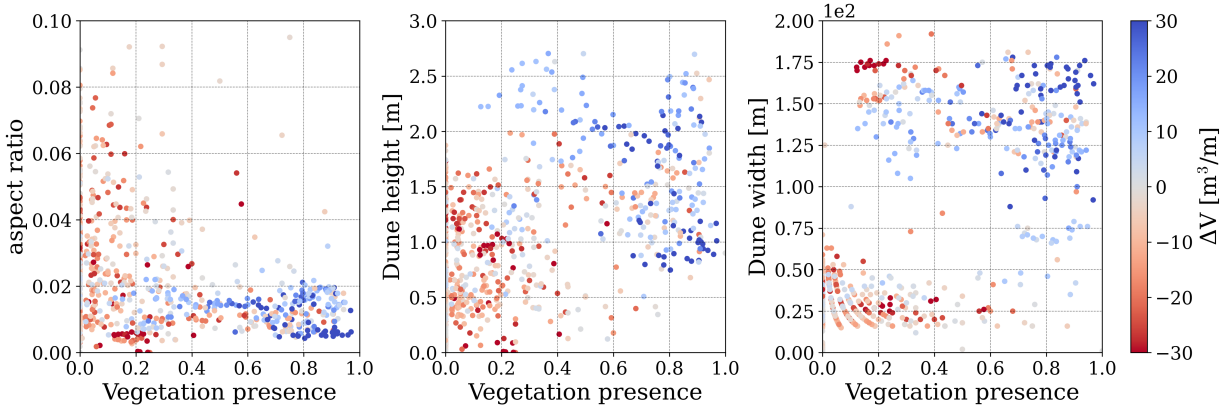

Figure 4.14: *NCI dune geomorphic characteristics vs eroded/deposited volumes vs vegetation. From left to right: the dune aspect ratio, dune height H, and dune width W are compared to volume changes and vegetation cover.*

4.3. Summary

This Chapter delved into the steps taken to process the pre and post-Hurricane Ian data and the analysis to determine the impact of the storm on two barrier islands located on the west coast of Florida, namely Lovers Key (LK) and North Captiva Island (NCI).

Historical high-resolution aerial imagery of the two islands reveals that erosional channels and breaches tend to develop in regions with preexisting unvegetated pathways that align with local bed-level depressions. During Hurricane Ian, LK transitioned entirely into the flooding regime, resulting in extensive erosion across areas with varying types of vegetation. Notably, the highest eroded volumes per transect were observed in regions with low vegetation presence.

In the case of NCI, a distinctive alongshore variability can be observed in which higher and wider dunes with more vegetation coverage are found at the northern end of the island. While the southern end has shorter and narrower dunes with less vegetation presence. Higher eroded volumes were found in areas with low vegetation and densely vegetated areas experienced less erosion. During the storm, the southern end of the island experienced mostly flooding regimes while the north remained in collision. These findings highlight a clear trend: areas with lower dunes, narrower widths, and limited vegetation presence are more susceptible to erosion compared to regions with higher dunes, broader expanses, and more substantial vegetation coverage.

5

Morphodynamic Modelling

This chapter discusses the morphological modelling of Lovers Key (LK) and North Captiva Island (NCI) with XBeach. The chapter is divided into two main sections. The first section centres on the methodology followed to model in XBeach the morphodynamic evolution of two barrier islands during Hurricane Ian. Including the different methods employed to represent vegetation in the model. The final section analyses the model results of several setups focused on vegetation's spatial and temporal inclusion in both barrier islands.

5.1. Modelling approach

This section delves into the approach to modelling morphodynamics with XBeach, encompassing the base model setup, methods employed to implement vegetation and the model evaluation process. First, the base model for both study cases is covered, including domain size, model resolution, bathymetry, boundary conditions and general model setup. Vegetation was implemented statically and dynamically by using three different types of LULC data and converted to other bed friction maps based on different classifications. Finally, the other model results are assessed based on performance metrics, nearshore processes and Sallenger storm regimes.

5.1.1. Model setup

The two models set up for LK and NCI used the hydrodynamic long wave resolving $surfbeat$ mode with XBeach version 1.23.5940M. The selection of the domains, computational grid, simulation time, bathymetry, boundary conditions, bathymetry, and general parameters are discussed in the following subsections.

Domain
The model domain was selected based on the local bathymetry and topography of LK and NCI. The model extent of both islands is shown in Fig. 5.1. Given the shallow nature of the Gulf of Mexico, the domain was cut off at a depth of 8 m relative to NAVD88. From that cutoff point, the model was extended to a virtual depth of 25 m, with a slope of 1/50 to avoid numerical instabilities at the boundary. Furthermore, to avoid complex interactions between the sea and bay, the barrier island inlets were not included in the domain.

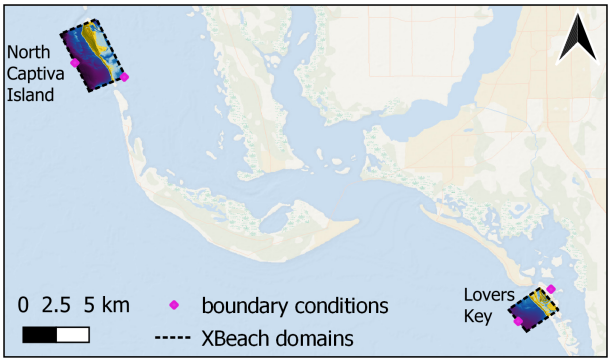

Figure 5.1: *Location of the two barrier islands XBeach domains and output locations (red dots) of the boundary conditions obtained from large-scale hydrodynamic models.*

Grid

The model grid resolution for the rectangular computational grids was selected based on the resolution of the bathymetric data and computing time. To capture enough details in the model a minimum cross-shore grid size of Δx_{min}= 1 m was selected for the dune areas. The grid then varies based on a constant Courant number up to an offshore resolution of Δx_{max} = 17 m based on a characteristic cross-shore profile. The characteristic profile was selected based on the maximum cross-shore elevations, to obtain higher resolutions as soon as the profile reaches shallow regions. The minimum cross-shore grid Δx_{min} was kept constant from the first point that the characteristic profile crosses a depth of 1 m and was increased back to a resolution Δx = 10 m on the bay side to reduce computation times. Fig. 5.2, shows the cross-shore grid resolution computed as explained above based on the characteristic profile. Using this method, the high-resolution area covers the entire dune area. The alongshore resolution of the models is Δy = 5 m, this resolution is kept constant throughout the model provides sufficient topographic details and does not miss critical local minimums (see Appendix Fig. A.1). The resulting grid setups for both the LK and NCI models are summarized in Table 5.1.

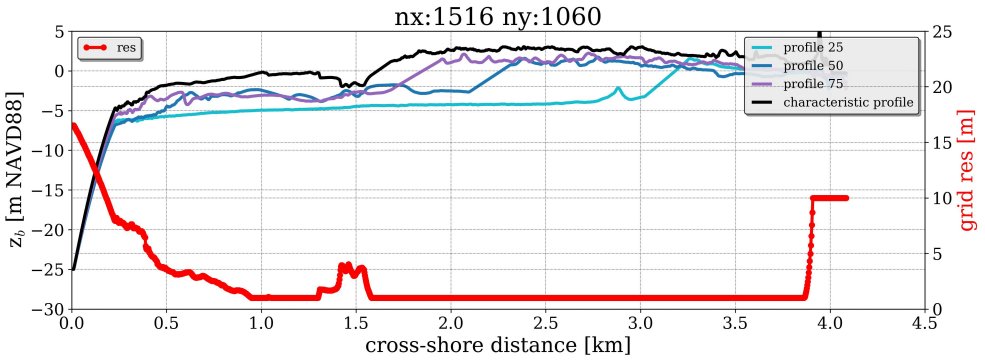

Figure 5.2: *NCI cross-shore profiles and cross-shore grid resolution. Red shows the cross-shore grid resolution based on the characteristic profile shown in black. The cyan, blue and purple lines are cross-shore profiles at 25%, 50% and 75% of the alongshore distance.*

Simulation duration

The simulation times were selected to be 48 hrs to capture the peak of the storm as well as back-flow events that take place during the ebb between the bay and the sea. The peak takes place approximately 24 hours from the start of the simulation.

Bathymetry

Two main bathymetry sources were used for this model, CUDEM (NOAA, 2018) and the 2018 LiDAR DEM (OCM-Partners, 2023b), these data sets are further described in Chapter 3. The bathymetry was obtained from the CUDEM data set, however, this data set does not include as many topographic details above the waterline as the LiDAR DEM does. The CUDEM data set misses the alongshore dune crest global minimum (see Appendix Fig. A.2), this can impact the accuracy of predicting breach locations with XBeach. To resolve this, a new bathymetry was constructed by merging the LiDAR data set with the CUDEM data set to provide the highest level of detail available in the dune area Fig. 5.3.

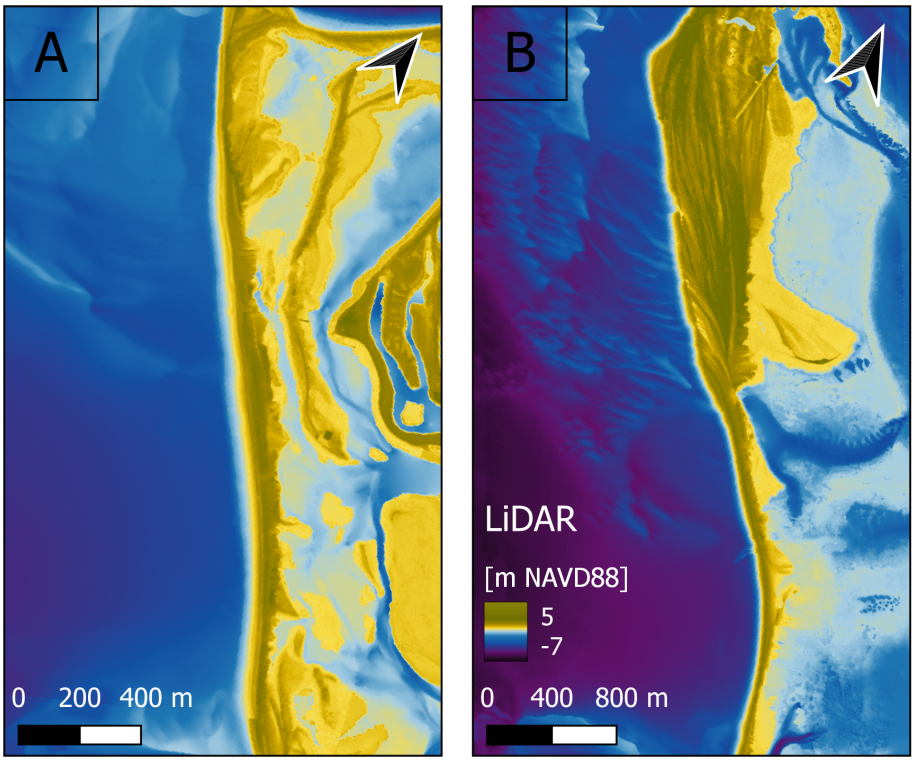

Figure 5.3: *Constructed bathymetries for LK and NCI using the CUDEM (NOAA, 2018) and the pre-storm LiDAR DEM (OCM-Partners, 2023b) data sets.*

Boundary conditions

The boundary conditions, which include water levels in the sea and bay side as well as the offshore wave conditions were derived from large-scale hydrodynamic models. With output locations for the XBeach model shown in Fig. 5.1. In this model, the forcing conditions for Hurricane Ian, are based on 6-hour forecast cycles, as a calibrated hindcast is not available yet. As a result, there remain certain uncertainties on how well it reproduces the water levels and wave heights. To consider this, a sensitivity analysis on varying water levels and wave heights is conducted to understand the effects those uncertainties would carry onto the morphodynamic model. For the flow boundary conditions, absorbing-generating 2D boundary conditions were selected for the offshore and landward sides. For the lateral conditions, the Neumann boundary conditions were selected to provide constant water levels at the lateral boundaries. The wave angle of approach is mostly shore-normal, as a result, the Neumann condition does not result in shadowing effects along the lateral boundaries.

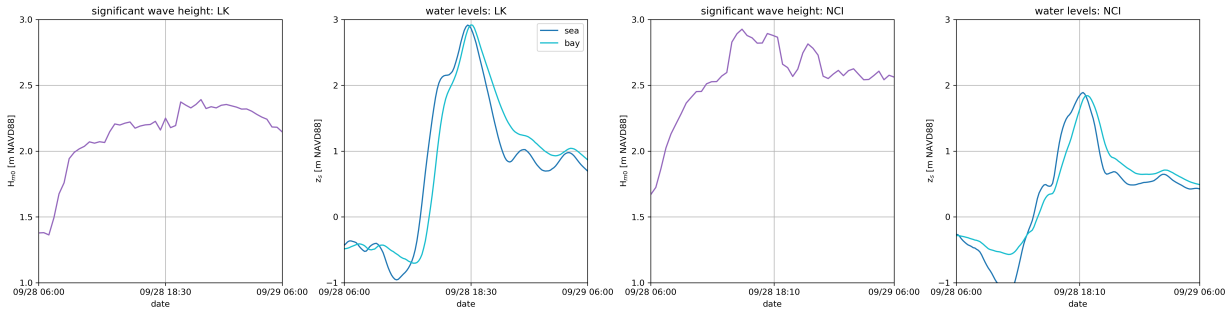

Figure 5.4: *Boundary conditions obtained from the large-scale hydrodynamic model used in both LK (left) and NCI(right) XBeach models. Note the large water level gradient between the seaside and bayside, over 1 m in some instances.*

General parameters

Bed roughness is set based on different vegetation maps using the Manning roughness coefficients as described in section 5.1.3. To reduce computational costs, a morphological acceleration factor ($morfac$) of 3 was selected. Table 5.1 summarizes all the parameters selected for the morphodynamic simulations in XBeach, all other parameters not included in the table are set with default values.

Grid parameters	Value	General parameters	Value
LK: nx/ny	1016/460	BC: front/back	abs2d
NCI: nx/ny	1516/1060	BC: left/right	Neumann
$\Delta x_{max}/\Delta x_{min}$	17/1 m	friction	Manning
Δy	5 m	$morfac$	3

Table 5.1: *XBeach physical parameters for LK and NCI*

5.1.2. Modelling vegetation

The objective of this study is to improve the inclusion of vegetation in XBeach to improve the accuracy of dune erosion forecasts during storms. Currently, there are several methods to include vegetation in XBeach models as discussed in Chapter 2. The most common approach is to increase the bed roughness where vegetation is present (Lodewijk et al., 2015; Schambach et al., 2018; Sherwood et al., 2021). This is done to reduce flow velocities locally as it is expected to occur when vegetation is obstructing the flow of water. This reduces the capacity of the water to carry sediment, and thus dune erosion is reduced along vegetated areas.

The first step is to determine how the vegetation is distributed spatially. Thanks to satellite imagery, there are now many ways to extract vegetation information to use in models. However, the accuracy of these data sets is varied and the influence of different vegetation classifications and resolutions is not fully explored. Furthermore, during storms vegetation is uprooted both from the effects of strong winds as well as the erosional and hydrodynamic processes taking place. These effects have been studied across several flume experiments and the temporal effects of vegetation removal have been included in XBeach models by Van Der Lugt et al., 2019 and Schweiger and Schuettrumpf, 2021a.

Spatial vegetation

Spatial vegetation can be obtained from many different types of data sources. Including satellite imagery, aerial imagery, and LiDAR or SfM measurements. Chapter 3 discusses some of the available LULC data sets that will be used in the XBeach models. For the XBeach models, four different spatial vegetation cases are tested. The no vegetation case, in which a commonly used Manning roughness coefficient of 0.02 [m/s$^{1/3}$] is used throughout the entire domain. This implies that the whole domain consists of a sandy bed. The second case uses the NLCD 2019 (Dewitz, 2021) data set, which has LULC data derived from satellites and has a low resolution of 30 m. The third case uses the NOPP 2019 data set which is another LULC data set that combines the latest higher-resolution imagery with satellite imagery to derive LULC data with resolutions varying between 1 and 30 m. For both the second and third cases, two different Manning roughness classifications are applied which are discussed in the following subsection. Finally, a high-resolution LULC map was derived from high-resolution aerial imagery taken pre-storm to provide the latest high-resolution data set. This case used a Supervised Machine Learning (SML) tool developed by (Buscombe et al., 2022; Buscombe & Ritchie, 2018) to derive the LULC map and is therefore named SML case. The difference between these data sets can be visualized in Fig. 5.5. The main differences are resolution differences, as well as classifications per XBeach cell. Note that NLCD and NOPP are from 2019, while SML was obtained with aerial images taken in 2022 pre-Ian. The classification shown is based on the compiled Manning roughness explained in the next subsection.

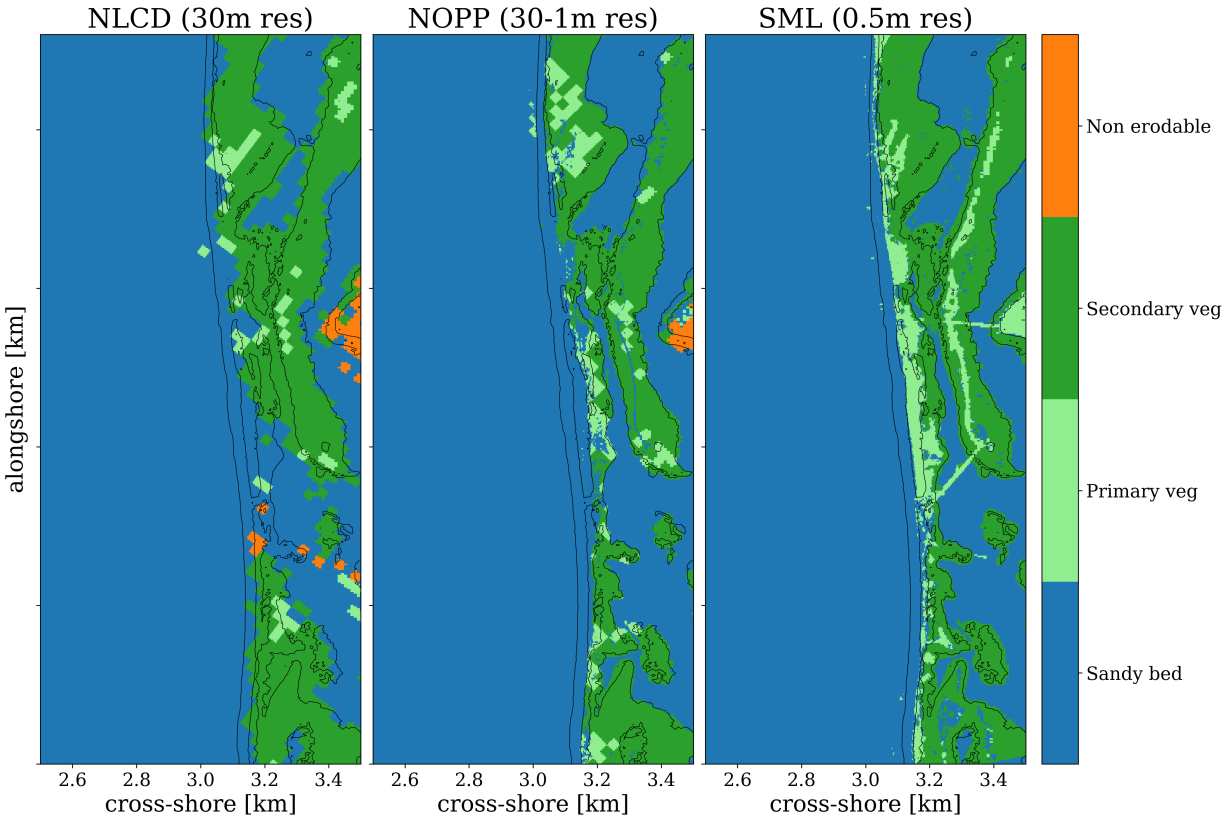

Figure 5.5: *Comparison of different LULC data sets with the compiled classification of Manning roughness coefficients. From left to right, NLCD 2019 has a 30 m resolution, NOPP 2019 has a 30 to 1m resolution and SML 2022 is derived from high-resolution RGB data with 0.5 m resolution.*

Temporal vegetation
The effects of temporal vegetation in this study are explored by using the best-performing spatial resolution data set and combining it with Van Der Lugt et al., 2019 temporal vegetation model. This model assumes a root depth of half a meter which is consistent with dune vegetation found in the state of Florida. However, to account for variation in vegetation and root depth, a sensitivity analysis is conducted in which varying root depths are used. The temporal vegetation case is then compared against the static vegetation and no vegetation cases. This is done by running the following configurations in XBeach as shown in Table 5.2. This table summarises the main runs in which different spatial vegetation data sets are tested, manning roughness classifications and the use of temporal (sometimes referred to as dynamic) vs. static vegetation. All additional calibration runs are shown in the tables in the results section.

	vegetation	classification	temporal
run 1	no vegetation		
run 2a	NLCD 2019	M&F2008	
run 2b		Compiled	
run 3a	NOPP 2019	M&F2008	
run 3b		Compiled	
run 4	SML	Compiled	
run 5	NOPP 2019	Compiled	✓

Table 5.2: *XBeach runs for different vegetation configurations. This runs test different spatial vegetation data sets, manning roughness classifications, and the use of temporal vegetation using the Van Der Lugt et al., 2019 method.*

5.1.3. Manning roughness

The Manning roughness coefficient is applied spatially across the XBeach domain. It represents the bed roughness and is standard practice to assign a value of 0.02 for any areas that consist of sandy beds. The Manning coefficient used for areas that are vegetated or urbanized varies across coastal modelling literature. Lodewijk et al., 2015 applies a constant value of 0.04 across all vegetated areas. But others, such as Makris et al., 2023; Schambach et al., 2018; Van Der Lugt et al., 2019 use LULC data and assign specific Manning roughness coefficients to different LULC classes. Schambach et al., 2018 use the Arcement and Schneider, 1989 Manning classification guide that composes a series of Manning values for different vegetation types located in flood planes and rivers. Van Der Lugt et al., 2019 use the Mattocks and Forbes, 2008 classification, which is a subset of the Arcement and Schneider, 1989 guide (shown in Table 5.3). Finally, Makris et al., 2023 compiled a new Manning classification based on an extensive survey of all the latest coastal modelling literature in which LULC data is used. Their purpose was to create a new Manning classification specific to coastal models, this classification can be found in the Appendix Fig. A.3.

The most common calibration parameters in XBeach include wave skewness, wave asymmetry and Manning roughness. However, the most important parameter is the roughness coefficient when it comes to overwash or inundation regimes (Lodewijk et al., 2015). Given that large sections of the islands selected for this study went into both overwash or inundation regimes Manning roughness is used as the calibration parameter and default values are used for wave asymmetry and skewness.

As a result, selecting appropriate Manning roughness coefficients to represent vegetation is a crucial modelling step. In this study, the Mattocks and Forbes, 2008 classification is used as it uses a constant value of 0.02 for sandy bed which corresponds with many other literature works, unlike the Makris et al., 2023 classification that uses a higher roughness for dune sand. However, one major drawback of these classifications is that they are based on old guides that come from the field of rivers. No specific classifications of coastal environments exist at the moment. In addition, the classification has over 20 different Manning roughness values for each LULC class.

Given the lack of certainty for these roughness values, in this work, a new classification is developed based on vegetation height and typical vegetation along a dune cross-shore profile. In Chapter 2 the different vegetation types found in coastal dune environments are sub-classified into primary vegetation, secondary vegetation and tertiary vegetation (see Fig. 2.3). The new classification is divided into, no vegetation, primary vegetation, secondary vegetation and non-erodible. Primary vegetation consists mostly of low vegetation such as dune grass and shrubs in the incipient dune areas. The secondary vegetation includes both secondary and tertiary vegetation which are located mostly in the foredune and hind dunes. Non-erodible classifications include all human infrastructure except for open-space urban areas. Table 5.3 provides a detailed summary of the NOPP class names and the newly compiled classification along with their corresponding Manning roughness coefficients.

NOPP class name	**Manning's n (Mattocks & Forbes, 2008)**	**Compiled classification**	**Manning's n**
Unconsolidated Shore	0.04		
Bare Land	0.09		
Open Water	0.02	Sandy bed	0.02
Palustrine Aquatic Bed	0.015		
Estuarine Aquatic Bed	0.015		
Cultivated Crops	0.037		
Pasture/Hay	0.033		
Grassland/Herbaceous	0.034	Primary vegetation	0.04
Palustrine Emergent Wetland	0.045		
Estuarine Emergent Wetland	0.045		
Scrub/Shrub	0.05		
Palustrine Forested Wetland	0.1		
Palustrine Scrub/Shrub Wetland	0.048	Secondary vegetation	0.05
Estuarine Forested Wetland	0.1		
Estuarine Scrub/Shrub Wetland	0.048		
Developed, High Intensity	0.15		
Developed, Medium Intensity	0.1	Non-erodible	0.1
Developed, Low Intensity	0.05		

Table 5.3: *Manning roughness coefficient classes for modelling dune vegetation in XBeach*

5.1.4. Evaluation methods

This study aims to identify the most effective approach for incorporating vegetation into XBeach models, specifically to enhance its predictive accuracy in forecasting dune erosion during storm events. The assessment of these various vegetation inclusion methods will be carried out through a comprehensive evaluation of model outcomes. The evaluation process will involve multiple facets, including a comparison between computed results and observed data, an analysis of how these methods impact critical erosional processes, and an assessment of their ability to accurately replicate the Sallenger, 2000 storm regimes.

To gauge the performance of the model and its incorporation of vegetation, we will rely on observed data obtained through Structure from Motion (SfM) techniques. This data was collected post-Ian and subsequently converted from a Digital Surface Model (DSM) to a Digital Elevation Model (DEM), as detailed in Chapter 4. This data set will serve as a crucial reference point for evaluating the model's predictions and validating the effectiveness of the various vegetation inclusion methods.

Metrics

To assess the performance of the model outputs in comparison to post-storm measurements, two key metrics are employed: the Brier Skill Score (BSS) and bias. These metrics are instrumental in quantifying the model's predictive accuracy and its tendency to overestimate or underestimate. Once the BSS is computed, we utilize a classification system as outlined in Table 5.4, which was originally proposed by Van Rijn et al., 2003. This classification system offers a structured means of evaluating the morphodynamic model's performance. It helps categorize the model's performance into different skill levels, providing a clear and concise assessment of its predictive capabilities. By applying these evaluation metrics and classification criteria, we can effectively gauge how well the model aligns with the observed data, offering valuable insights into its predictive accuracy and overall reliability in simulating dune erosion during hurricane events.

Qualification	skill
excellent	1.0 - 0.8
good	0.8 - 0.6
reasonable	0.6 - 0.3
bad	0.3 - 0.0
poor	< 0.0

Table 5.4: *Morphodynamic model qualification based on skill*

$$skill = 1 - \frac{\frac{1}{N}\sum_{i=1}^{N}(Y_i - X_i)^2}{\frac{1}{N}\sum_{i=1}^{N}(X_0 - X_i)^2} \tag{5.1}$$

$$bias = \frac{1}{N}\sum_{i}^{N}(Y_i - X_i) \tag{5.2}$$

The mathematical formulations for calculating BSS and Bias are presented in Equations 5.1 and 5.2, respectively. Where Y is the prediction, which in this case is the model output. X is the

observed data and X_0 is the baseline prediction or initial condition. Since the model operates in a 2D spatial domain, it offers the flexibility to assess its skill across different parameters and areas. The following list outlines the main variables that will be compared and evaluated:

- Breach location
- Post-storm bed levels map, above MHW: z_b map
- Post-storm bed levels dune, above 1.3 m above NAVD88 datum: z_b dune
- Post-storm sedimentation erosion map, above MHW: Δz_b map
- Post-storm sedimentation erosion dune, above 1.3 m above NAVD88 datum: Δz_b dune
- Alongshore dune crest elevation: z_{crest}
- Alongshore eroded volumes above MHW: V_{eroded}
- Alongshore deposited volumes above MHW: $V_{deposited}$

Processes
Dune erosion is predominantly driven by four key nearshore processes: avalanching, long waves, wave impact, and turbulence. The introduction of vegetation, using the Manning roughness coefficient, directly influences bed shear stresses, consequently impacting flow dynamics within the model. As a result, it is necessary to assess the ramifications of vegetation on nearshore processes that are tied to flow conditions, both spatially and temporally. These processes are currents, waves, infragravity waves, and water levels. To quantify these parameters current velocities are analyzed on a temporal scale by looking at the water level gradient Δz between the bay side and the ocean side. Significant wave heights H_s are studied at the dune toe, as this is the area where they will have the largest impact on dune erosion. Additionally, infragravity waves H_{ig}, also evaluated at the dune toe, are approximated utilizing the standard deviation of water levels (σ_{wl}), as described by the following equation:

$$H_{ig} \approx \sqrt{8\sigma_{wl}} \tag{5.3}$$

This spatiotemporal analysis will allow for a deeper understanding of how vegetation, through the Manning roughness coefficient influences flow-related nearshore processes and consequently changes the dynamics of dune erosion.

Storm regimes
The erosional impact of a storm can be categorized using the Sallenger, 2000 regimes and the storm surge ebb regime. The data analysis conducted in Chapter 4, identified areas that remained in the collision regime or areas that transitioned into the overwash or inundation regimes. To evaluate the model performance, these areas will be compared to determine if the storm regimes modelled align with observations. Literature studies such as Bryant et al., 2019 suggest that vegetation plays a role in storm regime transitions. Consequently, it is important to determine if including vegetation in the models also results in improved storm regime forecasts.

Moreover, establishing a connection between storm regimes and the inclusion of vegetation in XBeach models can provide insights into the practical applications of morphodynamic modelling with XBeach worldwide. For example, the Dutch coastal dunes are engineered to remain in the collision regime. This connection between vegetation and storm regimes can therefore provide valuable information for design practices with XBeach.

5.2. Results: XBeach

This section covers the results of several morphodynamic simulations conducted in XBeach to evaluate the spatiotemporal inclusion of vegetation in XBeach models. First, the effects of different bathymetry data sets are studied to determine the required level of bathymetric detail needed. Followed by an analysis of different spatial vegetation data sets, with different Manning roughness coefficient classifications. Once the best performing spatial vegetation data set, cases with no vegetation, static vegetation and dynamic vegetation were investigated. These different cases are summarized and labelled in Table 5.2. In addition to these runs, sensitivity runs were conducted on varying roughness coefficients, hydrodynamic conditions and root depths for the dynamic models. Subsequently, the three different vegetation cases are analyzed based on the nearshore processes that drive dune erosion and the ability of the model to reproduce storm regimes. To conclude, a detailed description of the best-performing models for both islands is provided. Given that the model domain for LK is much smaller than NCI, the LK model is used for calibration purposes and the NCI model is for validation to reduce computational costs.

5.2.1. Bathymetry

To establish a base model, two different bathymetry data sets were tested in the XBeach morphodynamic model. The first data set is the CUDEM 2018 and the second one is the LiDAR 2018 which is constructed as described in Section 5.1.1. The main distinction between these data sets is that the LiDAR data set has a higher resolution in the areas above MHW. Additionally, the CUDEM data set has a much wider and elevated beach profile with a much steeper sloping foreshore as depicted in Fig. 3.5. In contrast, the constructed LiDAR data set yields a much narrower beach with a milder sloping foreshore (as shown in Fig. 5.3). Both data sets result from the fusion of topographic data with bathymetric measurements, and the interpolation of nearshore data complicates the determination of which data set accurately replicates the beach profile.

For both bathymetry sets, XBeach simulations were executed without any vegetation, while all other conditions remained as outlined in Section 5.1.1. These simulations aimed to determine the significance of having high-resolution data in morphodynamic models. The model performance metrics are summarized in Table 5.5 and the resulting post-storm bed levels for both cases can be visualized in Fig. 5.6. The models severely overestimate erosion in both cases and their performance ranges from poor and bad, as no vegetation was included. Overwash fans and ebb fans extended over substantial distances, and dune crest elevations were much lower than post-storm observations. Multiple breaches manifested along the LK barrier island in both scenarios. Notably, LiDAR reproduces fewer breaches throughout the domain and successfully replicates the breach that was observed in reality at the same location. Conversely, the CUDEM model reproduces several breaches in the vicinity of the one that occurred but not at the same location.

run	**bathymetry**	**breach**	z_b **map**		z_b **dune**	
			skill	bias	skill	bias
run 1	LiDAR	✓	-0.02	-0.81	-0.12	-0.95
run 1-1	CUDEM	✗	0.07	-0.70	0.08	-0.78

Table 5.5: *XBeach bathymetry runs performance*

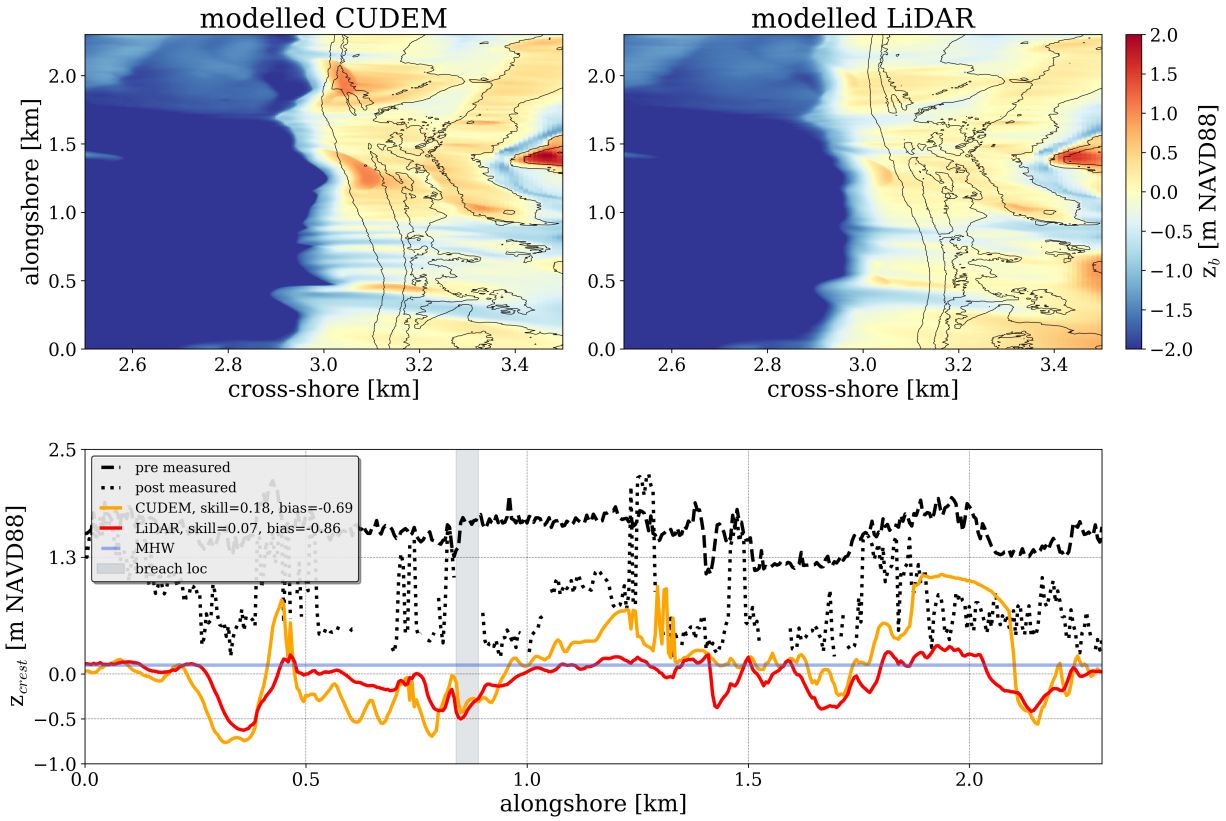

Figure 5.6: *LK model results for different bathymetries; CUDEM and LiDAR. The top two figures show the post-storm bed level for both bathymetries used. The bottom figure shows the alongshore dune crest measured pre and post-storm and computed with the two different bathymetries. The shaded area corresponds with the observed breach location, and the blue line is the MHW.*

Given that both models perform poorly and have no predictive skill (Table 5.5), the only distinctive difference was the prediction of the breach at the same location by the LiDAR data set. In addition, the LiDAR data was used throughout Chapter 4, therefore, for continuity, the LiDAR data set was used in the reminding XBeach simulations.

5.2.2. Spatial vegetation

Spatial vegetation was included in XBeach by converting LULC data into a Manning n bed friction file. There are two different data sets, the NLCD 2019 and the NOPP 2019, each of these data sets was converted to bed friction by using the Mattocks and Forbes, 2008 conversion table and a separate conversion was carried out for both data sets using the compiled version described in Section 5.1.3. Additionally, a fifth model used the SML-derived LULC map with the compiled version of the Manning roughness coefficients. Table 5.6 summarizes the different setups for each run along with their performance metrics. Finally, these models are compared against the no vegetation case and each other to determine the best vegetation data sets to use in the XBeach model.

Compiled vs Mattocks and Forbes, 2008

The main difference between the Mattocks and Forbes, 2008 and the compiled Manning roughness classification is a reduction of 25 different LULC classes to only 4 LULC classes (see 5.3). This is

a significant reduction, however, in reality, for the two barrier islands studied here, the reduction was from 10 different LULC classes to 4. This simplification can be observed in Fig 5.7. The most notable differences between Mattocks and Forbes, 2008 and the compiled method used here are the spatial changes in roughness coefficients. With higher roughness values at the front beach and back of the dune for the Mattocks and Forbes, 2008.

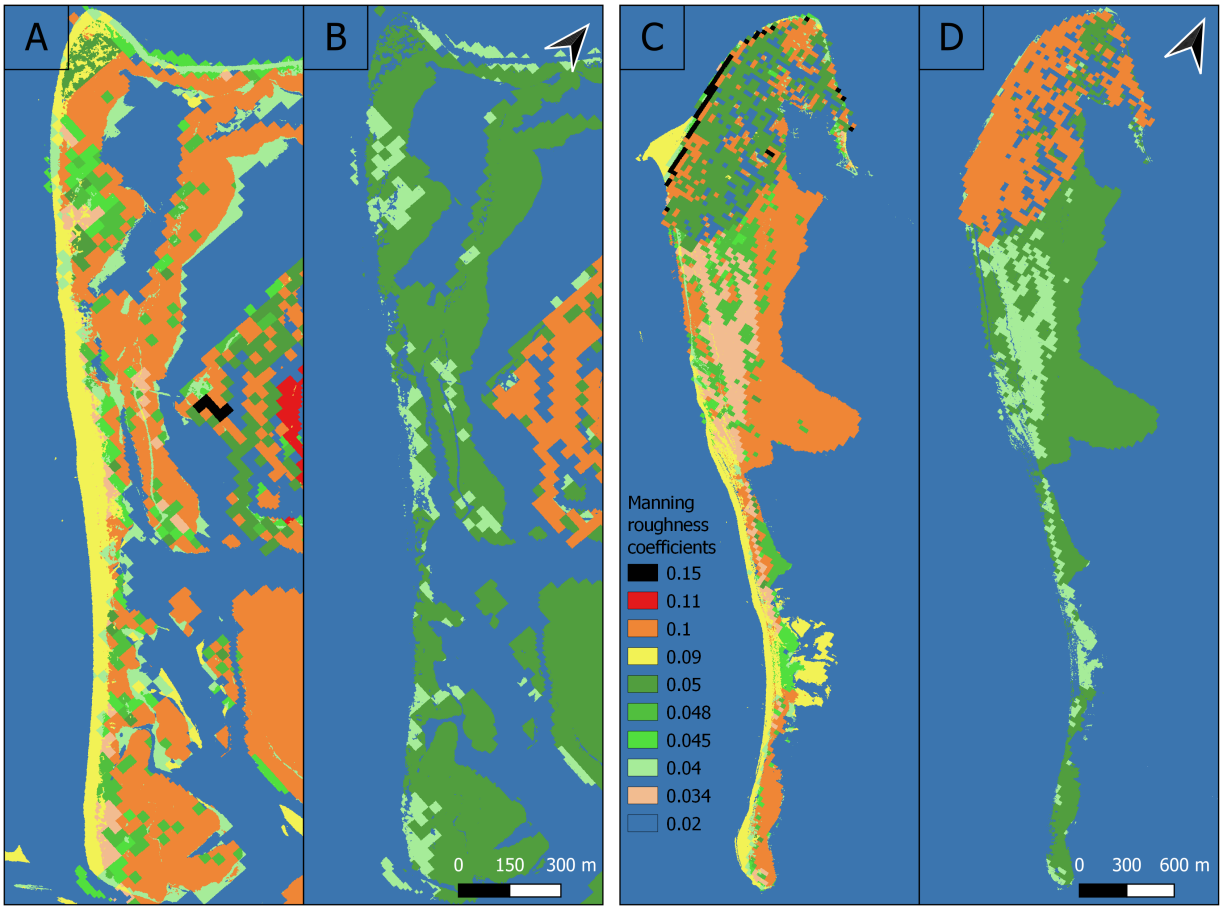

Figure 5.7: *A) LK NOPP 2019 with Mattocks and Forbes, 2008 classification for Manning roughness coefficients. B) LK NOPP 2019 with compiled classification for Manning roughness coefficients. C) NCI NOPP 2019 with Mattocks and Forbes, 2008 classification for Manning roughness coefficients. D) NCI NOPP 2019 with compiled classification for Manning roughness coefficients.*

In XBeach, the results of using different Manning roughness classifications do not produce major differences across different data sets. This can be visualized in Fig. 5.8, where post-storm bed level difference maps are plotted for the same data sets with different roughness coefficients. Larger differences were produced for the NOPP data sets, but this only occurs in the areas that breached, with deeper channels and larger ebb deposition for the non-compiled version. The performance metrics of all variables range between reasonable to good predictive skills but favour the compiled version across all variables, particularly in the dune areas, where the predictive skill is approximately 9% higher (Table 5.6). To summarize, the compiled version of the manning roughness coefficients performed better across the NLCD and NOPP data sets. This is a desirable result, as a classification of 25 different Manning roughness coefficients can be simplified to only four different classes in XBeach based on vegetation, and while the results do not differ significantly they improve the predictive skill of the model. Given the success of the compiled

Manning roughness classification. All remaining XBeach runs to determine the best spatial vegetation data sets, sensitivity runs, and temporal vegetation runs are done with the compiled classification.

run	vegetation	breach	z_b map		z_b dune		Δz_b map		Δz_b dune	
			skill	bias	skill	bias	skill	bias	skill	bias
run 1	no veg	✓	-0.02	-0.81	-0.12	-0.95	0.02	-0.83	-0.11	-0.95
run 2a	NLCD	✓	0.42	-0.35	0.67	-0.13	0.54	-0.28	0.67	-0.13
run 2b	NLCD comp	✓	0.44	-0.32	0.71	-0.08	0.57	-0.24	0.71	-0.07
run 3a	NOPP	✓	0.43	-0.36	0.71	-0.18	0.57	-0.28	0.72	-0.18
run 3b	NOPP comp	✓	0.46	-0.32	0.77	-0.12	0.60	-0.25	0.77	-0.12
run 4	SML comp	✓	0.43	-0.35	0.70	-0.12	0.56	-0.27	0.71	-0.12

Table 5.6: *XBeach spatial vegetation runs and unvegetated performance metrics. The best-performing model is highlighted in green.*

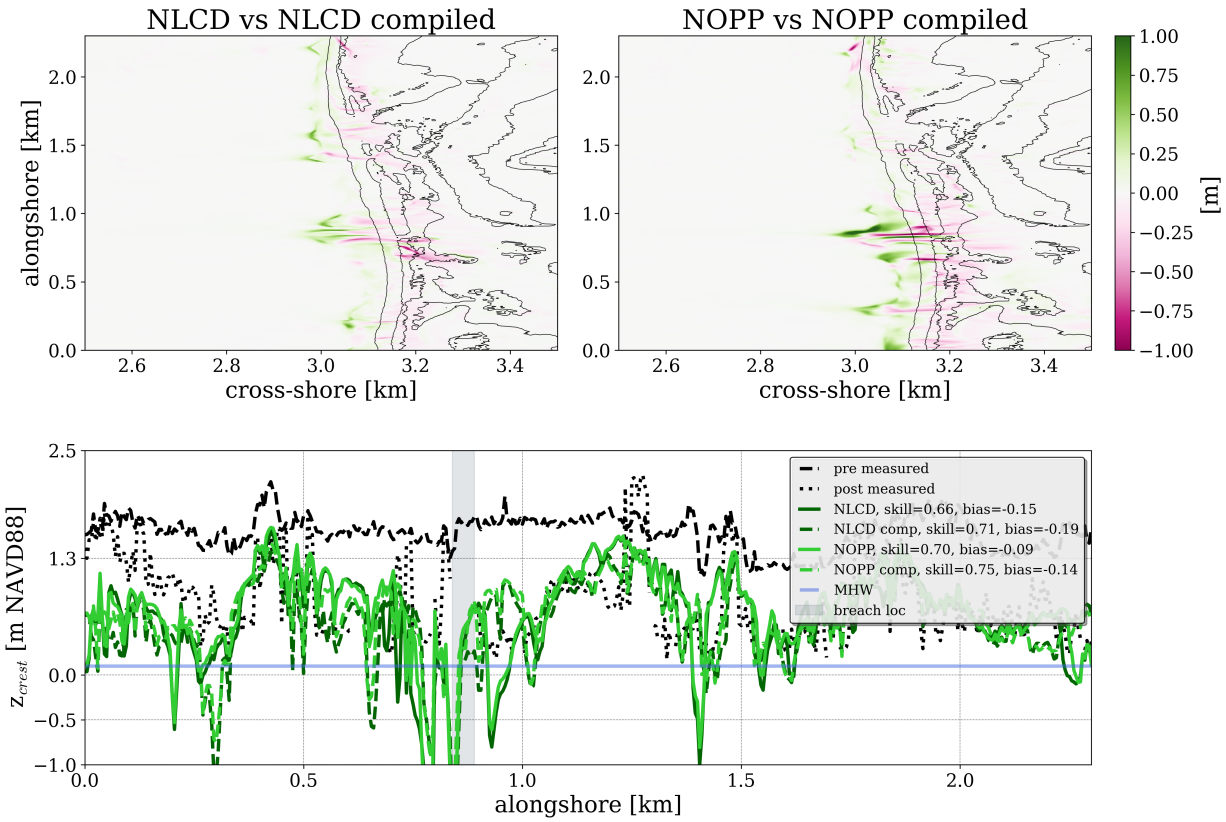

Figure 5.8: *Computed bed level differences between the Mattocks and Forbes, 2008 manning roughness conversion and the compiled version. The bottom figure shows the alongshore dune crest elevation on the resulting computed bed levels compared to the measured ones.*

Unvegetated vs vegetated

The three different LULC data sets used, namely NLCD (run 2b), NOPP (run 3b) and SML (run 4) are compared against the unvegetated model (run 1) to determine how important it is to include vegetation in XBeach models. Note that all these cases use the compiled Manning classification. In addition, these different vegetation data sets are pitted against each other to determine if there are significant differences between the spatial resolutions of LULC data. This will help establish what kind of vegetation resolution is needed to improve the forecasting skill of the morphodynamic model.

Overall, the improvement between the unvegetated and vegetated models is significant. The model predictive skill jumps across all variables from poor to reasonable and good across different variables (see Table 5.6). When comparing the models in Fig. 5.9, there is a drastic difference between the vegetated models and the unvegetated ones. The erosion overestimation in the unvegetated case is significantly reduced by all the vegetated cases. This can be observed in a

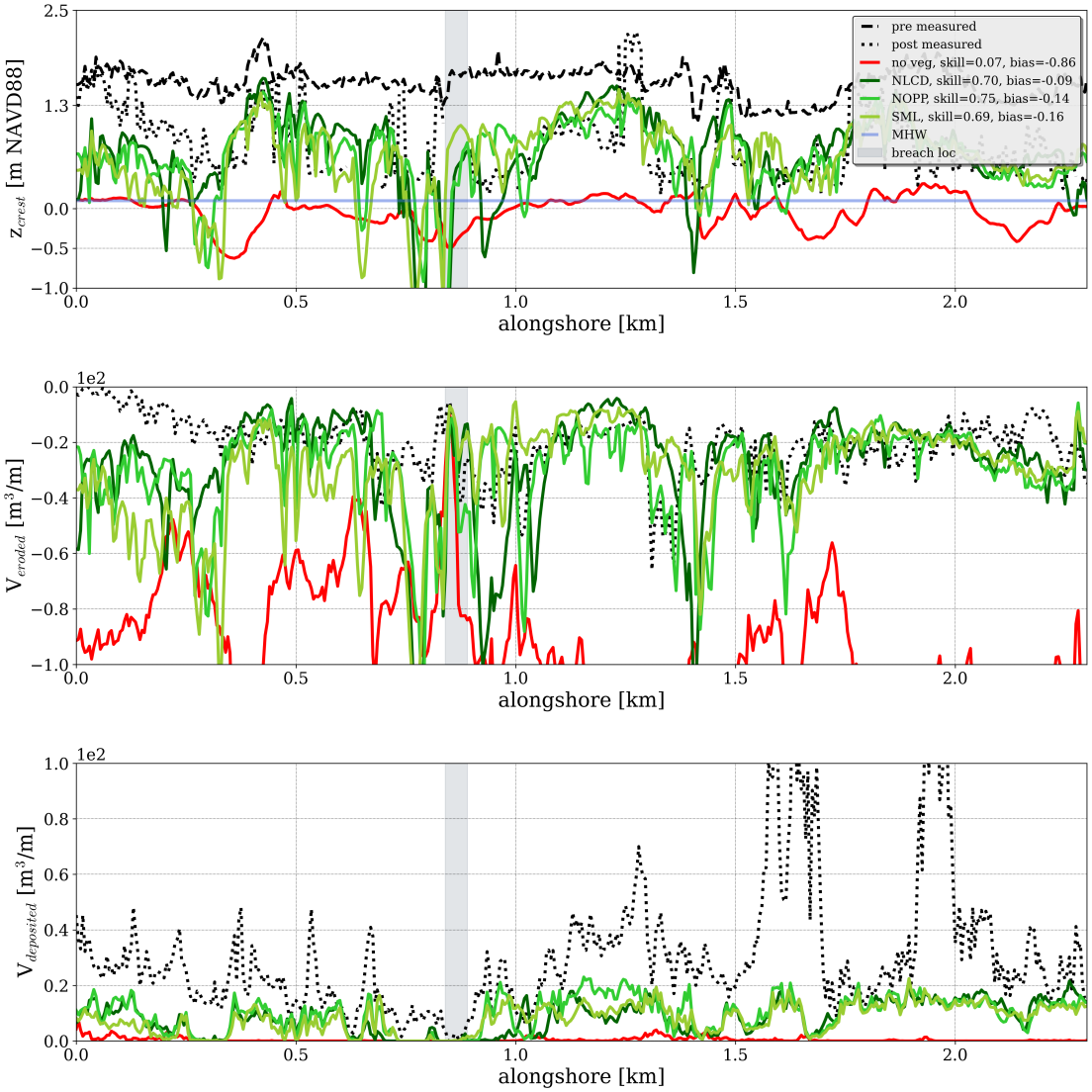

Figure 5.9: *Comparison measured and computed alongshore dune crest evolution over the storm, alongshore eroded volumes and alongshore sedimentation volumes for the different LULC including no vegetation, NLCD, NOPP and SML.*

reduction in the total number of breaches as well as a much-improved location prediction of the breached channel. The results of all models do not compare well with the measured sedimentation volumes alongshore. However, as mentioned in Chapter 4, the DEM derived from the SfM does contain some errors in areas where vegetation cannot be removed. This shows up as sedimentation in the measured data. However, this is not a problem in other areas and variables compared to the model, where less vegetation was present.

The differences between the vegetated models are minimal, however, the NOPP performs the best across all variables. With a maximum difference in predictive skill that favours the NOPP LULC data set by only 11% in the dune area for both final bed level, sedimentation and erosion. The outcome of this comparison is that vegetation must be included in all models and that higher accuracy can result in better predictive skills. However, this does not necessarily hold for all data sets. The high-accuracy SML data set, performed worse than the NOPP data. This could be a result of limitations in the SML tool developed by Buscombe et al., 2022; Buscombe and Ritchie, 2018. Nevertheless, including any form of LULC vegetation data significantly improves dune erosion predictions in XBeach from poor to reasonable or good. Given that the overall best predictions were obtained from the NOPP model, the NOPP (run 3b) LULC data set will be used for all the following XBeach simulations. These include the sensitivity analysis, the temporally varying vegetation and the NCI vegetated models.

5.2.3. Sensitivity

The LK model has many different input conditions that affect the prediction of morphological change throughout the storm. To account for these variations, a sensitivity analysis was conducted to determine the relative influence of varying conditions such as water levels, waves and bed friction. The sensitivity analysis consists of six different simulations in which the roughness, water levels and waves are changed for run 3b. The first simulation increases the primary vegetation from 0.04 to 0.06 and the secondary vegetation coefficients from 0.05 to 0.06. The second simulation decreases primary vegetation from 0.04 to 0.035 and the secondary vegetation coefficients from 0.05 to 0.045. The lower change for the second simulation is to not approach the sandy bed roughness coefficient as much. The following two simulations adjust the water levels by $\pm 10\%$ and the final two very the wave heights also by $\pm 10\%$ as done in Van Der Lugt et al., 2019. Table 5.7 summarizes the results of the different sensitivity runs.

run	**sensitivity**	**breach**	z_b **map**		z_b **dune**		Δz_b **map**		Δz_b **dune**	
			skill	bias	skill	bias	skill	bias	skill	bias
run 3b		✓	0.46	-0.32	0.77	-0.12	0.60	-0.25	0.77	-0.12
run 3b-1	roughness +	✓	0.47	-0.30	0.80	-0.04	0.62	-0.21	0.80	-0.03
run 3b-2	roughness -	✓	0.45	-0.35	0.73	-0.18	0.58	-0.27	0.74	-0.17
run 3b-3	water level +	✓	0.42	-0.39	0.67	-0.26	0.55	-0.32	0.68	-0.26
run 3b-4	water level -	✓	0.49	-0.26	0.82	0.03	0.63	-0.17	0.82	0.04
run 3b-5	waves +	✓	0.47	-0.30	0.78	-0.10	0.61	-0.22	0.78	-0.09
run 3b-6	waves -	✓	0.45	-0.34	0.75	-0.14	0.59	-0.26	0.75	-0.14

Table 5.7: *XBeach sensitivity runs for bed roughness coefficients, water levels and waves, along with their respective performance metrics.*

Bed roughness

Varying the bed roughness coefficients assigned to the primary vegetation and secondary vegetation classification results in small variations in model skill prediction. These variations range between 3% skill increase when increasing the roughness and a drop of approximately 4% when reducing the roughness. These percentage differences are applicable for the dune area, however, looking at all areas above MHW the differences become even less noticeable. These results show that reducing the roughness coefficients further towards the value of the sandy bed will not improve the results of the model. Moreover, the variances are significant along the dune area, which highlights the importance of increasing the roughness in vegetation for areas that undergo overwash as noted by Lodewijk et al., 2015. The sensitivity band for roughness shown in Fig. 5.10, shows that the roughness coefficient plays a more important role in the dune areas that still overestimate erosion but its role in other areas is not as important as water level variations. Alongshore variations to eroded volumes also respond to changing roughness values, particularly in areas that showed an overestimation of erosion across all models.

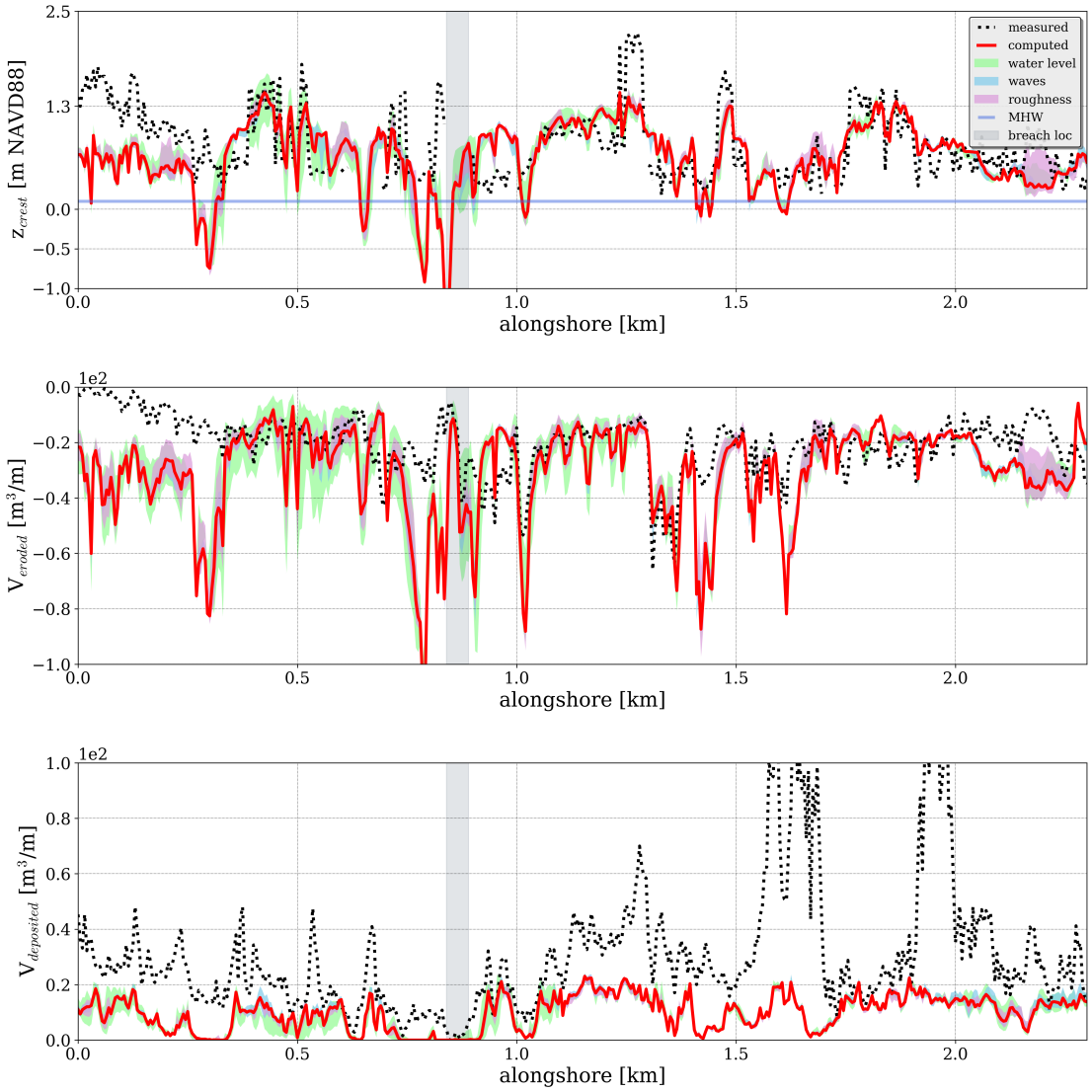

Figure 5.10: *Computed sensitivities of the model to water levels, wave height and vegetation roughness, for alongshore dune crest evolution over the storm, alongshore eroded volumes and alongshore sedimentation volumes.*

Water levels
Sensitivities to water level differences are important to determine as uncertainties from models that forecast hydrodynamic conditions can carry over into the morphodynamic model. These uncertainties produce the largest variations in model predictive skill. For the instance in which the water level increased by 10%, the skill was reduced by a maximum of 13%. However, this leads to a more conservative estimate of the damage caused by the storm. On the other hand, lowering the water levels by 10%, increased the model predictive skill by 6%. When comparing the evolution of the dune crest, the water level difference generates a much larger sensitivity band compared to roughness and waves (see Fig. 5.10 light green band). In some instances, the dune crest is eroded by approximately 40 cm, which results in additional breaches that did not occur in reality. The water level variations are also the only ones that caused significant changes to alongshore sedimentation volumes. For eroded volumes, they also cause major alongshore variations, but in that case, the bed roughness also plays an important role in areas that overestimate erosion in general.

Waves
Similarly to the water levels, the waves are forecasted by other hydrodynamic models that may carry uncertainties into XBeach. To account for this, the wave heights were adjusted by $\pm 10\%$ and the wave period was adjusted such that the wave steepness remained constant. These variations in the wave conditions caused very minimal differences in the predictive skill of the model, never exceeding 3%. The model showed little sensitivity to wave heights and did not cause significant bed elevation changes throughout the storm compared to variations in water level and roughness (see Fig. 5.10 light blue band).

5.2.4. Temporal vegetation

Temporal or dynamic vegetation refers to the processes that involve dune erosion and vegetation removal during a storm. This type of approach has been included in XBeach models in the past; it assumes that after erosion levels reach a certain root depth, the vegetation is removed (Schweiger & Schuettrumpf, 2021a; Van Der Lugt et al., 2019). In this study, the focus is on the dynamic vegetation model implemented by Van Der Lugt et al., 2019. This approach reduces the manning friction coefficient linearly as soon as it starts eroding in a vegetated area, up until the point that it reaches the value of a sandy bed or remains with an in-between value. This section will first focus on studying the sensitivity to varying root depths. It then will compare the temporal/dynamic case (run 5) to the static vegetation case (run 3b) and the unvegetated case (run 1). Table 5.8 summarizes the temporal vegetation runs and the static vegetation run performance metrics.

run	**root depth**	**breach**	z_b **map**		z_b **crest**		Δz_b **map**		Δz_b **crest**	
			skill	bias	skill	bias	skill	bias	skill	bias
run 3b		✓	0.46	-0.32	0.77	-0.12	0.60	-0.25	0.77	-0.12
run 5	0.5 m	✓	0.36	-0.42	0.60	-0.31	0.48	-0.36	0.61	-0.30
run 5-1	0.75 m	✓	0.38	-0.41	0.63	0.29	0.49	-0.35	0.63	-0.29
run 5-2	0.25 m	✓	0.39	-0.40	0.65	-0.27	0.52	-0.34	0.65	-0.27

Table 5.8: *XBeach dynamic vegetation runs, with varying root depths along with their respective performance metrics.*

Sensitivity: root depth

Varying root depth produced minimal differences between the dynamic vegetation models. Doubling the root depth results in a maximum increase in the predictive skill of 5% and halving the root depth also increases the skill by 8%. This is an interesting result, all previous results show relationships that either increase or decrease model skill. However, in this instance halving or doubling the root depth increases improves model skill. In Fig. 5.11 this becomes even more apparent as the sensitivity band does not always align with the base dynamic vegetation run with a root depth of 0.5 m. This is likely caused by the dynamic vegetation model as it also takes into account sedimentation. If sedimentation occurs, the roughness coefficient restores to the original vegetated value. The root depth has a large influence on the alongshore erosion volumes and has negligible influence on the sedimentation volumes.

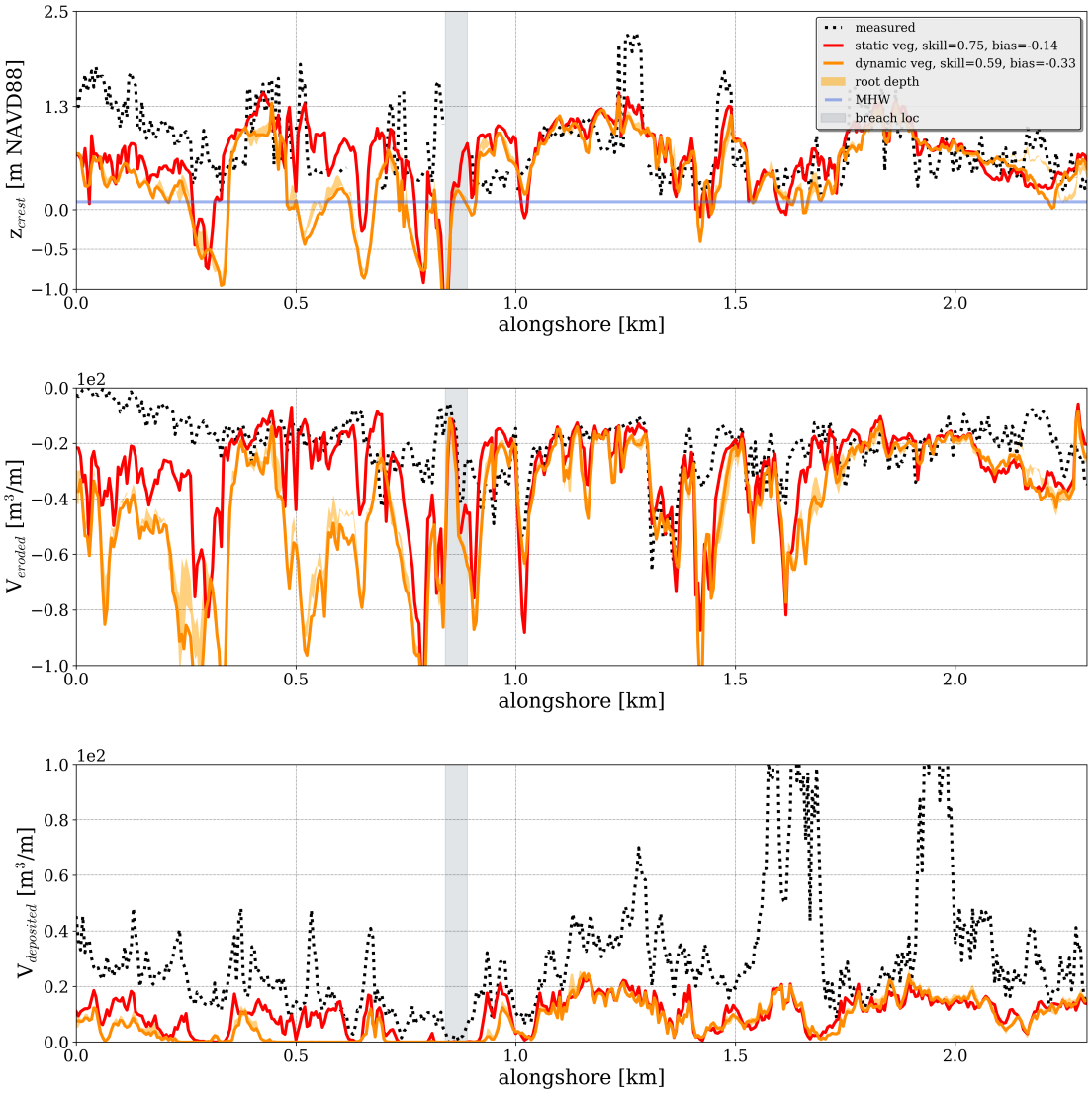

Figure 5.11: *Sensitivity of model to varying root depth and comparison of static vs dynamic roughness*

5.2.5. Unvegetated vs static vegetation vs dynamic vegetation

The predictive skill of dynamic vegetated models is significantly lower when compared to the static vegetation case. However, both models vegetated models scored significantly higher than the unvegetated case, which has poor predictive skill. The dynamic vegetation model currently overestimates erosion and results in a model that performs reasonably across the majority of the variables compared. In comparison, the static vegetation model predictive skill is near excellent for the best-performing case and good for all the different LULC data sets used. To compare the results see run 3b and run 5 in Table 5.8. The overestimation of erosion is caused by the assumption of a linear decrease of the roughness coefficient as soon as the bed level begins to lower in the Van Der Lugt et al., 2019 vegetation model. The differences in the different vegetation cases are also clearly visible in Fig. 5.12. In the unvegetated case, the island is almost entirely washed away and experiences a significant decrease in dune crest elevation. In some instances, the dune crest was lowered by more than 1.3 meters and large portions were below MHW after the storm (see Fig. 5.13). In comparison, the higher predictive skill of both the static and dynamic vegetation cases is visible in the spatial plots as only certain breaches formed along the island. The main breach that formed in the static case coincides with the one observed in reality. While this breach also occurs in the dynamic vegetation case, the additional breaches did not happen in reality. Based on the predictive skill scores for each case and the comparison of the final bed levels to the observed measurements, it is clear that the best-performing model is the static vegetation case using the NOPP land cover data set and the compiled manning roughness coefficients.

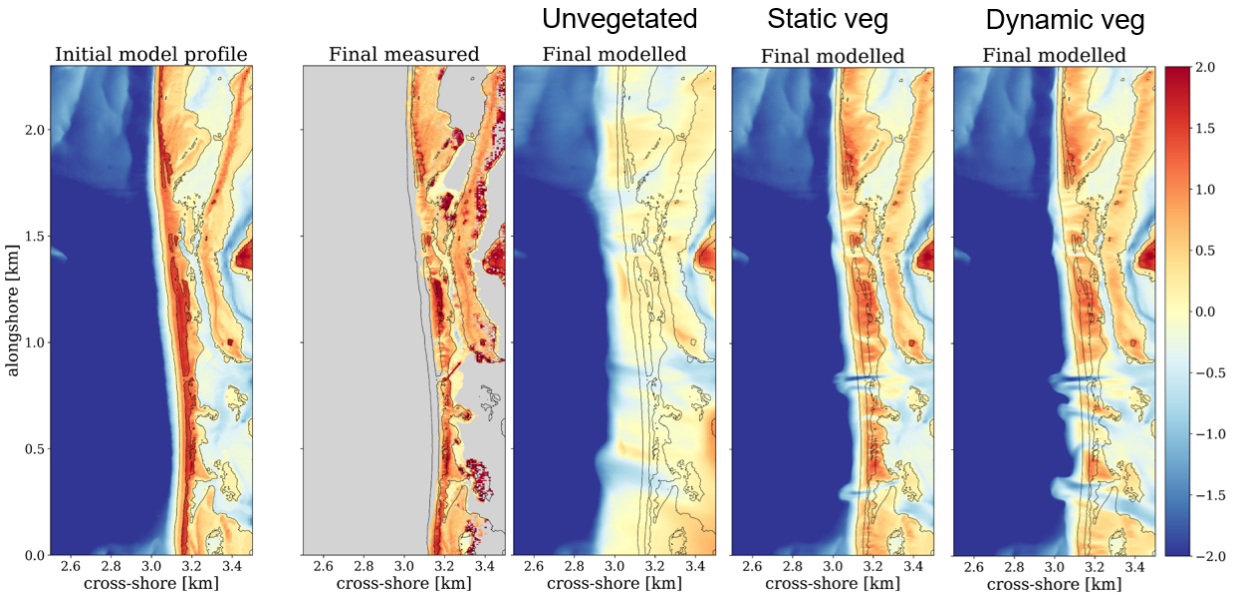

Figure 5.12: *LK vegetation effects in XBeach. From left to right: A) pre-storm topography of LK, B) post-storm measured DEM derived from SfM data at LK, C) XBeach model results for the unvegetated case, D) XBeach model results for the static vegetation case, and E) XBeach model results for the dynamic/temporal vegetation case.*

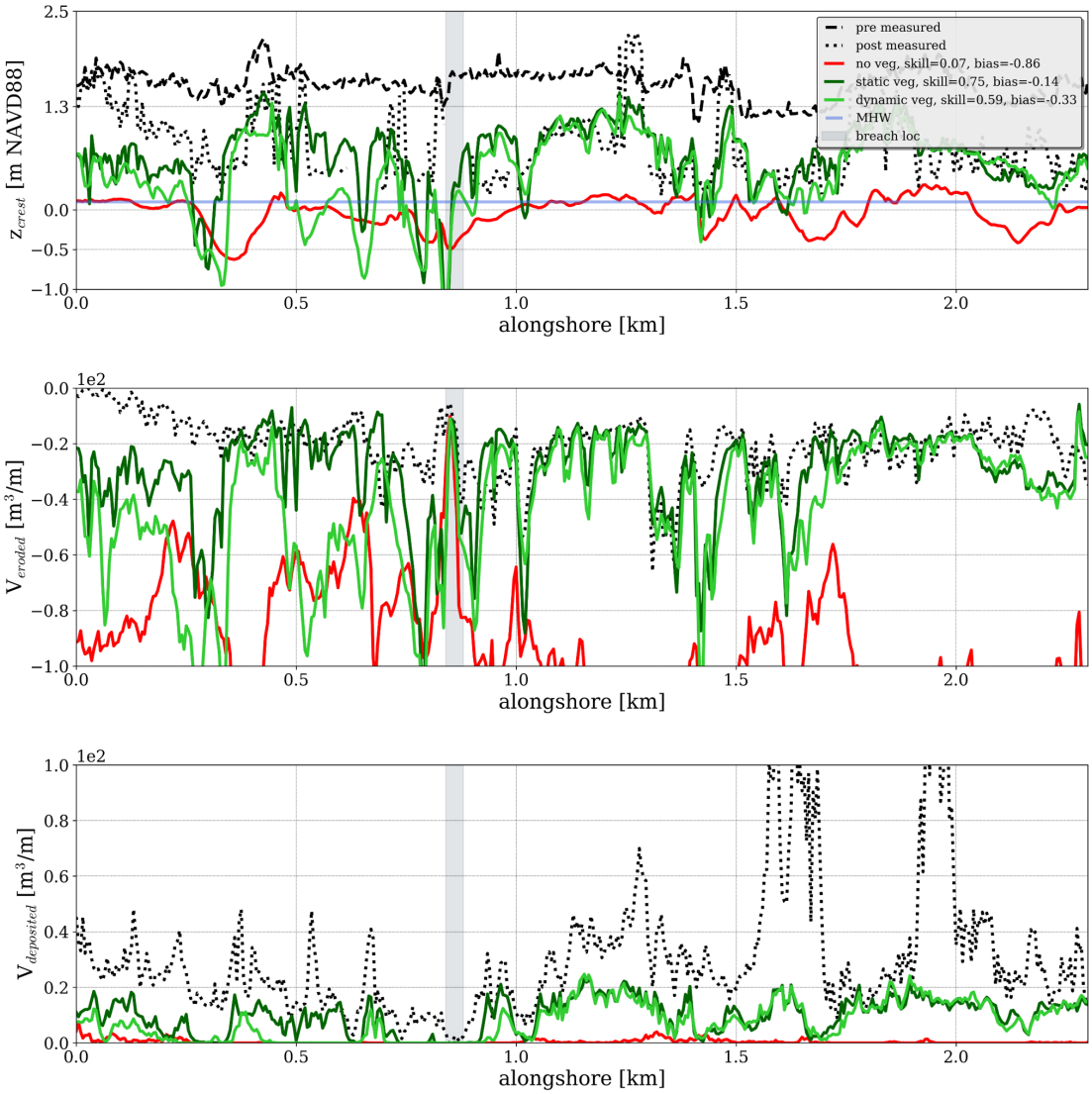

Figure 5.13: *LK XBeach alongshore model results for dune crest height, erosion and sedimentation volumes. In red is the unvegetated case, in dark green is the static vegetation case and in lime green is the dynamic vegetation case.*

5.2.6. Validation

To validate the results obtained from the LK model three NCI models. A no vegetation case, a static vegetation case and a dynamic vegetation case using the NOPP data set were run in XBeach. The bathymetry used for these models is the LiDAR-constructed one explained in Section 5.1.1. All other parameters were the same ones as the ones used for the LK models. Table 5.9 summarizes all three different runs and their respective performance metrics.

For NCI the unvegetated model has a reasonable to good performance across different parameters. However, it severely overestimates erosion, particularly at the southern end of the island (see Fig. 5.14C). When it comes to the dune crest evolution over the storm, the model also overestimates the erosion levels in both the south and the north, however, in the southern end, some areas experience over a meter of erosion compared to the post-storm measurements (see Fig. 5.15). The model improves significantly when vegetation is included both statically and dynamically. This is consistent with the results of models in LK island. The static vegetation model improves its model

run	vegetation	breach	z_b map		z_b crest		Δz_b map		Δz_b crest	
			skill	bias	skill	bias	skill	bias	skill	bias
NCI: run 1	no vegetation	✗	0.59	-0.41	0.75	0.31	0.62	-0.38	0.75	-0.31
NCI: run 2	NOPP static	✓	0.69	-0.30	0.89	-0.18	0.72	-0.28	0.89	-0.17
NCI: run 3	NOPP dynamic	✗	0.64	-0.37	0.81	-0.26	0.66	-0.35	0.82	-0.25

Table 5.9: *XBeach NCI runs, for the unvegetated case, static vegetation case and dynamic vegetation case along with their respective performance metrics. Highlighted in green is the best-performing model.*

predictive skill to excellent in the dune areas and to good in the areas above MHW, this means that the model increased in performance by approximately 19%. For the dune crest area, the static vegetation model is the only one that exactly predicts the breach location that occurred during the storm. Moreover, the static vegetation model is the only one that manages to keep the sediment on the island (Fig. 5.14D). The dynamic vegetation model still overestimates erosion throughout the model domain (see Fig. 5.14E). With model performance ranging between reasonable and good.

The most notable difference in these results is that including vegetation is crucial for low-lying barrier islands that are likely to suffer from overwash and inundation regimes. This becomes clear when analyzing Fig. 5.15, NCI is characterized by a southern end that is much lower in elevation compared to the northern end of the island. This difference in dune crest height results in completely different predictions from all models. For the lower dune heights found in the southern end, all models overestimate erosion, in some instances lowering the dune crest elevation by more than a meter compared to the measurements. Both the unvegetated and the dynamic vegetation model, predict a lowering of crest bed levels to below MHW over a distance of over 1 km. In contrast, the static vegetation model only breaches at the location of the actual breach. In contrast, the northern end (which starts from around km 2.7 alongshore), shows a much better predictive

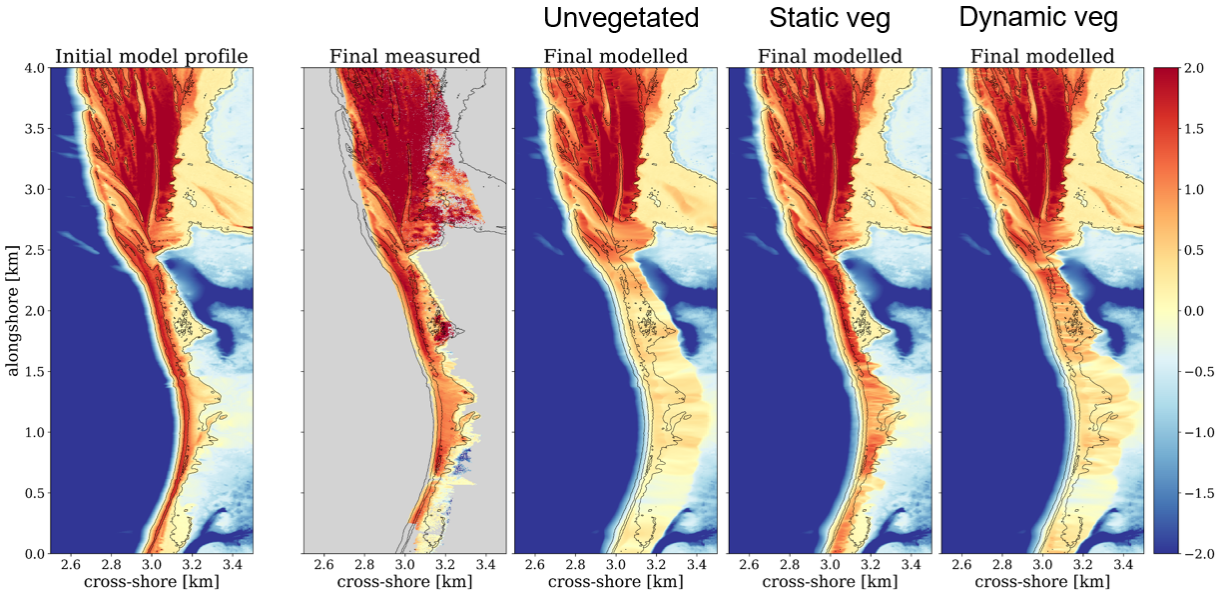

Figure 5.14: *NCI vegetation effects in XBeach. From left to right: A) pre-storm topography of NCI, B) post-storm measured DEM derived from SfM data at NCI, C) XBeach model results for the unvegetated case, D) XBeach model results for the static vegetation case, and E) XBeach model results for the dynamic/temporal vegetation case*

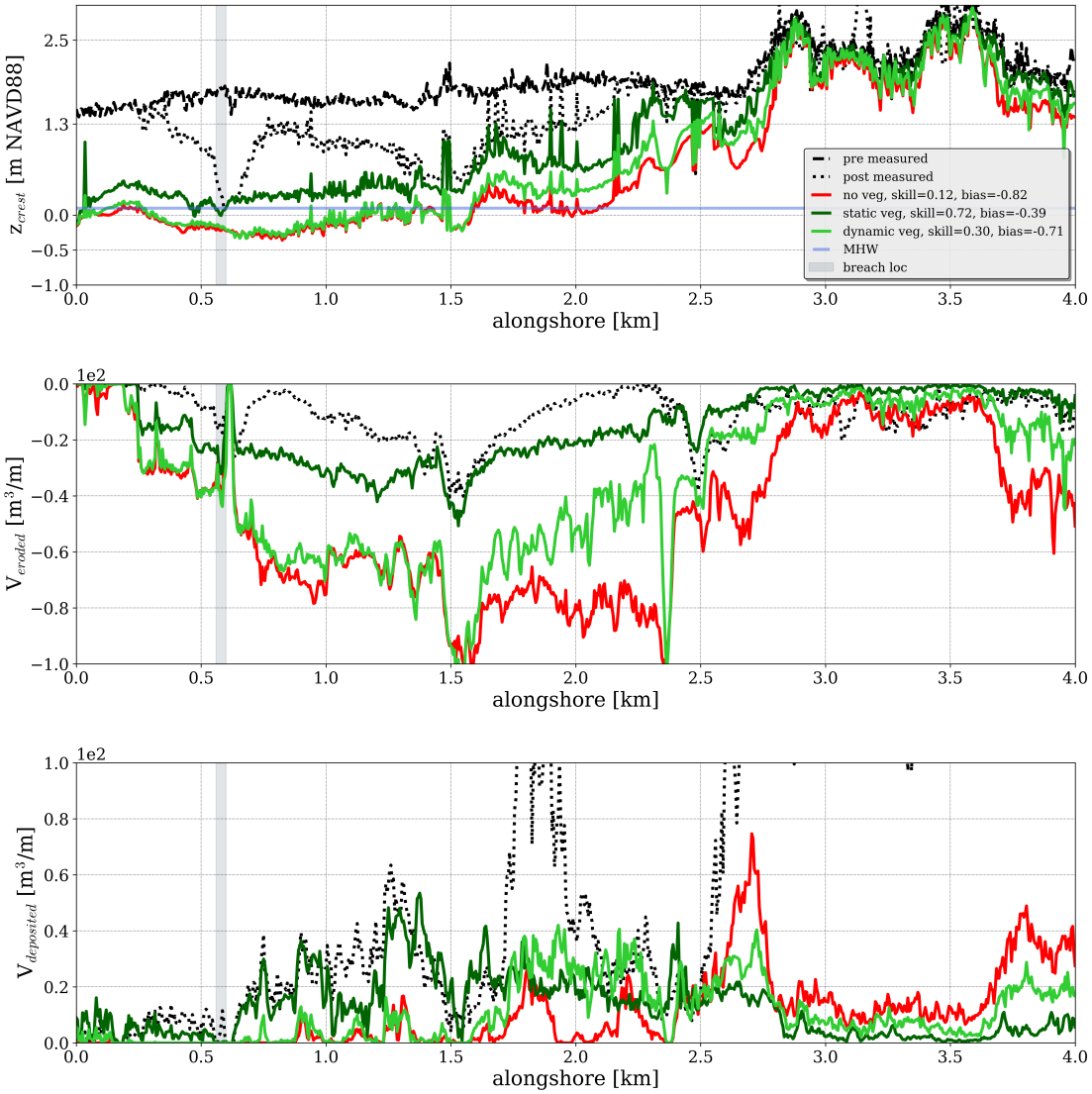

Figure 5.15: *NCI XBeach alongshore model results for dune crest height, erosion and sedimentation volumes. In red is the unvegetated case, in dark green is the static vegetation case and in lime green is the dynamic vegetation case.*

skill when compared to the measurements for all models. However, the unvegetated model still over-predicts erosion.

Overall, the NCI model results are consistent with the ones from LK. The best-performing models use static vegetation, with the NOPP land cover data set, along with the compiled Manning classification. These are desirable results as the compiled version of the vegetation data can allow for easy calibration of the roughness parameters. Moreover, the dynamic vegetation case adds more variables and uncertainty to a complex model that already carries many uncertainties.

5.2.7. Dune erosion processes

The main nearshore processes that are linked to flow conditions are the ones affected directly by changing the bed roughness coefficients to represent vegetation. It is important to understand the effects different roughnesses have on the hydrodynamics driving dune erosion, namely water levels, currents, long waves and short waves. This will understand the applicability of vegetation across different XBeach models. Since these processes drive erosion, changing the roughness coefficients also produces different erosional patterns. For example, across all the model simulations, the extent of flood and ebb fans varied significantly.

To understand these effects of having no vegetation, static vegetation, or dynamic vegetation; different cross-shore profiles were analyzed across LK and NCI. These cross-shore profiles were selected in areas that breached, experienced overwash and remained in collision regime. These profiles are shown in Figures 5.16 and 5.18. At each profile, the temporal evolution of the dune crest bed level was compared to different hydrodynamic conditions. Including, the water level gradient, which provides insight into the current velocities experienced across the profile, the short wave heights and infragravity waves at the toe of the dune. The temporal evolution of the profiles is also studied at four different time steps during the storm along with the spatial and temporal evolution of vegetation as shown in Figures 5.17 and 5.19.

Bed level changes

The bed levels varied significantly when vegetation was not included. These mainly result in cross-shore profiles that extend far into the sea. The erosional processes caused by storm surge ebb lead to strong sediment transport in the offshore direction. Resulting in large ebb fans across the entire domain. When little to no vegetation is present, the profiles of the models including vegetation extend just as far but the opposite occurs when vegetation is present (see Fig. 5.17 and 5.19, yellow vs dark green). Similar results are observed when it comes to flooding, as the unvegetated case shows far more deposition in the bay side compared to the vegetated cases. These occur for the dynamic case to a lesser extent. Particularly in areas where the vegetation was completely removed after the storm. The crest bed levels without vegetation have a more steep decline over time and in some instances, the lowering of the bed level starts before the ones including vegetation. Suggesting a delay in the storm regime transition.

Water levels

The water levels vary significantly between the seaside and the bayside as can be seen by the fluctuations in the water level gradient in Figures 5.16E and 5.18E. The largest gradient occurs a few hours before the peak of the storm and coincides with the maximum lowering of the dune crest. As a result, the main driver of dune erosion in the model is the cross-shore currents driven by water level gradients between the sea and the bay once an island is inundated or a breach occurs. The gradient continues to fluctuate after the peak of the storm, however, the erosional processes are significantly reduced for areas that did not breach. In those areas, the crest bed level remains constant after the peak of the storm (see Fig. 5.16D). However, the profiles with the most dune crest lowering suffer from a second major morphological change some time after the storm surge peak. This coincided with the moment in which cross-shore currents started flowing seawards due to the higher water levels on the bay side. In this instance, water level gradients are significantly higher again, and the currents caused by the gradient drive sediment transport offshore. This is the process responsible for creating ebb fans that can be at the third time step of Fig. 5.17. Overall, vegetation causes no difference to the water levels but it significantly reduces

the currents caused by the water level gradients once the island is inundated or breached. This in turn reduces the level of morphodynamic change; this can be observed by smaller overwash and ebb fans in addition to a lower rate of dune crest bed level change.

Short waves
The largest significant wave heights align for both models with the peak of the storm surge. However, the wave heights are already considerably higher before the peak of the storm, already reaching above 2 m (see Figures 5.16F and 5.18F). The combination of high water levels and wave height likely caused the initial dune crest lowering that occurs before the peak of the storm. Interestingly, the profiles that were lowered significantly during the maximum water level gradients suffered secondary reduction after the peak of the storm. At this time, the water level gradients are higher again but the significant wave heights are at their peak too, this suggests that waves may have contributed to this secondary erosion. This process is reinforced with more erosion, as the lower bed levels and higher water levels allow waves to break much later and carry more energy to impact the dune. Vegetation only affects the wave heights as morphological changes occur within the model for different vegetation models, but vegetation has no direct impact on the short waves in the model.

Long waves
Similarly to the significant wave heights, the infragravity waves are calculated at the toe of the dune. The largest infragravity wave heights also occur shortly after the peak of the storm surge and their peak aligns with that secondary reduction observed across certain cross-shore profiles. This suggests that long waves also play a role in the second major morphological changes that occur after the peak of the storm. Long waves were not impacted by variations in vegetation and reproduced the same infragravity wave heights across all vegetation cases studied in this section.

To summarize, the major changes in bed level occurred before the storm surge peak when the water level gradients between the bay and sea were at their highest and the island was inundated or breached. The sediment is mostly transported landward by the cross-shore currents caused by the gradient. Vegetation affected the steepness in which bed levels were reduced and in some instances, a delay was observed when comparing the unvegetated and static vegetation cases. Short waves and long waves reached their peak at the same time as the storm surge ebb peak. It is believed that the waves play a role in increasing the sediment available for transport by the offshore directed currents. This combination of waves and storm surge ebb drives the secondary erosional process occurring in areas that suffered major morphodynamic change. Overall, including vegetation as a bed roughness coefficient only causes differences in currents and has no influence over water levels, wave heights and infragravity waves.

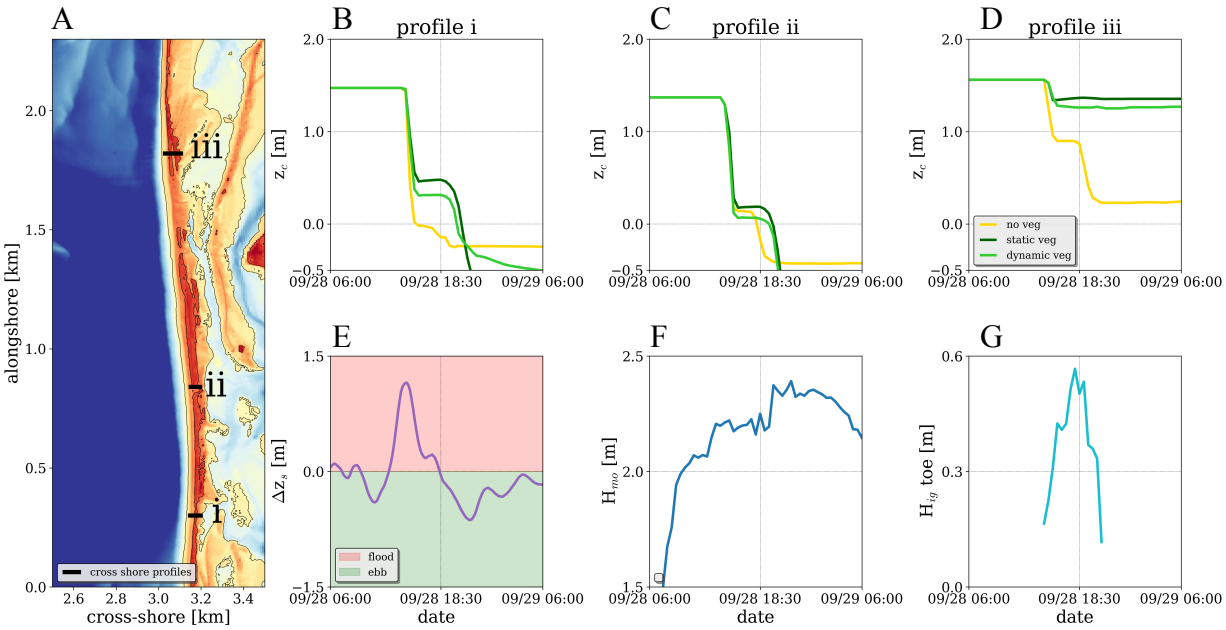

Figure 5.16: *LK bed level change and hydrodynamic conditions at three distinctive cross-shore profiles for the unvegetated, static vegetation and dynamic vegetation cases. A) Location of the three profiles along the island. The top row including Fig B, C and D shows the temporal evolution of the dune crest bed level for the three vegetation cases. E) Water level gradient between bay and sea. F) the significant wave height and G) the infragravity wave height*

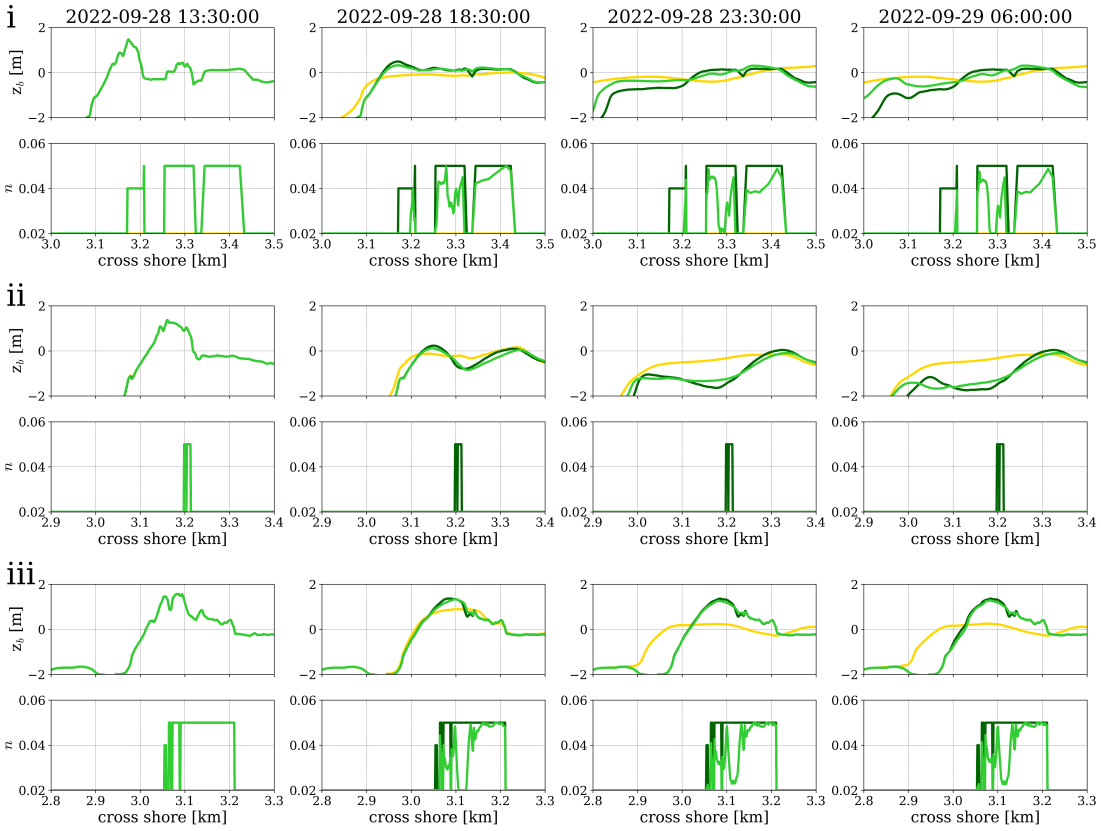

Figure 5.17: *LK cross-shore profile and vegetation as Manning roughness coefficient evolution over time.*

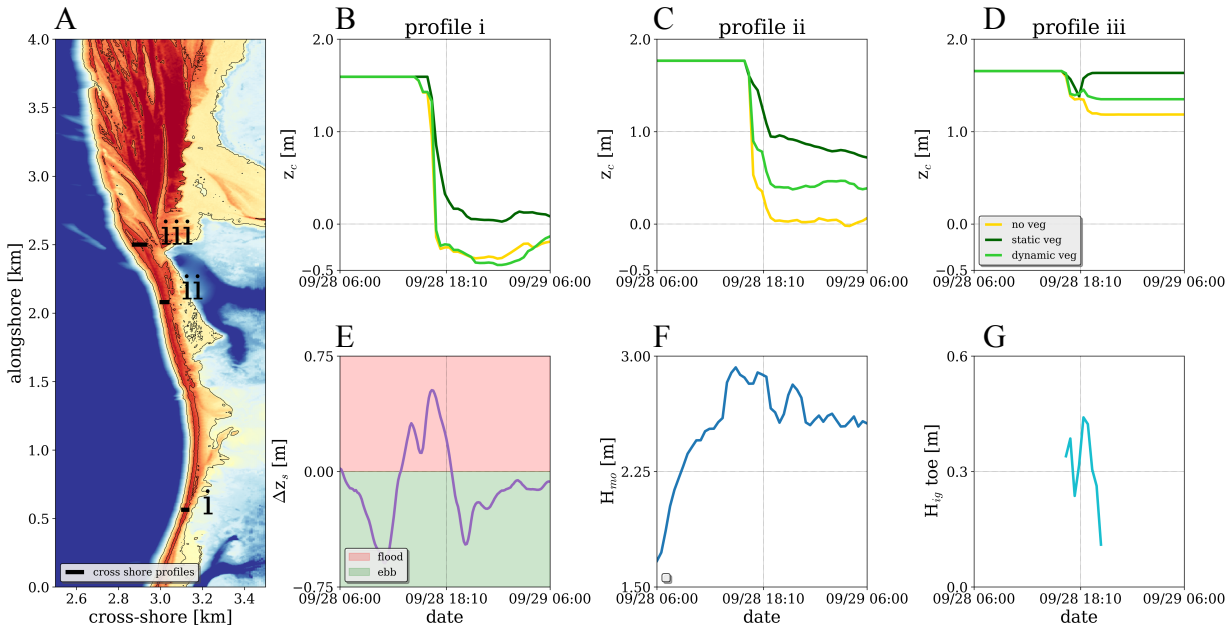

Figure 5.18: *NCI bed level change and hydrodynamic conditions at three distinctive cross-shore profiles for the unvegetated, static vegetation and dynamic vegetation cases. A) Location of the three profiles along the island. The top row including Fig B, C and D shows the temporal evolution of the dune crest bed level for the three vegetation cases. E) Water level gradient between bay and sea. F) the significant wave height and G) the infragravity wave height*

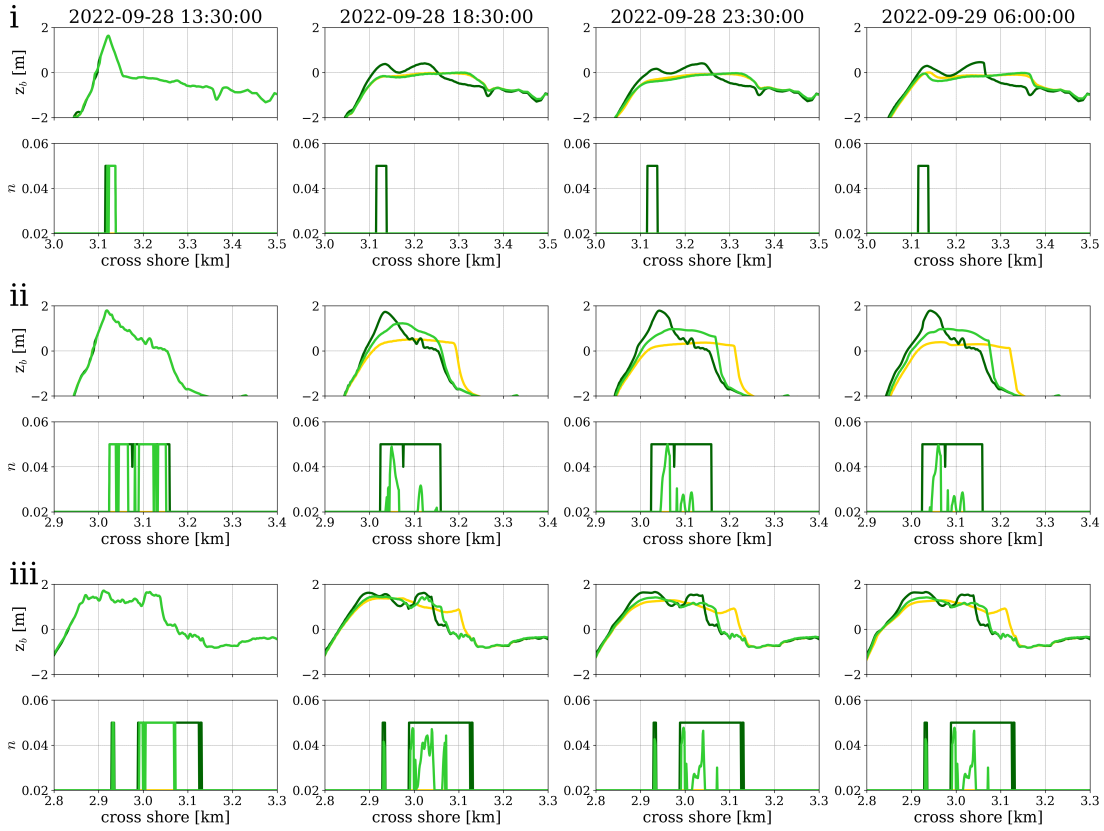

Figure 5.19: *NCI cross-shore profile and vegetation as Manning roughness coefficient evolution over time.*

5.2.8. Storm regimes

Understanding the effects of including vegetation by means of the Manning roughness coefficient across different Sallenger, 2000 storm regimes is crucial for its application in other regions across the globe. Three different areas are identified in which the collision, overwash and inundation regimes occur. LK island suffered complete inundation as the storm surge water level was much higher than its maximum dune crest elevation. The southern end of NCI island was mostly in the overwash regime with a few areas that went into the inundation regime, particularly near the breach. The northern end of NCI remained in the collision regime throughout the storm. These three areas are further analyzed to determine the influence of the unvegetated, static vegetation and dynamic vegetation models across different regimes.

Collision
The northern end of NCI island remained mostly in the collision regime throughout the storm. This area suffered significantly less erosion when compared to the other areas that went into overwash or inundation regimes. In Fig. 5.15, it can be observed that in the northern end, which starts after approximately 2.5 km alongshore, the different vegetation models approximate the measurements well. The unvegetated model overestimates the erosion slightly, but the variations between the vegetated models in the collision regime are negligible compared to the differences for the overwash or inundation regime. Nevertheless, when analyzing the metrics for the alongshore dune crest elevation and the erode volumes, the static vegetation performs the best. In Fig. 5.18, the profile iii is located in a collision regime area. However, the vegetated and dynamic vegetation models both lower the dune crest, meaning that that particular area went at least into the overwash regime for those two models. The static vegetation model in this instance, maintains the pre-storm dune crest elevation. The different vegetation cases result in minimal differences when a region remains in a collision regime. This suggests that in areas with large dunes that remain in collision throughout storms, vegetation can be ignored in models. Nevertheless, the overall performance of the model is much better when vegetation is included.

Overwash
The southern end of NCI experienced mostly the overwash regime and had significant morphological change. Several overwash fans developed throughout the storm. In this area, the vegetation models differ significantly across multiple variables. The unvegetated model performs poorly across all variables and severely overestimates erosion. The best-performing model is the static vegetation, not only does it have an excellent predictive sill but it also predicts the exact location of the breach. It is particularly good in replicating deposited volumes, this becomes more apparent when observing the spatial extent of the overwash fans and how they are in the same order of magnitude as the measured ones. Ultimately, areas that experience overwash regimes need to include vegetation in XBeach models.

Inundation
The whole of LK island went into the inundation regime. The scenario is similar to the overwash one, when vegetation is not included, erosion is severely overestimated and the models perform poorly. When an island is inundated and vegetation is included, the erosional impact is reduced by reducing sediment transport both landward and seaward. This results in improved storm erosion forecasts with XBeach models.

5.2.9. Best performing models

The best-performing models for both LK and NCI are the ones with the static vegetation using the NOPP 2019 data set, with the compiled version of the Manning roughness coefficients.

Lovers Key

The LK model has a reasonable to good predictive skill across multiple variables. Remarkably, the model predicts the breach location (at 0.8 km alongshore) with extreme accuracy and the location of other channels that did not breach during the storm in the northern end. The only downside is that the model predicts a breach that did not occur at the south end of the island. This breach is likely caused by a poor representation of the vegetation located in that area. For instance, it did not occur when using the NLCD data set. Nevertheless, including vegetation in the model improved results significantly. Particularly when using the static vegetation with the compiled roughness classes.

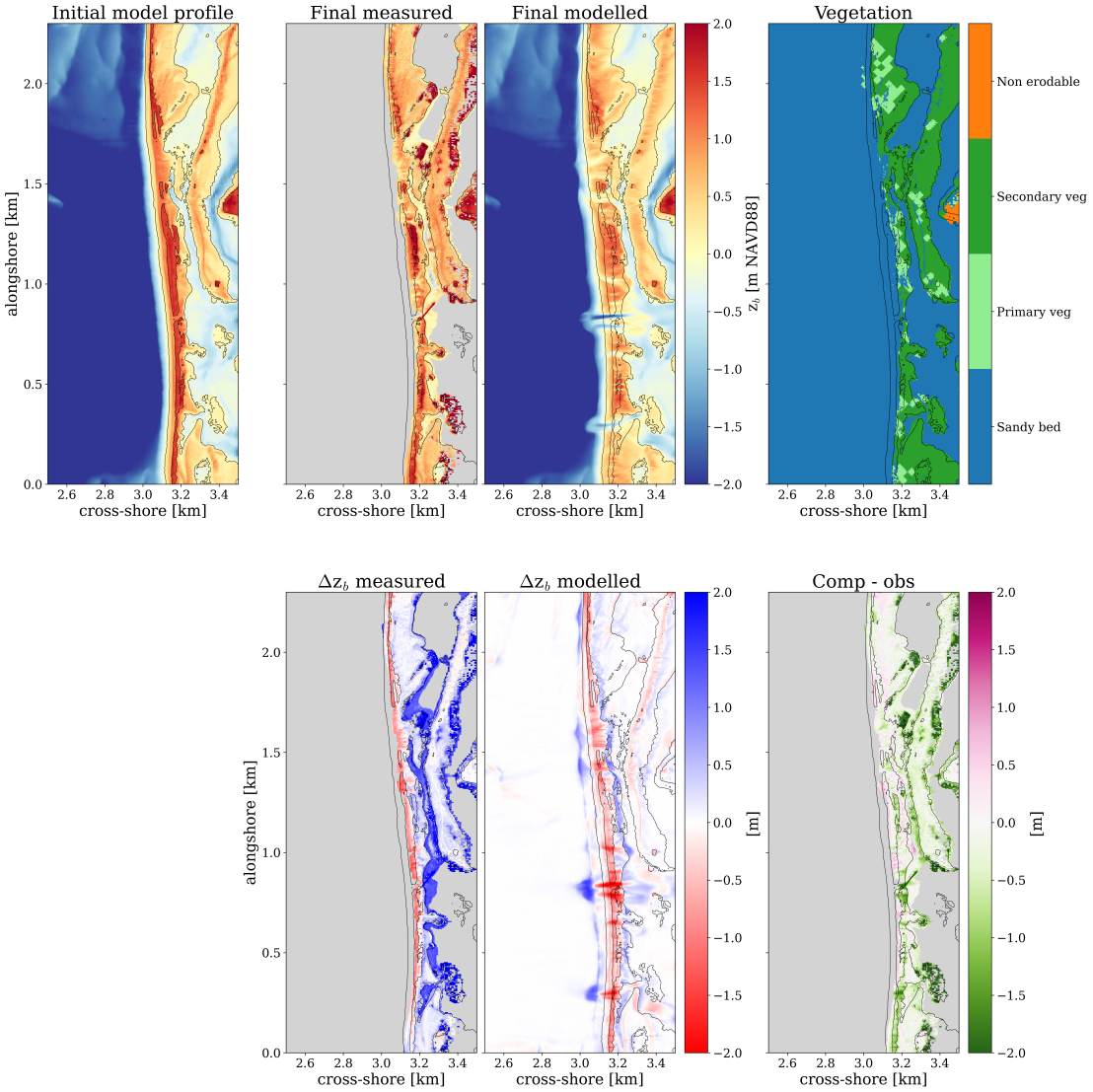

Figure 5.20: *LK XBeach model results for best performing configuration. run 3b, with static vegetation based on the NOPP land cover data and using the compiled Manning coefficients.*

North Captiva Island

The NCI model has good to excellent predictive skills across all the variables analyzed in this section. This model accurately predicted the breach location and managed to retain all the sediment in the island as can be seen in Fig. 5.21 final modelled and in 5.21 Δz_b modelled. This also can be observed in the measurements. Another success is the extent of the overwash fan near the breach at approximately 3.2 km cross-shore and 0.6 km alongshore. The spatial extent of the breached fan in XBeach is similar to the extent of the measured fan. These model results were only achieved when the static vegetation model was used. Including vegetation statically in the model played an important role in improving the prediction of the southern end of the island that experiences overwash and inundation regimes.

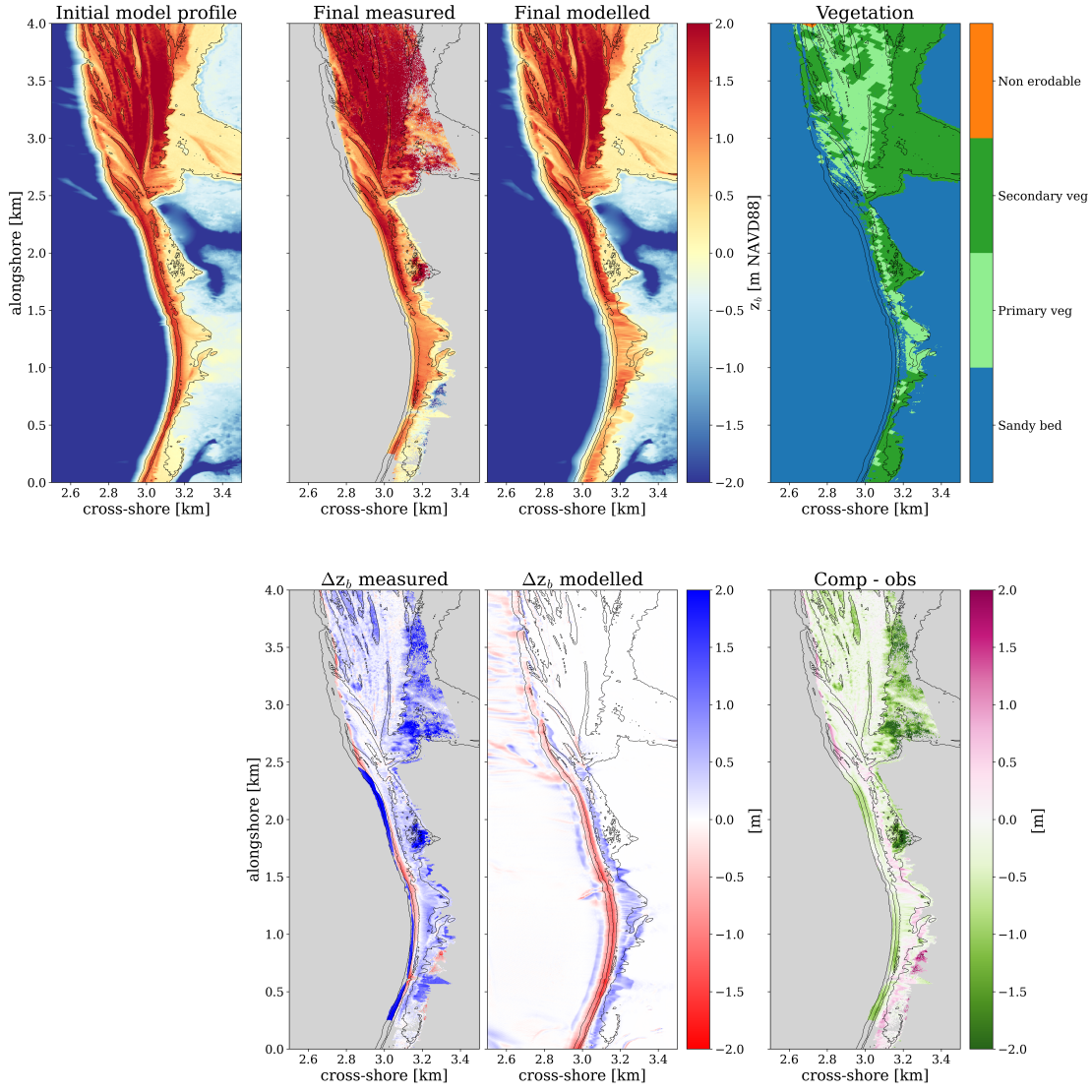

Figure 5.21: *NCI XBeach model results for best performing configuration. NCI: run 2, with static vegetation based on the NOPP land cover data and using the compiled Manning coefficients.*

5.3. Summary

This chapter describes the approach taken to model morphodynamics in XBeach and covers the results of applying varying vegetation conditions to the model.

The first section discusses the modelling approach, covering the base model setup, vegetation implementation, and model evaluation methods. The base model setup includes a constant domain size, grid resolution, bathymetry, boundary conditions, and general XBeach parameters that are used for all simulations. Vegetation is implemented both statically and dynamically using various LULC data. These vegetation data sets were converted into bed roughness using the Mattocks and Forbes, 2008 table or the complied version described in this chapter. The model's results are assessed using performance metrics and the Sallenger storm regimes.

The XBeach models were set up with three main scenarios: unvegetated, static vegetation, and dynamic vegetation cases. The findings indicate that all models tend to overestimate erosion but the static vegetation case was the best-performing model for both LK and NCI. This model was able to predict the exact breach location for both islands. From all the different runs with varying roughnesses and data sources, the best LULC data set to use was the NOPP 2019, using the compiled version of the bed roughness coefficients. This section also examines the effects of vegetation on the main drivers of dune erosion, including water levels, currents, short waves, and long waves. Vegetation primarily influences currents and wave heights but not water level gradients and infragravity waves. The model results highlight the importance of including vegetation in models that experience overwash and inundation regimes. However, for areas in the collision regime, all the differences between the cases are less significant but the static vegetation model is still the best case.

6

Discussion

This chapter discusses the results of the data analysis and the morphodynamic models conducted with XBeach. First, the different methods of including dune vegetation are discussed based on the model results for Lovers Key (LK) and North Captiva Island (NCI). These methods included several static vegetation data sets from varying sources and dynamic vegetation models that account for vegetation removal during a storm. This is followed by a discussion of the influence of vegetation in dune erosion processes based on the data analysis and model results. The data analysis lacked hydrodynamic data and this missing information was investigated by analyzing the effects of vegetation on hydrodynamic conditions and storm regimes based on model results. Subsequently, the model uncertainties are discussed based on their level of impact in XBeach. Finally, the limitations of these studies are outlined, which include the use of data gathered 4 years before Hurricane Ian, the analysis of a single storm, the processing of the available data, and the modelling practices and model limitations.

6.1. Influence of vegetation on dune erosion

The influence of dune vegetation during storms was done by conducting a thorough data analysis of dune geomorphic features, erosion volumes and dune vegetation for LK and NCI. From the data collected for Hurricane Ian, visual data indicated that unvegetated paths that align with local elevation depressions are potential weak points in barrier islands. Coincidentally, some of these paths align with areas that have high human traffic that may hinder vegetation growth and lower ground elevation even further. It is also possible that the vegetation surrounding the unvegetated path further increases erosion along the path. The observations taken during this storm are not sufficient to validate this hypothesis. To prove this, additional data is needed from different areas and storms where breaches occurred where vegetation was present. The data needs to be a combination of pre and post-storm, aerial images, topographic surveys and vegetation measurements.

The analysis of elevation maps along with vegetation data indicate that areas with high vegetation coverage suffered less erosion than the less vegetated areas. That is the case for LK, however, NCI island also had higher and wider dunes in the areas with more vegetation coverage. This means that for NCI there is a strong correlation between vegetation coverage and high and broad dunes. This was found mostly in the northern end of the island, where coincidentally lower erosion volumes per transect occurred during the storm. In contrast, the southern end of the island experiences flooding and higher erosion volumes which coincides with low-narrow dunes and with low vegetation presence. The results from both islands indicate that vegetation is indeed

correlated to erosion volumes. In the case of both islands higher vegetation coverage results in lower erosion volumes. However, it is not possible to discern from this data if vegetation alone was responsible for this trend, as higher and wider dunes were found in the highly vegetated areas. More measurements taken across different storms need to be analyzed to determine if vegetation alone can reduce dune erosion levels. Another possibility is that the dynamic interactions of dune vegetation with dune geomorphic features result in reduced erosion levels when more vegetation is present. Higher vegetation helps build up dunes by increasing the deposition of sediments transported by aeolian transport (Van Puijenbroek et al., 2017). This likely means that dune growth and vegetation play a dynamic reinforcing mechanism (Maximiliano-Cordova et al., 2021), therefore is not surprising to find the more robust dunes where vegetation coverage is higher.

Unfortunately, without hydrodynamic measurements near the island, it is impossible to determine vegetation's influence relative to the hydrodynamic conditions that drove the erosion processes. To understand the effects caused by vegetation on hydrodynamics, the results of the models that included vegetation can be compared to the unvegetated model to determine the effects of dune vegetation on hydrodynamics and storm regimes.

6.1.1. Effects on hydrodynamic

The effects of including vegetation in XBeach as a roughness parameter had significant effects on the current velocities and wave heights. The effect on currents was not surprising, as the bed friction coefficient directly affects the flow in XBeach. By reducing the current, the sediment transport capacity is reduced and as a result, the overwash fans and ebb fans are significantly reduced in extent. These effects are similar to what would be expected to occur in reality.

Water levels were affected due to the inclusion of vegetation as the vegetated dunes underwent a delay and more gradual dune crest lowering. This resulted in variations in water level gradients between the sea and bay. Which were the primary drivers of dune erosion. Similarly to water levels, the wave heights were mainly affected by the inclusion of vegetation due to the changes in morphodynamics. The unvegetated cases had a faster dune lowering which resulted in higher wave heights at the toe of the dune. Including vegetation in XBeach affects wave heights and water levels indirectly through different morphodynamic changes.

Infragravity wave heights were not affected by the inclusion of vegetation. This is an expected result as infragravity waves are able to travel all the way to the coast and reach the toe of the dunes without breaking (Bertin et al., 2018).

6.1.2. Effects on storm regimes

The Sallenger storm regimes can be determined by analyzing pre and post-storm elevation data. However, the transition moment cannot be determined without hydrodynamic data. The simplified collision and flood regimes described in Chapter 4 required knowledge of the maximum water level during the storm. With that hydrodynamic information, it is possible to combine elevation data and the maximum water level to determine if a certain area experienced a flood or remained in the collision regime. Those results show that LK went fully into flood regime and 55% of NCI experienced flooding as well. The areas that experienced flooding had lower dunes which aligns with the research conducted by (Houser et al., 2008; Maximiliano-Cordova et al., 2021).

From that analysis it can only inferred that vegetation had more presence in areas that remained in collision, however, these areas also align with higher and broader dunes. To determine if

vegetation affects storm regimes, the data from the XBeach models was used. In the models, it was observed that models with vegetation experienced delays in dune crest lowering compared to the case where no vegetation was included. This delay in dune crest lowering could be associated with a delay in regime transition due to vegetation. This type of delay in regime shift has been observed in flume experiments that tested vegetated and unvegetated dunes (Bryant et al., 2019).

6.2. Inclusion of dune vegetation in XBeach

Dune vegetation was not initially included in XBeach models, it was until much later that some studies began to test the inclusion of dune vegetation in XBeach models. Lodewijk et al., 2015 included vegetation based on satellite data and applied a uniform friction coefficient for all vegetated areas. Later on, Passeri et al., 2018; Schambach et al., 2018 included vegetation based on LULC data. These methods here are defined as static vegetation methods. New methods have been implemented by Schweiger and Schuettrumpf, 2021a; Van Der Lugt et al., 2019 to take into account vegetation removal during storms. These are the dynamic vegetation methods. The static vegetation method and the dynamic vegetation method by Van Der Lugt et al., 2019 were tested in this study to determine the best method to include vegetation in XBeach to predict dune erosion during Hurricanes; the results are discussed here.

6.2.1. Manning roughness coefficients

Vegetation maps derived from LULC data are commonly used for coastal modelling applications. This is done by assigning Manning roughness coefficients to different vegetation classes. One of the most caused conversion tables is the Mattocks and Forbes, 2008 table, which has 25 different roughness classes derived from river engineering applications. Similar to that table, Makris et al., 2023 developed a new classification for coastal models, with up to 36 different classes. The Manning roughness coefficients are very specific in these two conversion tables. This can provide a false sense of choosing the exact values specific to a type of vegetation or sediment. When in reality, these values are not validated by physical models or measurements. Simplifying these tables proved to be successful in this study. The Mattocks and Forbes, 2008 table was reduced from 25 classes to just 4. The results of using the compiled classification not only improved the model skill but also eased the process of calibrating with bed roughness coefficients. This approach can streamline the coastal modelling process of including dune vegetation as it provides a more straightforward implementation method. The simplified bed roughness classification improved the model results for the two barrier islands, however, this is the case for a single storm and areas with similar features. To determine if the compiled method improves results, it must be tested at different locations during different storms.

6.2.2. Static vegetation in XBeach

Three different LULC data sets were tested statically in XBeach to determine the importance of varying spatial resolutions of vegetation. These were compared only using the compiled roughness classification. The three different data sets tested in the model had varying resolutions ranging from 30 to half a meter resolution. Overall, the NOPP data set (30-1m resolution) provided the most accurate predictions. However, the differences between data sets were at a maximum of 11% and all models had good predictive skill. This is a desirable result, as LULC data like the NLCD or NOPP data set can be used when available for coastal models like XBeach. The LULC data set

computed using a supervised machine learning (SML) model also performs well. This type of model can be used to quickly classify aerial images taken right before the storm. Thus providing the most up-to-date vegetation data to the model. This is particularly useful for locations that do not have public LULC data sets. Further research in this area is necessary to improve the classification methods of vegetation from aerial images. To summarize, implementing vegetation statically improved the model skill for all the different data sets tested, especially when compared to the unvegetated case. The high-resolution LULC data set provided better results, but the main finding is that vegetation must be included to improve the XBeach model output regardless of the LULC data set used.

6.2.3. Dynamic vegetation in XBeach

Dynamic vegetation in this research was included by using the Van Der Lugt et al., 2019 model. This model performed much better than the no vegetation case but fell short of the static vegetation model across all variables compared. The model overestimates dune erosion due to its linear decrease in roughness as soon as the bed is eroded. This does not follow the natural uprooting process of plants (Schweiger & Schuettrumpf, 2021a, 2021b). The plant in most instances will remain in place until strong currents are able to uproot it instantly or the bed level has eroded all the way to the bottom of the roots. In numerical models, it is difficult to include sudden changes like the uprooting process as they may lead to numerical instabilities. For this reason, decreasing the bed roughness linearly prevents instabilities. However, this is a poor representation of what occurs in reality, therefore other studies have suggested an exponential decrease Schweiger and Schuettrumpf, 2021a. Alternatively, instead of reducing the bed friction as soon as erosion begins, a buffer can be implemented to maintain the roughness coefficient and after a certain erosion depth reduce the friction coefficient linearly up to the root depth. Overall, the static vegetation model performed significantly better than the dynamic vegetation model. Suggesting that the dynamic vegetation model may not be essential for achieving the best results at this time. To improve this dynamic vegetation model, the uprooting process must be further researched. With the help of flume experiments or field observations.

6.3. Sensitivities

Understanding the sources of uncertainty in models like XBeach can help guide future areas of research aimed at reducing the uncertainties of the model. The results of this study have provided insights into the input parameters that provide the uncertainties in predicting dune erosion during storms. To start, the following list summarizes the input parameters to which the model displayed higher sensitivity.

- **Bathymetry:** Differences in bathymetry can cause significant differences in model skill, some areas experienced differences in crest lowering of up to 1 m. Higher resolution bathymetric data was able to reproduce breach location more accurately as local dune depressions are more accurately represented in the model.
- **Inclusion of vegetation:** Including vegetation as a roughness parameter compared to the cases without vegetation improved model skill from poor to good and excellent in some instances. With vegetation improving model skill by 13% to 30% depending on the variable studied. The model results are extremely sensitive to the inclusion of vegetation and it should be included.

- **Water levels:** The model results can differ significantly based on the water levels. It is therefore necessary to improve the forecasting of water levels when derived through other models. However, in coastal applications achieving errors of 10 to 20 cm in water levels is extremely difficult. Thus morphodynamic modellers must take into account these uncertainties in water level predictions.

Other input parameters displayed sensitivities in the model results. However, these were not as significant as the ones discussed above. The next list comprises the parameters to which the model showed less sensitivity.

- **Spatial resolution vegetation:** The differences in model performance provided by LULC data with different resolutions are minimal. This is likely related to the fact that most data sets are derived from satellite or aerial images. However, in this case, the higher-resolution data set performed the best. As a result, when available the highest resolution data set should be used. Public LULC data sets are not available for all locations and are published every 4 years in the case of the USGS data sets. It is therefore important to improve machine learning algorithms like the machine learning model by Buscombe and Ritchie, 2018. With these data sets the most up-to-date vegetation data can be included in models.
- **bed friction coefficients:** Variations to the bed friction coefficients for each vegetation class do not change model skill significantly. With a simplified classification for different vegetation, this parameter can be easily calibrated to improve model results.
- **wave heights:** The model sensitivities to waves were minimal with variations in skill never going over 3%. This means that improving the accuracy of models that predict water levels is more important than improving the accuracy of wave models when using XBeach as the morphodynamic model.
- **root depth:** Changing the root depth in the dynamic vegetation model caused small differences in model skill. This value should be selected based on the local vegetation and a better understanding of the uprooting process.

To summarize, XBeach models require detailed bathymetries, inclusion of dune vegetation and accurate water level conditions to provide an accurate prediction of dune erosion during storms.

6.4. Limitations

This section describes the major limitations encountered in this research. Including spatiotemporal evolution of the studied areas over the time gap between available data sets, use of one single storm, processing of the available data, uncertainties in model parameters such as the bed friction coefficients, and models.

Spatiotemporal evolution

This study conducted most of the analysis using data that dated 3 to 4 years back from the date of Hurricane Ian. This is a large time span in which the barrier islands studied underwent several changes, including morphology, vegetation growth/reduction, and urban development. With the current data, pre-storm aerial images compared to images taken four years prior showed some vegetation growth, little urban development and some morphological changes along the coast. The area with the most morphological change is excluded from the analysis. Furthermore, the time gap as the pre and post-storm data was of high quality and no extreme events occurred in that time frame that resulted in major changes to both islands.

One storm one location
This study focused on Hurricane Ian and analyzed the area impacted by this single storm. Which consists of low-lying barrier islands. To further validate the results of this study, other storms and areas with different geomorphic features need to be investigated. This will allow not only for validation of these results but also for understanding the influence of vegetation in coastal dunes at a much larger scale. Studying a broader spectrum of dunes and their vegetation will help coastal managers worldwide apply morphodynamic models such as XBeach. Other studies have used vegetation in coastal models and showed promising results (Lodewijk et al., 2015; Makris et al., 2023; Passeri et al., 2018; Schambach et al., 2018; Van Der Lugt et al., 2019). Nevertheless, more research needs to be conducted to account for all possible vegetation conditions and the best ways to introduce them in coastal models such as XBeach.

DEM to DSM
This study relied heavily on post-storm data collected with SfM technology. This data was available as a DSM that was converted to a DEM using the ROTO tool developed by Lindsay, 2018. Unfortunately, no other data was available such as ground points to validate the conversion from the DSM to DEM.

Bed friction coefficients
Traditionally, the bed friction coefficients are common calibration parameters for hydrodynamic and morphological models. Since vegetation is now included as a roughness coefficient which is derived from conversion tables, there are many uncertainties associated with the selection of each roughness value for different land cover classifications. To get the appropriate manning coefficients for each land cover class, several physical experiments and measurements need to take place (Mckay & Fischenich, 2011). This would be a lengthy and expensive undertaking, therefore it is likely that the bed friction coefficient will continue to be used as a calibration parameter in numerical models.

XBeach
XBeach is a numerical model that simulates several processes. This research is limited by the limitations of this model. Several uncertainties occur within this model, which come mainly from the simplification and parametrization of physical processes that drive dune erosion. One major limitation, in the $surfbeat$ mode is that short waves are not resolved and the effect of short waves on sediment transport is not clear. A more accurate implementation of both the long waves and short waves in XBeach can potentially improve model results. In terms of vegetation, including vegetation only as a bed roughness coefficient has no effect in damping the waves in the model, it only reduces the flow. This is another limitation of the XBeach model. Including a wave damper where vegetation is present would be closer to the effects that occur in reality. This has been done by means of the XBeach vegetation module, but it requires more detailed data such as vegetation stem diameter and density. This data would be difficult to obtain in many areas and it is difficult to parameterise. The best-performing models for the two barrier islands studied have impressive results in XBeach. Breaches were replicated in the exact locations, and the final bed levels resemble the observed post-storm morphological changes. While XBeach still has many limitations, the current model is an excellent tool that can provide excellent insights and forecasts of dune erosion during hurricanes.

7

Conclusion and recommendations

7.1. Conclusions

The objective of this master thesis was to ***improve the inclusion of vegetation in XBeach models to reduce uncertainty in predicting dune and beach erosion during storms***. Hurricane Ian was selected as the storm for the study and extensive data analysis and morphodynamic modelling of two barrier islands Lovers Key (LK) and North Captiva Island (NCI) located in southwest Florida was conducted. The results show that Hurricane Ian caused significant morphological change and that including vegetation in XBeach models is crucial to accurately predict dune erosion.

The overall research objective was divided into four research questions and their individual conclusions are outlined below:

1. **What was the erosional impact of Hurricane Ian and the influence of vegetation?**

Section 4.2 of Chapter 4 analyzed the data pertaining to Hurricane Ian and its impact on the regions of NCI and LK. The storm caused substantial erosional effects on both islands, resulting in breaches, extensive overwash fans and storm surge ebb fans. Upon visual inspection, it was evident that the two breaches occurred predominantly along pathways devoid of vegetation, aligning with local topographic depressions. This observation suggests that these pathways are potential weak points susceptible to breaching during similar storm events. However, more empirical observations are needed to corroborate this hypothesis.

When comparing dune vegetation coverage and dune geomorphic features to the eroded volumes, a significant correlation was discovered. Regions with higher vegetation density experienced less erosion during the storm, whereas areas with low vegetation coverage exhibited higher eroded volumes along both islands. Additionally, dunes characterized by greater height and width experienced less erosion compared to their shorter and narrower counterparts. However, based on this data analysis alone, it remains inconclusive whether vegetation alone was solely responsible for the reduction in eroded volumes along the islands. Thus, it is deduced that higher and wider dunes, coupled with dense vegetation cover, tend to endure less erosion when compared to lower, narrower dunes with sparse vegetation. Further investigations are necessary to delineate the individual contributions of these factors in erosion mitigation.

2. **How can we improve the inclusion of dune vegetation in XBeach?**

In Chapter 5, several XBeach model setups with varying vegetation parameters were tested. Vegetation in this study is implemented by converting LULC data into bed friction coefficients. To do this, the Mattocks and Forbes, 2008 classification table was used and a compiled version of it. The compiled version simplifies the 25 classes of Mattocks and Forbes, 2008 into four different classes based on urban features, two vegetation zones and sandy beds. These two classification tables were tested across two LULC data sets and while the differences in the model skill were small, the compiled classification improved the model skill overall. Improving the model skill by means of a reduction in Manning classes is a success as it eases the calibration of roughness coefficients to improve model prediction.

The importance of the spatial resolution was tested by three different LULC data sets. Two were obtained from public data sets and one was derived by means of a supervised machine-learning model (SML). The results were best for the high-resolution data set, but the differences in model skill were not significant. This is also a meaningful result as when no high-resolution LULC data is available, lower-resolution data sets will also perform well. Furthermore, the SML model showed promising results, this type of classification system can be used to classify images taken just before the storm, thus providing the most up-to-date data.

Finally, three main cases were compared, no vegetation, static vegetation and dynamic vegetation. Both vegetated models demonstrated a significant improvement compared to the unvegetated case. However, the dynamic model tended to overestimate erosion, exhibiting a model skill ranging from reasonable to good (BSS: 0.48 to 0.63). Conversely, the static vegetation model showcased good model skill (BSS: 0.6 to 0.77). Based on the findings of this study, incorporating vegetation using a reduced classification system derived from a high-resolution LULC data set is presently considered the most effective method to integrate vegetation as bed roughness into XBeach models.

3. **What are the largest uncertainties in the inclusion of vegetation in XBeach models?**

The largest uncertainty in including vegetation in XBeach models is not including it at all. The results between the unvegetated case and the two vegetated cases are drastically different. The unvegetated model skill ranged from poor to bad (BSS: -0.12 to 0.18) and the vegetated model skills improved to good and excellent (BSS: 0.6 to 0.89). Once vegetation is included, three major uncertainties are encountered: spatial resolution of vegetation, the value of manning roughness coefficients, and dynamic or static vegetation. The major uncertainty is choosing the dynamic model which can reduce model skill by up to 20%. Compared to 10% for the vegetation spatial resolution and 8% for roughness coefficients. It must be noted that the sensitivities also varied depending on the Sallenger storm regime encountered. Areas that remained in the collision regime were less sensitive to the presence of vegetation. However, the results were not negatively affected by the inclusion of vegetation.

Moreover, vegetation is not the only major source of uncertainties in XBeach models. Two other major uncertainties were identified, bathymetries and water levels and to a lesser extent wave heights. Varying water levels by $\pm$ 10% caused differences in predictive skills of up to 13%. The use of high-resolution bathymetry data sets is important. The lower-resolution data set that did not capture local dune depressions was not able to predict breaches with high accuracy. Varying

wave heights by ± 10% on the other hand, only result in 3% differences in model skill. These additional sources of uncertainty are just as important as the main vegetation ones. To summarize, XBeach models require detailed bathymetries, need dune vegetation to be included and require accurate water level conditions to provide an accurate prediction of dune erosion during storms.

7.2. Recommendations

7.2.1. Steps to improve dune erosion predictions in XBeach

The following list summarizes the recommended steps to improve predictions of dune erosion in vegetated areas:

- Include high-resolution pre-storm bathymetry; if available less than 30m.
- Numerical grid resolution that captures enough critical topographic details such as topographic lows in dune crests. If computationally feasible, use the same resolution as your bathymetry resolution.
- Include accurate hydrodynamic forcing and limit were possible its uncertainties.
- Use high-resolution LULC data and convert it into a simplified data set based on dune vegetation zones.
- Convert these classes into bed friction coefficients and calibrate them when necessary.

These steps highlight the need for accurate pre-storm data sets. More measurements are needed in order to provide more up-to-date data sets and reduce uncertainties from time gaps between the last collected data set and the date of the storm.

7.2.2. Understanding of the role of vegetation in erosion processes

There is a consensus that vegetation plays an important role in dune resiliency to storms. However detailed physical processes that take place during storms are not well understood. This is highlighted by the recent findings of Feagin et al., 2023 in which it was found that vegetation accelerates dune erosion in extreme storms. It is clear that more studies need to be conducted that focus on the effects that vegetation causes on hydrodynamics and sediment transport during dune erosion. In addition, the physics of key processes such as uprooting and their effects need to be better understood.

7.2.3. Dynamic vegetation

The dynamic vegetation model by Van Der Lugt et al., 2019 reduces the roughness coefficient linearly as soon as the bed level begins to lower. This does not accurately reproduce what occurs in reality in the uprooting process. This can be improved by adding a buffer that vegetation remains constant up until a percentage of the root depth and then reduces linearly. Alternatively, the vegetation can be reduced exponentially. Schweiger and Schuettrumpf, 2021a developed another dynamic vegetation model that uses the same linear approximation as Van Der Lugt et al., 2019 and reduces the critical velocity by a factor instead of changing the bed friction. This model is yet to be tested in 2D prototype-scale XBeach models.

7.2.4. LULC

LULC generally can be found as public data derived from satellite imagery. The classification analyzes each pixel and classifies it based on certain image data sets in machine learning models. With recent advancements in machine learning technology and artificial intelligence, our capabilities to classify different vegetation types from different image sources. Current LULC data is applied at very large scales and does not often have a focus on coastal environments. Work has already been done to improve algorithms to classify coastal areas (Buscombe et al., 2022; Buscombe & Ritchie, 2018). Further research into LULC classification for coasts can significantly improve the spatial inclusion of vegetation in XBeach models.

7.2.5. Nearshore bathymetry

The current bathymetry used for XBeach models combines topographic dune measurements from LiDAR or SfM with data from bathymetric surveys. The resulting data set has almost an entirely interpolated nearshore. As a result, important morphological features can be lost in the interpolation. In general, nearshore bathymetries are hard to measure due to wave action. Satellite-derived bathymetries can be used for these shallow areas to avoid interpolation in the nearshore.

Bibliography

Arcement, G. J., & Schneider, V. R. (1989). Guide for selecting manning's roughness coefficients for natural channels and flood plains. *U.S. Geological survey water-supply paper 2339*. https://doi.org/10.3133/wsp2339

Bertin, X., De Bakker, A., Van Dongeren, A., Coco, G., André, G., Ardhuin, F., Bonneton, P., Bouchette, F., Castelle, B., Crawford, W. C., Davidson, M., Deen, M., Dodet, G., Guérin, T., Inch, K., Leckler, F., McCall, R., Muller, H., Olabarrieta, M., … Tissier, M. (2018). Infragravity waves: From driving mechanisms to impacts. *Earth-Science Reviews*, *177*, 774–799. https://doi.org/https://doi.org/10.1016/j.earscirev.2018.01.002

Bhatia, K. T., Vecchi, G. A., Knutson, T. R., Murakami, H., Kossin, J., Dixon, K. W., & Whitlock, C. E. (2019). Recent increases in tropical cyclone intensification rates. *Nature Communications*, *10*, 1–9.

Blackburn, S., Pelling, M., & Marques, C. (2019). Megacities and the coast: Global context and scope for transformation. *Coast and Estuaries*, 661–669.

Bryant, D. B., Bryant, M. A., Sharp, J. A., Bell, G. L., & Moore, C. (2019). The response of vegetated dunes to wave attack. *Coastal Engineering*, *152*. https://doi.org/10.1016/j.coastaleng.2019.103506

Bucci, L., Alaka, L., Hagen, A., Delgado, S., & Beven, J. (2023). Hurricane ian. *National Hurricane Center Tropical Cyclone Report*, *AL092022*. https://www.nhc.noaa.gov/data/tcr/AL092022_Ian.pdf

Buscombe, D., Goldstein, E. B., Sherwood, C. R., Bodine, C., Brown, J. A., J. Favela, S. F., Kranenburg, C. J., Over, J. R., Ritchie, A. C., Warrick, J. A., & Wernette, P. (2022). Human-in-the-loop segmentation of earth surface imagery. *Earth and Space Science*, *9*. https://doi.org/https://doi.org/10.1029/2021EA002085

Buscombe, D., & Ritchie, A. C. (2018). Landscape classification with deep neural networks. *Geosciences (Switzerland)*, *8*. https://doi.org/10.3390/geosciences8070244

Cohn, N., Ruggiero, P., García-Medina, G., Anderson, D., Serafin, K. A., & Biel, R. (2019). Environmental and morphologic controls on wave-induced dune response. *Geomorphology*, *329*, 108–128. https://doi.org/10.1016/j.geomorph.2018.12.023

Davidson, S. G., Hesp, P. A., & Da Silva, G. M. (2020). Controls on dune scarping. *Progress in Physical Geography*, *44*, 923–947. https://doi.org/10.1177/0309133320932880

De Battisti, D., & Griffin, J. N. (2020). Below-ground biomass of plants, with a key contribution of buried shoots, increases foredune resistance to wave swash. *Annals of Botany*, *125*, 325–333.

De Doncker, L., Troch, P., Verhoeven, R., Bal, K., Meire, P., & Quintelier, J. (2009). Determination of the manning roughness coefficient influenced by vegetation in the river aa and biebrza

river. *Environmental Fluid Mechanics*, *9*, 549–567. https://doi.org/10.1007/s10652-009-9149-0

De Vries, S., Southgate, H., Kanning, W., & Ranasinghe, R. (2012). Dune behaviour and aeolian transport on decadal timescales. *Coastal Engineering*, *67*, 41–53.

Dewitz, J. (2021). National land cover database (nlcd) 2019 products. https://doi.org/10.5066/P9KZCM54

Doyle, T. B., & Woodroffe, C. D. (2018). The application of lidar to investigate foredune morphology and vegetation. *Geomorphology*, *303*, 106–121. https://doi.org/10.1016/j.geomorph.2017.11.005

FDEP. (2005). Florida department of environmental protection: Lovers key state park approved management plan. *Geomorphology*. https://floridadep.gov/parks/parks-office-park-planning/documents/lovers-key-state-park

Feagin, R. A., Furman, M., Salgado, K., Martinez, M. L., Innocenti, R. A., Eubanks, K., Figlus, J., Huff, T. P., Sigren, J., & Silva, R. (2019). The role of beach and sand dune vegetation in mediating wave run up erosion. *Estuarine, Coastal and Shelf Science*, *219*, 97–106. https://doi.org/10.1016/j.ecss.2019.01.018

Feagin, R. A., Innocenti, R. A., Bond, H., Wengrove, M., Huff, T. P., Lomonaco, P., Tsai, B., Puleo, J., Pontiki, M., Figlus, J., Chavez, V., & Silva, R. (2023). Does vegetation accelerate coastal dune erosion during extreme events? *Science Advances*, *9*. https://doi.org/10.1126/sciadv.adg7135

Figlus, J., Sigren, J. M., Feagin, R. A., & Armitage, A. R. (2022). The unique ability of fine roots to reduce vegetated coastal dune erosion during wave collision. *Frontiers in Built Environment*, *8*. https://doi.org/10.3389/fbuil.2022.904837

Figlus, J., Sigren, J. M., Power, M. J., & Armitage, A. R. (2017). Physical model experiment investigating interactions between different dune vegetation and morphology changes under wave impact. *Coastal Dynamics*, *59*.

Goff, J. A., Allison, M. A., & Gulick, S. P. (2010). Offshore transport of sediment during cyclonic storms: Hurricane ike (2008), texas gulf coast, usa. *Geology*, *38*, 351–354. https://doi.org/10.1130/G30632.1

Goff, J. A., Swartz, J. M., Gulick, S. P., Dawson, C. N., & de Alegria-Arzaburu, A. R. (2019). An outflow event on the left side of hurricane harvey: Erosion of barrier sand and seaward transport through aransas pass, texas. *Geomorphology*, *334*, 44–57. https://doi.org/10.1016/j.geomorph.2019.02.038

Harter, C., & Figlus, J. (2017). Numerical modeling of the morphodynamic response of a low-lying barrier island beach and foredune system inundated during hurricane ike using xbeach and cshore. *Coastal Engineering*, *120*, 64–74. https://doi.org/10.1016/j.coastaleng.2016.11.005

Houser, C., Hapke, C., & Hamilton, S. (2008). Controls on coastal dune morphology, shoreline erosion and barrier island response to extreme storms. *Geomorphology*, *100*, 223–240. https://doi.org/10.1016/j.geomorph.2007.12.007

Hsu, S. A., & Yan, Z. (1998). A note on the radius of maximum wind for hurricanes. *Journal of Coastal Research*, *14*(2), 667–668. Retrieved July 31, 2023, from http://www.jstor.org/stable/4298820

Itzkin, M., Moore, L. J., Ruggiero, P., Hacker, S. D., & Biel, R. G. (2021). The relative influence of dune aspect ratio and beach width on dune erosion as a function of storm duration and surge level. *Earth Surface Dynamcis*, *9*. https://doi.org/https://doi.org/10.5194/esurf-9-1223-2021

Kelly, E. W., & Jose, F. (2021). Geomorphologic recovery of north captiva island from the landfall of hurricane charley in 2004. *Geosciences*, *11*. https://doi.org/https://doi.org/10.3390/geosciences11090358

Lennon, G. (1991). The nature and causes of hurricane-induced ebb scour channels on a developed shoreline. *Journal of Coastal Research*, 237–248.

Lentz, E. E., & Hapke, C. J. (2011). Geologic framework influences on the geomorphology of an anthropogenically modified barrier island: Assessment of dune/beach changes at fire island, new york. *Geomorphology*, *126*. https://doi.org/https://doi.org/10.1016/j.geomorph.2010.10.032

Lindsay, J. (2018). A new method for the removal of off-terrain objects from lidar-derived raster surface models. *unpublished*, 1–17.

Livingston. (n.d.). Coastal vegetation and sand dunes: Information sheet, accessed on 2023-08-18. https://www.livingstone.qld.gov.au/downloads/file/2310/coastal-vegetation-and-sand-dunes-information-sheet

Lodewijk, P., De Vet, M., Mccall, R. T., Den Bieman, J. P., Stive, M. J. F., & Van Ormondt, M. (2015). Modelling dune erosion, overwash and breaching at fire island (ny) during hurricane sandy. *The Proceedings of the Coastal Sediments*. https://doi.org/10.1142/9789814689977_0006

Luijendijk, A., Hagenaars, G., Ranasinghe, R., Baart, F., Donchyts, G., & Aarninkhof, S. (2018). The state of the world's beaches. *Scientific Reports*, *8*. https://doi.org/10.1038/s41598-018-24630-6

Makris, C., Mallios, Z., Androulidakis, Y., & Krestenitis, Y. (2023). Coastflood: A high-resolution model for the simulation of coastal inundation due to storm surges. *Hydrology*, *10*. https://doi.org/https://doi.org/10.3390/hydrology10050103

Martínez, M. L., & Psuty, N. P. (2004). Coastal dunes: Ecology and conservation. *Ecological Studies*, *171*. https://doi.org/10.1007/978-3-540-74002-5

Masselink, G. (1995). Group bound long waves as a source of infragravity energy in the surf zone. *Continental Shelf Research*, *15*, 1525–1547.

Mattocks, C., & Forbes, C. (2008). A real-time, event-triggered storm surge forecasting system for the state of north carolina. *Ocean Modelling*, *25*, 95–119. https://doi.org/10.1016/j.ocemod.2008.06.008

Maximiliano-Cordova, C., Martínez, M. L., Silva, R., Hesp, P. A., Guevara, R., & Landgrave, R. (2021). Assessing the impact of a winter storm on the beach and dune systems and erosion

mitigation by plants. *Frontiers in Marine Science*, *8*. https://doi.org/10.3389/fmars.2021.734036

McCall, R. T., Van Thiel De Vries, J. S., Plant, N. G., Van Dongeren, A. R., Roelvink, J. A., Thompson, D. M., & Reniers, A. J. (2010). Two-dimensional time dependent hurricane overwash and erosion modeling at santa rosa island. *Coastal Engineering*, *57*, 668–683. https://doi.org/10.1016/j.coastaleng.2010.02.006

Mckay, S. K., & Fischenich, J. C. (2011). Robust prediction of hydraulic roughness. *US Army Corps of Engineers*, 1–19.

McLachlan, A. (1991). Ecology of coastal dune fauna. *Journalof Arid Environments*, *21*, 229–243. https://doi.org/https://doi.org/10.1016/S0140-1963(18)30684-0

Mitasova, H., Hardinb, E., Starek, M. J., Harmon, R. S., & Overton, M. F. (2011). Landscape dynamics from lidar data time series. *Geomorphometry*. https://geospatial.ncsu.edu/geoforall/pubpdf/Mitasova2011geomorphometry.pdf

NGS. (2023a). 2015-2023 noaa ngs color coastal oblique imagery. *NOAA National Centers for Environmental Information*. https://www.fisheries.noaa.gov/inport/item/67562.

NGS. (2023b). 2017 noaa ngs emergency response imagery: Hurricane irma. *NOAA National Centers for Environmental Information*. https://www.fisheries.noaa.gov/inport/item/52284.

NGS. (2023c). 2017 noaa ngs ortho-rectified oblique imagery of the gulf coast. *NOAA National Centers for Environmental Information*. https://www.fisheries.noaa.gov/inport/item/48432.

NGS. (2023d). 2022 noaa ngs emergency response imagery: Hurricane ian. *NOAA National Centers for Environmental Information*. https://www.fisheries.noaa.gov/inport/item/67923.

NOAA. (2018). Continuously updated digital elevation model (cudem) - ninth arc-second resolution bathymetric-topographic tiles. https://chs.coast.noaa.gov/htdata/raster2/elevation/NCEI_ninth_Topobathy_2014_8483/FL/

NOAA. (2023). Digital coast: Data access viewer, accessed on 2023-08-15. https://coast.noaa.gov/dataviewer/#/lidar/search/-9161589.336204654,3068564.5005084006,-9148289.293283034,3088132.3797494057

OCM-Partners. (2023a). 2006 usgs southeast u.s. imagery. *NOAA National Centers for Environmental Information*. https://www.fisheries.noaa.gov/inport/item/49578.

OCM-Partners. (2023b). 2018 usgs/nrcs lidar dem, southwest fl from 2010-06-15 to 2010-08-15. *NOAA National Centers for Environmental Information*. https://www.fisheries.noaa.gov/inport/item/59010.

OCM-Partners. (2023c). 2018 usgs/nrcs lidar, southwest fl from 2010-06-15 to 2010-08-15. *NOAA National Centers for Environmental Information*. https://www.fisheries.noaa.gov/inport/item/59010.

Over, J.-S. R., Brown, J. A., Sherwood, C. R., Hegermiller, C., Wernette, P. A., Ritchie, A. C., & Warrick, J. (2021). A survey of storm-induced seaward-transport features observed during the 2019 and 2020 hurricane seasons. *Shore Beach*, *89*, 31–40.

Passeri, D. L., Long, J. W., Plant, N. G., Bilskie, M. V., & Hagen, S. C. (2018). The influence of bed friction variability due to land cover on storm-driven barrier island morphodynamics. *Coastal Engineering*, *132*, 82–94. https://doi.org/10.1016/j.coastaleng.2017.11.005

Roelvink, D., Reniers, A., Van Dongeren, A., Van Thiel De Vries, J., McCall, R., & Lescinski, J. (2009). Modelling storm impacts on beaches, dunes and barrier islands. *Coastal Engineering*, *56*, 1133–1152. https://doi.org/10.1016/j.coastaleng.2009.08.006

Ruessink, B. G., Miles, J. R., Feddersen, F., Guza, R. T., & Elgar, S. (2001). Group bound long waves as a source of infragravity energy in the surf zone. *Journal of Geophysical Research: Oceans*, *106*, 22451–22463.

Sallenger, A. H. (2000). Storm impact scale for barrier islands. *Journal of Coastal Research*, *16*, 890–895.

Schambach, L., Grilli, A. R., Grilli, S. T., Hashemi, M. R., & King, J. W. (2018). Assessing the impact of extreme storms on barrier beaches along the atlantic coastline: Application to the southern rhode island coast. *Coastal Engineering*, *133*, 26–42. https://doi.org/10.1016/j.coastaleng.2017.12.004

Schweiger, C., & Schuettrumpf, H. (2021a). Considering the effect of belowground biomass on dune erosion volumes in coastal numerical modelling. *Coastal Engineering*, *168*. https://doi.org/10.1016/j.coastaleng.2021.103927

Schweiger, C., & Schuettrumpf, H. (2021b). Considering the effect of land-based biomass on dune erosion volumes in large-scale numerical modeling. *Journal of Marine Science and Engineering*, *9*. https://doi.org/10.3390/jmse9080843

Sherwood, C. R., Van Dongeren, A., Doyle, J., Hegermiller, C. A., Hsu, T.-J., Kalra, T. S., Olabarrieta, M., Penko, A. M., Rafati, Y., Roelvink, D., van der Lugt, M., Veeramony, J., & Warner, J. C. (2021). Modeling the morphodynamics of coastal responses to extreme events: What shape are we in? *Annual Review of Marine Science*, *14*, 457–92. https://doi.org/10.1146/annurev-marine-032221

Shiflett, S. A., & Backstrom, J. T. (2023). Impacts of hurricane isaias (2020) on geomorphology and vegetation communities of natural and planted dunes in north carolina. *Journal of Coastal Research*, *39*. https://doi.org/https://doi.org/10.2112/JCOASTRES-D-22-00108.1

Sigren, J. M., Figlus, J., & Armitage, A. R. (2014). Coastal sand dunes and dune vegetation: Restoration, erosion, and storm protection low-frequency wave dynamics in the nearshore during hurricane attack view project coastal ridge-runnel migration view project. *Shore and Beach*, *82*, 5–11. https://www.researchgate.net/publication/270822597

Sigren, J. M., Figlus, J., & Armitage, A. R. (2023). Coastal sand dunes and dune vegetation: Restoration, erosion, and storm protection. *Shore and Beach*, *82*. https://doi.org/10.1126/sciadv.adg7135

Sigren, J. M., Figlus, J., Highfield, W., Feagin, R. A., & Armitage, A. R. (2018). The effects of coastal dune volume and vegetation on storm-induced property damage: Analysis from hurricane ike. *Journal of Coastal Research*, *34*, 164–173. https://doi.org/10.2112/JCOASTRES-D-16-00169.1

Small, C., & Nicholls, R. J. (2003). A global analysis of human settlement in coastal zones. *Journal of Coastal Research*, *19*, 584–599.

Stockdon, H. F., Doran, K. S., & Jr., A. H. S. (2009). Extraction of lidar-based dune-crest elevations for use in examining the vulnerability of beaches to inundation during hurricanes. *Journal of Coastal Research*. https://doi.org/https://doi.org/10.2112/SI53-007.1

USGS. (2023). Short-term network data portal, accessed on 2023-08-15. http://water.usgs.gov/floods/FEV/.

Van Der Lugt, M. A., Quataert, E., Van Dongeren, A., Van Ormondt, M., & Sherwood, C. R. (2019). Morphodynamic modeling of the response of two barrier islands to atlantic hurricane forcing. *Estuarine, Coastal and Shelf Science*, *229*. https://doi.org/10.1016/j.ecss.2019.106404

Van Puijenbroek, M. E. B., Nolet, C., De Groot, A. V., Suomalainen, J. M., Riksen, M. J. P. M., Berendse, F., & Limpens, J. (2017). Exploring the contributions of vegetation and dune size to early dune development using unmanned aerial vehicle (uav) imaging. *Biogeosciences*, *14*, 5533–5549. https://doi.org/https://doi.org/10.5194/bg-14-5533-2017

Van Rijn, L. C. (2009). Prediction of dune erosion due to storms. *Coastal Engineering*, *56*, 441–457.

Van Rijn, L., Walstra, D., Grasmeijer, B., Sutherland, J., Pan, S., & Sierra, J. (2003). The predictability of cross-shore bed evolution of sandy beaches at the time scale of storms and seasons using process-based profile models. *Coastal Engineering*, *47*. https://doi.org/https://doi.org/10.1016/S0378-3839(02)00120-5

Van Rooijen, A. A., Van Thiel De Vries, J. S., McCall, R. T., Van Dongeren, A. R., Roelvink, J. A., & Reniers, A. J. (2014). Modeling of wave attenuation by vegetation with xbeach. *E-proceedings of the 36th IAHR World Congress*.

Van Thiel De Vries, J., Van Gent, M., Walstra, D., & Reniers, A. (2008). Analysis of dune erosion processes in large-scale flume experiments. *Coastal Engineering*, *55*, 1028–1040.

Wernette, P., Houser, C., & Bishop, M. P. (2016). An automated approach for extracting barrier island morphology from digital elevation models. *Geomorphology*, *262*.

A

Appendix

A.1. Alongshore resolution

Figures showing alongshore resolution of the dune crest with different grid sizes in XBeach and different bathymetry data sets.

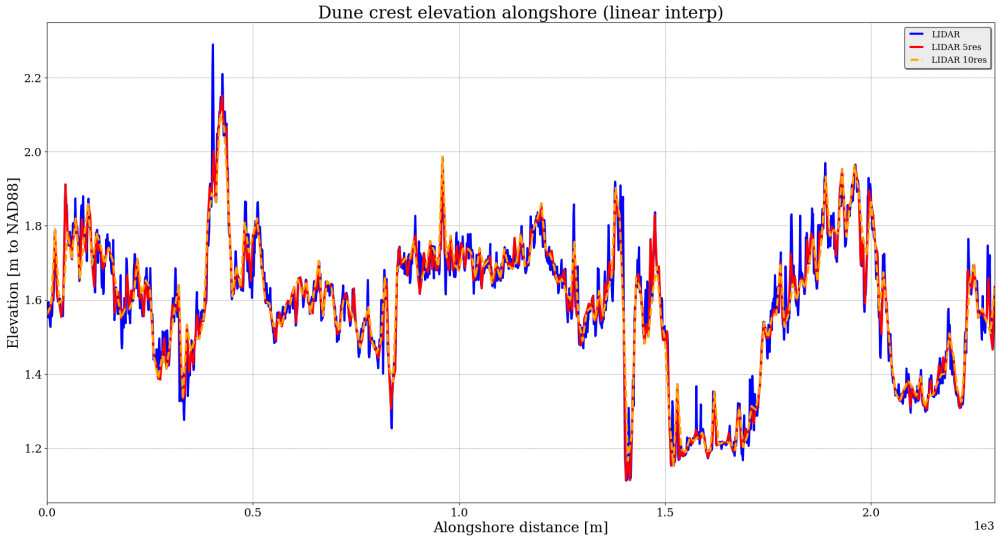

Figure A.1: *Different dune crest alongshore resolutions and the effects on topographic details captured*

Different bathymetry data sets are compared to see the amount of details captured. Note that the CUDEM data set misses a global minimum when compared to the LiDAR data set. This can have serious implications for the outcome of XBeach simulations, such as breach location.

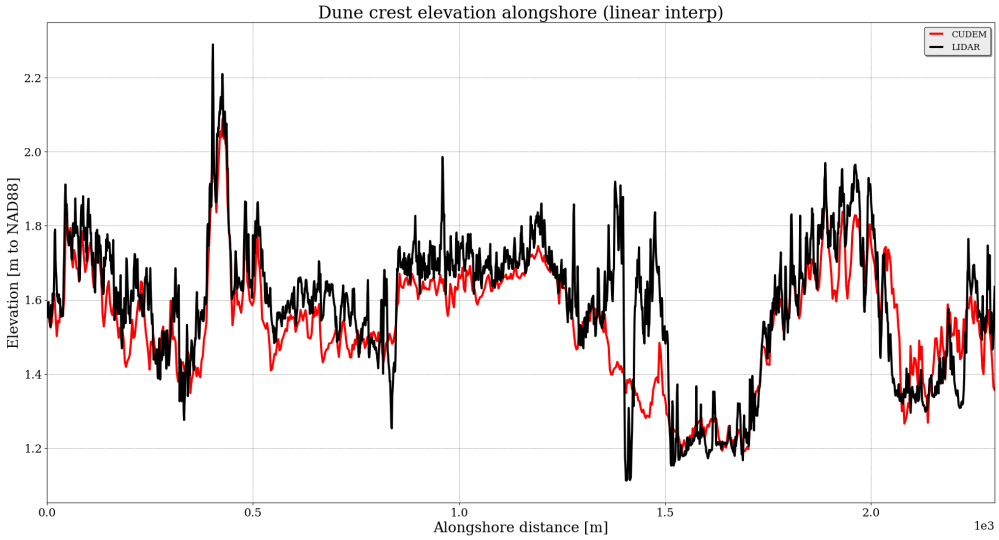

Figure A.2: *CUDEM vs LiDAR alongshore dune crest.*

A.2. Makris et al. 2023, roughness coefficients

Makris et al., 2023 compiled manning roughness values for different LULC classifications from different literature studies related to coastal modelling. The figure shows their new proposed classification system.

A/A	n	Description of Areas' Characteristics
1	0.001	open water
2	0.0115	concrete surfaces
3	0.010	rural driveways (dirt road and granules)
4	0.012	urban land uses (asphalt mixtures and other urban surface features: artificial stones, paving blocks, lightweight aggregate concrete), concrete rooftop, playground, yard, barren land
5	0.013	main asphalt roads (national, regional highway networks, autobahns, etc.)
6	0.015	brick terrain, unidentified high and low development urban environment, inland open waters (reservoirs, lakes, ponds, lagoons, estuaries)
7	0.017	city streets (asphalt, concrete, etc.)
8	0.018	unidentified/unclassified urban terrain
9	0.020	clean to gravelly earth pathways (pebbles with a small portion of cobbles), muddy/sandy open waters and sandy terrains, sea bottom (saturated wet sand or silt-sand) and channel beds
10	0.030	bare unidentified/unclassified soil
11	0.022	bare land, stone paved road and ceramic sett, or paving sett pathways
12	0.029	stony cobble lands, pastures, and farmlands
13	0.025	manmade structures, gravel beds and pathways (pebbles with nominal diameter: d_{n50} = 4–64 mm, cobbles: d_{n50} = 64–256 mm)
14	0.0375	cultivated fields and pasture, grassland (including prairies, steppes, plains)
15	0.0425	isolated sand/gravel(mixed) pits, estuary channels, and uneven urban areas
16	0.029	emerged sloping sandy beaches, sand dunes
17	0.030	managed grasslands
18	0.0115	unclassified/unidentified rural areas
19	0.033	grass surfaces
20	0.035	short stiff grass areas
21	0.0575	weeds with or without structure
22	0.0555	heavy brush floodplains
23	0.040	arable land plains, heavy/coarse gravel (boulders: d_{n50} >= 256 mm) areas, unclassified grassland, and shrubs (including savannah, meadow, veldt, pampa, tundra)
24	0.050	unclassified trees, open development areas (containing parks, streets of rural character)
25	0.055	herbaceous wetlands
26	0.067	emerged barriers
27	0.140	hardwood woodland and cultivated woodland
28	0.086	unclassified wetlands (including watersheds, salt/fresh marshes, bottomland hardwood, swamps, mangrove swamps, seagrass flats, forest swamps)
29	0.100	forest land and unidentified forest trees evergreen forest, pasture, hay, crop, vegetation
30	0.120	deciduous forest, natural grassland, herbaceous lands
31	0.150	mixed forest, shrubs, scrub, emergent herbaceous wetlands
32	0.240	cultivated vegetation
33	0.300	unidentified densely built urbanized zones (uncharacterized structures)
34	0.320	very dense tall (long trunk) trees forest (jungles, etc.)
35	0.368	very dense and/or stiff grasslands (reedy bamboo, etc.)
36	0.400	very dense small forest trees and thick shrubs

Figure A.3: *(Makris et al., 2023) proposed Manning roughness coefficients for different LULC classifications.*